Process Intensification in Crystallization: Submicron Particle Generation Using Alternative Energy Forms

Norbert Radácsi

Process Intensification in Crystallization: Submicron Particle Generation Using Alternative Energy Forms

Norbert RADÁCSI

Process Intensification in Crystallization: Submicron Particle Generation Using Alternative Energy Forms

Proefschrift

ter verkrijging van de graad van doctor
aan de Technische Universtiteit Delft,
op gezag van de Rector Magnificus Prof. ir. K.C.A.M. Luyben,
voorzitter van het College voor Promoties,
in het openbaar te verdedigen
op maandag 1 oktober 2012 om 15:00 uur

door

Norbert RADÁCSI

Master of Science in Physics, University of Debrecen
geboren te Debrecen, Hungary

Dit proefschrift is goedgekeurd door de promotor:

Prof. dr. ir. A.I. Stankiewicz

Copromotor:
Dr. ir. J.H. ter Horst

Samenstelling promotiecommissie:
Rector Magnificus	Voorzitter
Prof. dr. ir. A.I. Stankiewicz	Technische Universiteit Delft, promotor
Dr. ir. J.H. ter Horst	Technische Universiteit Delft, copromotor
Dr. A.E.D.M. van der Heijden	TNO Technical Sciences
Prof. dr. ir. A. Schmidt-Ott	Technische Universiteit Delft
Prof. dr. E. Vlieg	Radboud University Nijmegen
Prof. Dr. Dr. h.c. J. Ulrich	Martin-Luther-Universität Halle-Wittenberg
Prof. dr. T. Leyssens	Université catholique de Louvain
Prof. dr. J. Westerweel	Technische Universiteit Delft (reservelid)

Contents

Chapter 9. On the reliability of sensitivity test methods for submicron-sized energetic particles   **143**

1   **Introduction**

Crystallization is one of the oldest separation and purification techniques. In the middle ages, this unit operation was already used to obtain salt from seawater by evaporation of water. Nowadays, crystallization is among the most important processes in the chemical industry; it is the most convenient and cost effective method to produce pure solids and can give desired properties to the final product. In the future, the role of crystallization is expected to be increased in industrial processes. It is expected that several advances will be made to control crystal properties and reach high quality products. The main crystal quality aspects are crystal shape, crystal size distribution, purity and polymorphic fraction. Since nucleation and crystal growth determine the final product quality, it is crucial to understand and control these processes. By combining crystallization processes with new techniques, several opportunities emerge to allow the control of crystal quality.

1.1 Importance and drivers for crystallization research and development and process intensification in crystallization

Crystallization can be defined in many ways. It can be defined as a phase-change process in which solid crystals precipitate from a solution, melt, or even directly from gases. Crystallization is also a chemical solid–liquid separation technique, in which mass transfer of a solute from the liquid solution to a pure solid crystalline phase occurs. Crystallization and precipitation from solutions are responsible for 70% of all solid materials produced by the chemical industry [1], whereby the variation of the solubility conditions of the solute in a solvent causes crystallization during the precipitation process, as opposed to precipitation due to a chemical reaction. Thus crystallization is an important separation and purification process, which is widely used from laboratory scale to industry. Nowadays, a broad spectrum of products is produced by crystallization, and the application of crystallization processes continues to increase in the industry. For instance, crystallization is a main process in the chemical, food or pharmaceutical industries, as well as in biotechnology. Via crystallization, it is possible to reach extremely high product purity (>99.9%) in a single step, determine the end product crystal size, reach narrow size distribution of the product or obtain a desired polymorph of a crystal [2].

Despite its high importance, crystallization has hardly developed in the past centuries. For instance, batch crystallization is still widely used in the chemical industry due to its simplicity, flexibility and low cost. However, crystallization in batch has many disadvantages, namely relatively high operation costs, long operation times due to shutdowns after every batch, poor reproducibility and broad crystal size distribution. Thus, there is a need for developing crystallization techniques in order to cut costs and improve the crystalline product quality.

Process Intensification (PI) is a part of chemical engineering aiming at achieving substantial increases in the efficiency of chemical processes. The European Roadmap for Process Intensification [3] defines PI as a set of often radically innovative principles ("paradigm shift") in process and equipment design, which can bring significant (more than a factor 2) benefits in terms of process and chain efficiency, capital and operating expenses, quality, wastes, process safety, etc.

PI focuses on developing novel methods and equipment addressing four fundamental domains: spatial, thermodynamic, functional and temporal [4]. The

basic elements of PI in the thermodynamic domain are alternative forms/sources and transfer mechanisms of energy for improved processing, which belong to PI methods (Figure 1-1). Examples of such alternative energy forms and transfer mechanisms are centrifugal fields, ultrasounds, microwaves, solar energy, electric fields, or plasma [5].
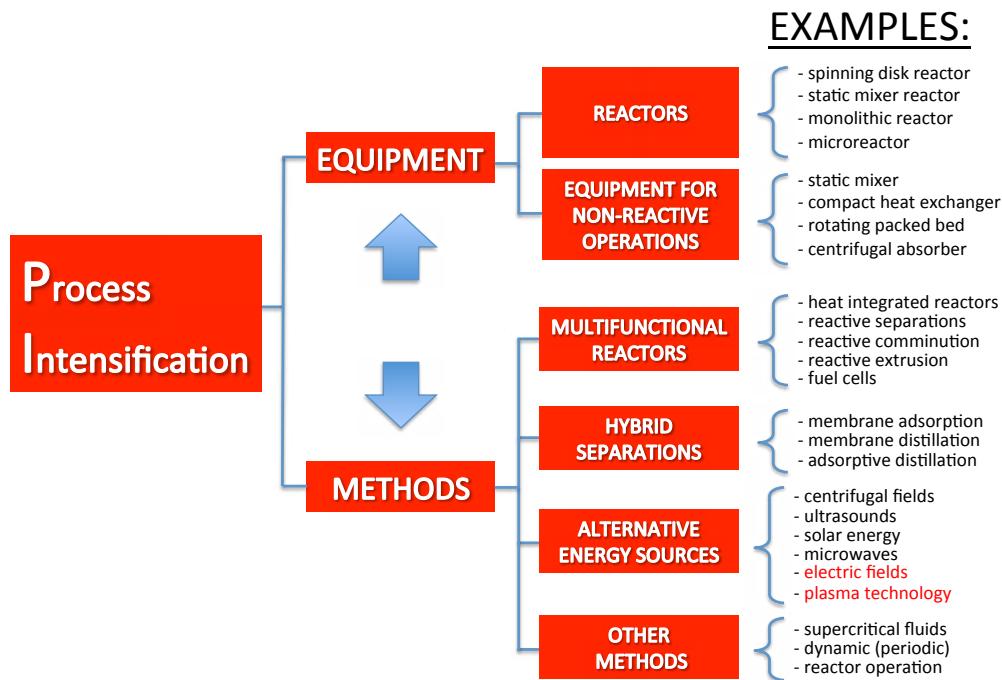
Figure 1-1. Elements of Process Intensification [5].

In the last few decades, few advances have been made in the crystallization research area and new types of crystallizers have emerged. Such developments include the transition of some crystallization processes from batch to continuous mode. Continuous processing is widely used nowadays since this mode of crystallization operation has the advantages of speed, low costs, and better reproducibility than the batch mode. In recent years, considerable progress has also been achieved in using ultrasounds [6] in crystallization processes. However, plasma technology and electric fields were hardly investigated for improving crystallization processes. Therefore, this thesis gives a detailed insight about the application of plasma technology in producing submicron organic particles with improved properties, and investigates the effects of constant electric fields on crystallization.

1.2 Crystal quality

The crystallization process parameters can significantly affect the final crystal product properties - the crystal shape, crystal size distribution (CSD), purity and polymorphic fraction - being the main crystal product quality aspects [1]. A compact crystal shape is generally associated with high quality, while elongated, needle-like crystals are associated with low crystal quality. Crystal size is generally investigated as a property of a distribution of crystals rather than a property of an individual crystal, where a narrow CSD is the sought after outcome in industrial applications. The purity gives information about the amount of a foreign substance present in a crystal. By applying crystallization, very high product purity (>99.9%) can be achieved [2].

Polymorphism is often characterized as the ability of a substance to exist as two or more crystalline phases that have different arrangement and/or conformation of the molecules in the crystal lattice [7]. These different crystal forms of the same material usually have different properties, specifically for polymorphs of drugs, which may have different effects *in vivo*. Thus, during drug production it is very important to produce the desired polymorphic form of the compound.

The crystal quality also depends on the presence of imperfections. In theory, crystals have a perfectly arranged crystal structure. But in practice crystals are (almost) never perfect [7]. If the crystal structure is disrupted in some way the crystal is said to contain imperfections [8]. There are different kinds of imperfections that can occur such as point defects, line defects or surface defects. Point defects can be caused by a foreign atom present in the crystal lattice that cause the atoms in the crystal to be slightly displaced since the impurity atoms do not really fit in the perfect lattice structure. The displacement of the atoms causes a strain in the crystal. Another type of point defects is due to the presence of vacancies in the crystal. A vacancy is simply a lattice site in which there is no atom. Another type of imperfection is known as a line defect. The dislocation is a weak point in the crystal. If a solvent or a foreign substance is entrapped within the crystal structure, it is called an inclusion. Inclusions highly diminish the crystal quality, since they are generally in the micron size range, and can cause three-dimensional defects.

Crystals can vary in size and shape and also the faces of a particular crystal can vary considerably. The latter variation is referred to as the crystal habit. Crystals can grow more rapidly in one direction, which results in elongated needle-like shapes while stunted growth yields flat plate-like shaped particles.

Interestingly crystal habit increases when crystals are smaller, especially in the submicron size range.

1.3 Crystal quality control

1.3.1 Impurities

In many instances, small amounts of impurities have dramatic effects on nucleation, crystal growth and crystal quality [8]. In industrial crystallization operations in particular, the presence of impurities can influence the whole crystallization process. The interactions of solvent and impurities at the interface play a central role in all aspects of crystallization and impact the crystal size, shape, and purity [8]. To diminish the effects of impurities, there is a need for the improvement of crystallization processes. Because of the requirement of high-purity crystalline products, an understanding of the effects of solvents on purification is important. The solvent can influence the separation efficiency through its effect on crystallization kinetics, solution thermodynamics, and crystal interface structure [8]. A poor initial choice of solvent can thermodynamically and kinetically limit the effectiveness of the separation, irrespective of all other factors, including the crystallizer design and cost. Some solvents can also incorporate into the crystal structure, and solvates can be formed.

The solvent and impurities thus influence the crystal structure and growth rates of faces, which determine the crystal shape. The shape of a crystal is determined by the relative growth rates of the individual faces of a crystal, and can be strongly influenced during crystallization by the presence of impurities, and even the solvent itself. During crystallization, fast growing faces normally grow out of existence, leaving the crystal bounded by the slowest growing faces [8]. Impurities or solvents that adsorb or interact with the crystal face in such a way to slow the growth rate can further increase its relative area.

1.3.2 Nucleation

Crystallization from solution can be thought of as a two-step process. The first step is the phase separation, or "birth" of new crystals. The second step is the growth of these crystals to larger sizes. These two processes are known as nucleation and crystal growth, and determine the crystal product, since the

nucleation and crystal growth rates give the residence time and induction time of a crystallization process [9]. Nucleation is the step where the solute molecules in the solvent start to gather into small clusters. Molecules attach and detach, until a critical size is reached and a stable nucleus is formed. If a cluster is not stable, it redissolves in the solution. In general, a few hundred molecules can form a stable nucleus, which is in the nanometer scale [7].

Nucleation can be categorized into primary and secondary nucleation (Figure 1-2). Primary nucleation occurs in the absence of crystalline surfaces when a specific supersaturation (metastable supersaturation) is reached in the system [10]. There are two types of primary nucleation: homogeneous nucleation (HON) and heterogeneous nucleation (HEN). HON rarely occurs in practice, since it can only occur if the solution contains neither solid foreign particles nor crystals of its own type [10]. In an industrial crystallizer, primary HON is not possible due to the low levels of supersaturation employed and due to the presence of impurities [8]. In practice, usually HEN is the one to occur and can be induced by the presence of impurities, wall or any foreign substances in the crystallization system.

Secondary nucleation involves the presence of crystals and their interaction with the crystallizer environment. It occurs for instance when fragmentation of a present crystal is under the influence of fluid shear, or by attrition due to interactions with the crystallizer wall, another crystal, stirrer or impeller. Secondary nucleation can also occur when nucleation is induced by the presence of a crystalline solute or 'seed' crystals [11]. In an industrial crystallizer mainly secondary nucleation takes place [12, 13].
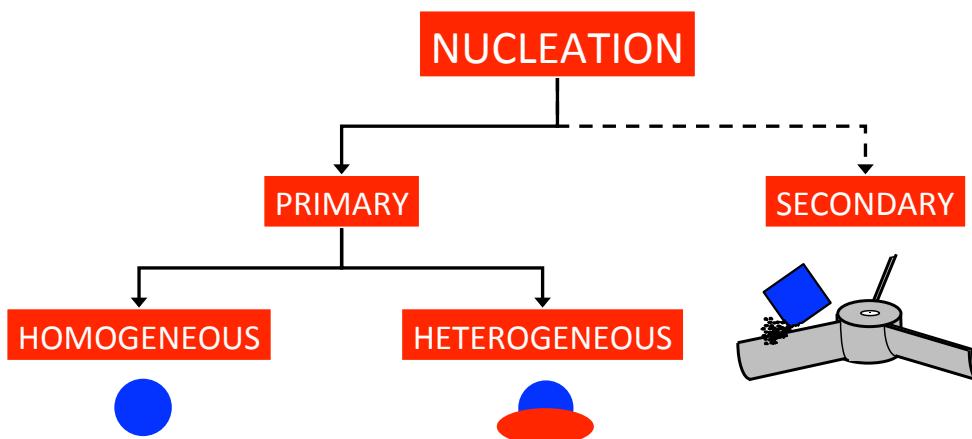
Figure 1-2. The main types of nucleation.

1.3.3 Crystal growth

Crystal growth is the next stage after the nucleation process, where the nucleus grows larger by the addition of solute molecules from the supersaturated solution. Crystal growth, along with nucleation, controls the final particle size distribution obtained in the system. In addition, the process conditions and rate of crystal growth have a significant impact on the product purity and the crystal habit. An understanding of the crystal growth theory and experimental techniques for examining crystal growth from solution are important and very useful in the development of industrial crystallization processes.

1.4 Conventional and state of the art crystallization techniques for submicron crystal production

There are several techniques for producing nanoparticles. Conventional methods involve milling or pyrolysis, while advanced methods include thermal plasma [14], or rapid expansion of supercritical solutions [15]. The latter techniques are often used for nanoparticle production. Thermal plasmas offer an effective, cost efficient way of nanoparticle production with narrow size distribution [14]. However, thermal plasmas are not suitable for organic compounds as high temperatures can cause decomposition reactions. The rapid expansion of supercritical solutions process is anticipated to have high surface quality since the small crystal size distribution is achieved by direct crystallization, without physical grinding, where damage to the crystal surface occurs [15]. Unfortunately, rapid expansion of supercritical solutions cannot be implemented in industry since it is a very complex and costly technique.

1.5 Motivation and thesis outline

The motivation of this thesis is to further develop crystallization techniques by using alternative energy forms to improve existing techniques and open new fields that can be applicable for crystallization. Two alternative energy forms, plasma technology and electric fields, were used in various crystallization systems.

In **Chapter 2** the thermodynamic and kinetic properties of the used materials, RDX, niflumic acid and isonicotinamide, are investigated. The solubility curve

and metastable zone width of these materials were determined, and the crystal growth rate of RDX was measured.

In **Chapters 3, 4** and **5,** an advanced crystallization technique, electrospray crystallization, for the production of nano-sized crystals is presented. Electrospray crystallization uses high voltage to create a large electric field in a nozzle tip through which a conductive solution is pumped. This process results in spraying ultra-fine solution droplets, and upon solvent evaporation, nano-sized crystals are produced.

An innovative crystallization technique, plasma-assisted crystallization, is discussed in **Chapters 6** and **7**. A specific plasma, surface dielectric barrier discharge, was used at atmospheric pressure and close to room temperature for the first time to produce organic nanoparticles. A nebulizer injects an aerosol of solution droplets into the plasma reactor, where the plasma charges and heats the droplets, and after disruption and solvent evaporation, nano-sized crystals are produced. The produced RDX, niflumic acid, and its excipient, Poloxamer 188 are characterized in these chapters.

In **Chapter 8** the effect of a constant high electric field is investigated during cooling crystallization experiments. Changes in fluid dynamics, crystal growth rates, and polymorphism are described in this chapter.

Chapter 9 discusses the applicability and reliability of conventional small-scale sensitivity test methods for nano-sized energetic crystals. Submicron-sized energetic crystals were produced by electrospray crystallization and plasma-assisted crystallization. The product was tested for sensitivity by impact and friction sensitivity tests and ballistic impact chamber test. The observations from the friction and ballistic impact chamber stress the need for revisiting these standard sensitivity tests, and recommendations are given to develop new tests that are also applicable for submicron/nano-sized energetic materials.

In **Chapter 10** a conclusion is made about the advantages and disadvantages of the electrospray and plasma-assisted crystallization techniques, and the effects of the electric field on crystallization are summarized. Finally, the outlook on some possible designs towards a perfect, future electrospray or plasma crystallizer is discussed.

References

[1]   M. Giulietti, M. M. Seckler, S. Derenzo, M. I. Ré, E. Cekinski *Brazilian Journal of Chemical Engineering* 2001, 18, 423-440.

[2]   C. M. Van't Land *Industrial Crystallization of Melts* M. Dekker: New York, Taylor & Francis: London, 2004

[3]   *European Roadmap for Process Intensification*, 2007.

[4]   T. van Gerven, A. Stankiewicz, *Industrial & Engineering Chemistry Research* 2009, 48, 2465-2474.

[5]   A. Stankiewicz, *Chemical Engineering and Processing* 2003, 42 137-144.

[6]   G. Ruecroft, D. Hipkiss, T. Ly, N. Maxted, P. W. Cains *Organic Process Research & Development*, 2005, 9, 923-932.

[7]   J. W. Mullin *Crystallisation,* 4th Edition Butterworth-Heinemann Ltd.: Oxford, 2001.

[8]   A. S. Myerson *Handbook of Industrial Crystallization* Butterworth-Heinemann Ltd.: Oxford, 1993.

[9]   J. D. Seader, E. J. Henley, D. K. Roper *Separation Process Principles* John Wiley & Sons Inc.: Hoboken, New Jersey, 2010.

[10]   A. Mersmann *Crystallization Technology Handbook* M. Dekker: New York, 1995.

[11]   G. Youngquist, A. D. Randolph *AIChE Journal* 1972, 18, 421.

[12]   N. S. Tavare, *Chemical Engineering Communications* 1987, 61, 259-318.

[13]   A. E. D. M. van der Heijden *Secondary nucleation and crystallization kinetics,* PhD Thesis, University of Nijmegen, The Netherlands, 1992.

[14]   N. Rao, S. Girshick, J. Heberlein, P. McMurry, S. Jones, D. Hansen, B. Micheel *Plasma Chemistry and Plasma Processing* 1995, 15 581-606.

[15]   V. Stepanov, L. N. Krasnoperov, I. B. Elkina, X. Zhang *Propellants, Explosives, Pyrotechnics* 2005, 30, 178-183.

2 Thermodynamic and kinetic properties of the used model materials

To understand the crystallization behavior of the used model materials, it is necessary to characterize their properties. In this chapter, the thermodynamic and kinetic properties of a high explosive material, RDX, and two pharmaceutical compounds, niflumic acid and isonicotinamide, are discussed. The solubility line and the metastable zone width were determined for all the used materials by small scale in situ crystallization experiments using a multiple reactor crystallization setup, Crystal16. The crystal growth rate of RDX was estimated using a recently developed multiple reactor station, Crystalline, which has an on-board camera system for in situ monitoring of cooling crystallization.

2.1 Introduction

Knowledge of the thermodynamic and kinetic properties of materials that are being crystallized is essential for developing crystallization processes. The solubility characteristics are the first data that should be known about a crystallizing system. In industrial applications, knowledge of the solubility and phase relations may provide useful guidelines for the method of operation and choice of the crystallizer type [1]. Therefore the solubility curve, metastable zone width (MSZW) and crystal growth rate of the model materials of this thesis, RDX, niflumic acid (NIF) and isonicotinamide (INA), are determined.

Royal Demolition Explosive (RDX, chemical name: hexahydro-1,3,5-trinitro-1,3,5-triazine) is a white crystalline powder, and also a widely used military explosive [2]. In addition, RDX has also been used as the model material for many studies investigating the relationship between crystal properties and sensitivity [3].

NIF is a yellow, elongated, needle-like crystalline powder. It is an important anti-inflammatory drug and also has a weak analgesic effect [4]. NIF is primarily used to treat different forms of rheumatism, like rheumatoid arthritis or arthrosis, and to decrease other inflammatory diseases [5].

INA is a white crystalline powder. Its chemical structure is based on the nicotinamide structure, but in which the amide is in the 4-position instead of the 3-position. INA possesses strong anti-tubercular, anti-pyretic, fibrinolytic and anti-bacterial properties [6]. It is also commonly used as a co-former in co-crystallization for tuning the physical properties of drug molecules, e.g. bioavailability, and is being investigated for Huntington's disease and for its anti-inflammatory benefits [7].

All of the used materials are organic crystals, where crystallization is generally used as one of the unit operations during the production process. In order to select the proper solvent and to design an optimized crystallization process, it is necessary to know the solubility of the compund in different solvents. The temperature dependent solubility of a compound is a guide to determine solution concentrations to use for crystallization experiments. The first step in crystallization is nucleation, which is created by molecules forming a cluster. This step determines the final product. An important parameter of the nucleation process is the Metastable Zone Width (MSZW). The MSZW is the difference between the saturation temperature of a solution and the temperature at which crystals are first detected - the metastable zone limit (MSZL) - during

cooling crystallization of a clear solution with a constant cooling rate [8]. The MSZL is a key parameter in cooling crystallization; it indicates the temperature at which nucleation can commence at a given solution concentration.

After a stable nucleus is formed, crystal growth occurs, whereby atoms, ions or molecules are attached to the nucleus. The velocity of crystal growth is typically expressed in terms of micrometers per unit time. The crystal growth rate depends on the supersaturation; the higher the supersaturation, the higher the growth rate [9].

In this chapter the thermodynamic and kinetic properties of the mainly used model materials used in the thesis, RDX, NIF and INA, are determined by two multiple reactor setups, the Crystal16 and Crystalline Particle Viewer.

2.2 Experimental section

2.2.1. Materials

RDX was used as the model energetic material (cyclotrimethylene trinitramine), and was purchased from Chemring Nobel AS, Norway. Niflumic acid (2-[[3-(trifluoromethyl)phenyl]amino]-3-pyridinecarboxylic acid) and isonicotinamide (pyridine-4-carboxamide) were used as the model pharmaceutical compounds. The two latter materials were supplied by Sigma-Aldrich. Different concentrations of solutions were made with acetone purchased from Merck and 1,4-Dioxane (1,4-Diethyleneoxide) purchased from Sigma-Aldrich. Figure 2-1 shows the molecular structure of the used materials.
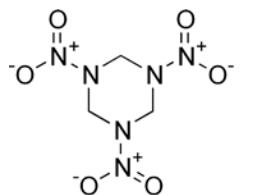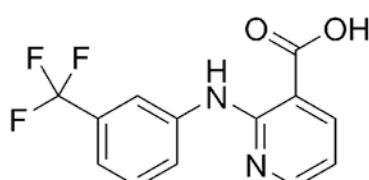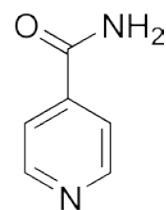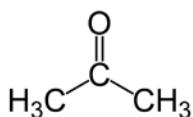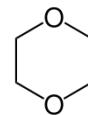
Figure 2-1. The molecular structure of the used materials. The three used crystalline materials can be seen at the top, and the two used solvents at the bottom.

2.2.2 Solubility, metastable zone width and crystal growth rate measurements

The Crystal16 multiple reactor station (Figure 2-2), developed by Avantium Technologies BV, was used to determine the solubility of all of the used materials. With the Crystal16 cloud points and clear points of sixteen 1 mL solution aliquots can be determined in parallel and automatically based on the measurement of the solution turbidity. The temperature at the point at which the suspension becomes a clear solution (clear point) upon slow heating (0.3 °C per minute) was taken as the saturation temperature of the measured sample of which the composition was established beforehand. The cloud point refers to the point at which solid material first appears upon a decrease of temperature. During a MSZW measurement a suspension is heated above the clear point and then the clear solution is cooled below the cloud point, usually at a constant rate. One boundary of the metastable zone is determined by the saturation temperature of the measured solution, which is given by the solubility curve (clear points), while the other boundary is determined by the temperature at which the crystals are first detected (cloud points), the MSZL. The MSZW is then determined by the difference between the solubility line and the MSZL. This difference exists because nucleation takes place before the growing crystals

could be detected. The detection largely depends on the resolution of the technique used [10]. A large MSZW is associated with a large supersaturation needed to nucleate the crystal product.

The crystal growth rate was measured in a stirred cooling crystallization process. For this purpose the Crystalline Particle Viewer station (Figure 2-2), also developed by Avantium Technologies BV, was used to visualize the suspension during cooling crystallization of RDX with an on-board camera. 3 mL suspension of RDX in acetone was prepared. The sample was heated above its saturation temperature in order to obtain a clear solution. Then, it was cooled down to -15 °C using a cooling rate of 0.5 °C min^{-1}. The crystal growth rate of INA and NIF samples was not investigated in a stirred cooling crystallization process. The Crystalline Particle Viewer station combines turbidity measurements with four independent real time particle visualization modules. This device is capable of taking images every second and its software analyzes and calculates particle size, distribution and shape. The median crystal diameter at every one minute was determined from the collected images using the Crystalline software. The average crystal growth rate during the crystallization process can then be estimated by dividing the size increase by the time period during which the growth occurred.
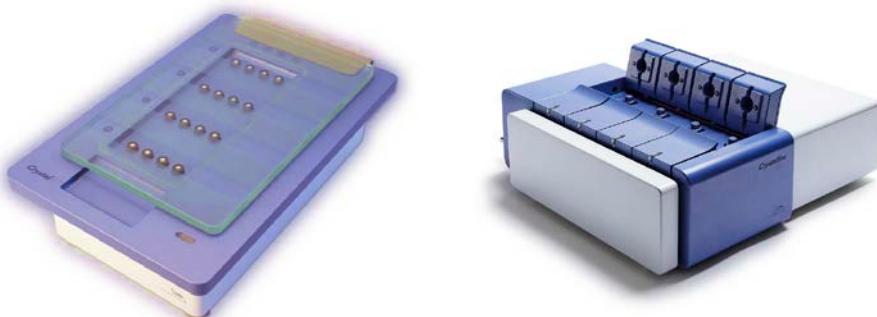
Figure 2-2. The Crystal16 multiple reactor crystallizer on the left and the Crystalline Particle Viewer multiple reactor station on the right.

2.3 Results and discussion

2.3.1 Solubility and metastable zone width

Figure 2-3 shows the solubility line and MSZL of RDX in acetone determined from the saturation temperature measurements and carried out with Crystal16, respectively. At 45 °C the solubility for RDX in acetone is 111 mg mL^{-1}. The

MSZW was determined for RDX to be around 9 °C. The solubility of RDX in acetone increases with temperature.
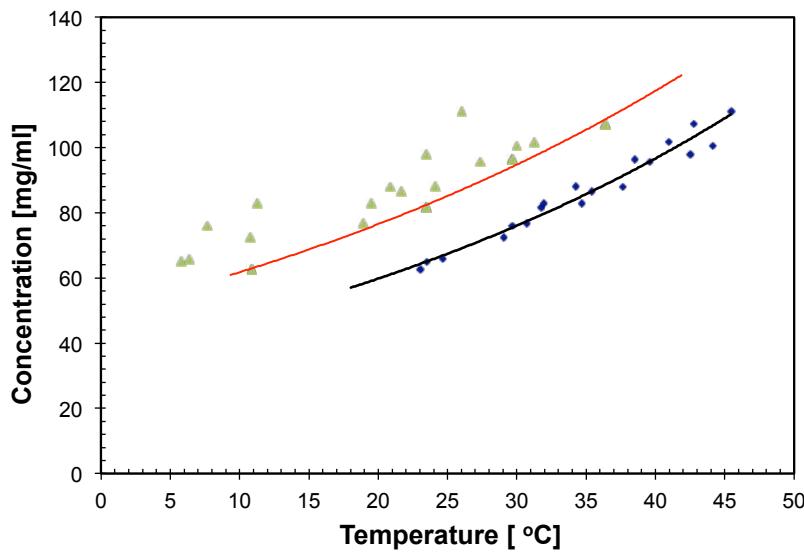
Figure 2-3. Solubility line of RDX in acetone (black line) with the metastable line (red line) as a function of temperature.

The solubility of NIF is around 111 mg mL^{-1} in acetone at room temperature (Figure 2-4). It also increases with the temperature when dissolved in acetone. The MSZW of NIF in acetone is around 10.5 °C.
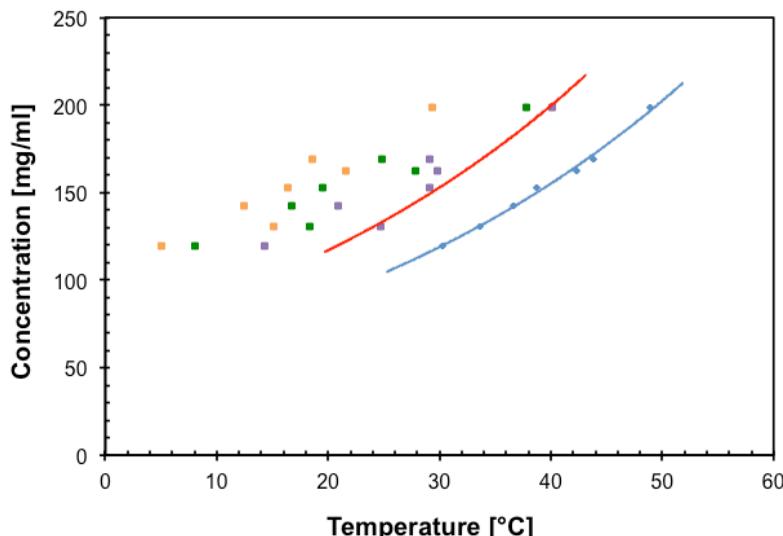
Figure 2-4. Solubility line of NIF (blue line) with the metastable line (red line) in acetone as a function of temperature.

Figure 2-5 shows that the solubility curve of INA together with the MSZL also increases with the temperature when crystallized in 1,4-dioxane. The MSZW of INA is determined to be around 10.5 °C in 1,4-dioxane.
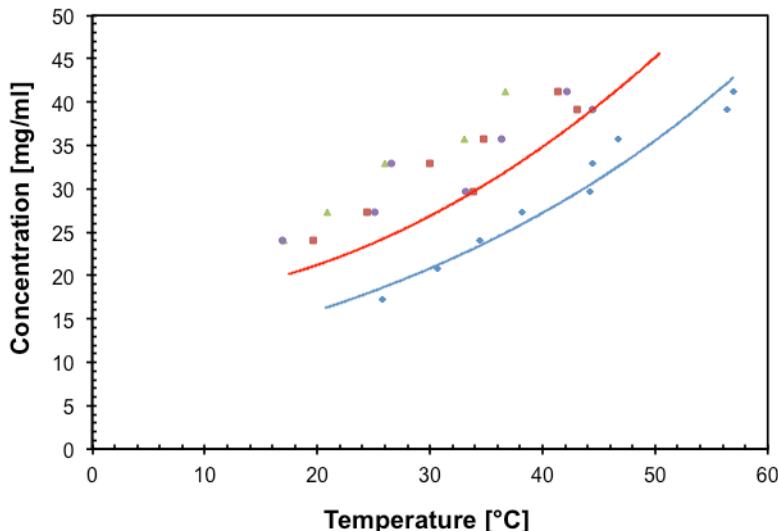
Figure 2-5. Solubility line of INA (blue line) with the metastable line (red line) in 1,4-dioxane as a function of temperature.

2.3.2 Crystal growth rate

Cooling crystallization experiments were performed with the Crystalline Particle Viewer station (Figure 2-2). During cooling crystallization of RDX in acetone, the solution was monitored *in situ* by measuring the transmission of light through the solution and by taking images simultaneously (Figure 2-6). The evolving crystal size was monitored after a sufficient number of crystals was present. Since the resolution of the on-board camera is sufficiently high (5-10 µm/pixel) to identify crystals above 30 µm size, only crystals beyond this size were taken into account. Figure 2-7 shows the average size of the RDX crystals as a function of time. Initially the size seems to be constant slightly above 30 µm. After around 10 minutes, the size seems to increase roughly linearly with time, leading to an average growth rate of about 3.7 µm min^{-1} for RDX in acetone (see Figure 2-7). These values are typical for the crystal growth of organic compounds from solutions [11,12].

Figure 2-6. Crystal growth of RDX visualized with the Crystalline Particle Viewer. The crystal size rapidly increases with the time.
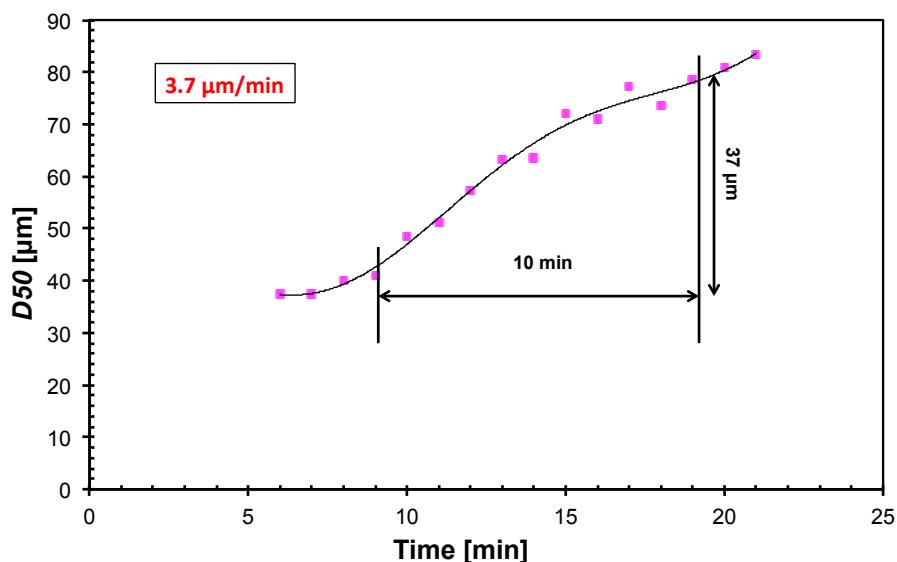
Figure 2-7. Crystal growth rate of RDX during cooling crystallization.

2.4 Conclusions

The solubility curves of a high military explosive, RDX, and two pharmaceutical compounds, INA and NIF, were determined in several solvents. In all cases the solubility increased with increasing temperature. The metastable zone width (MSZW) was determined for RDX, INA and NIF, by determining the metastable zone limit. The MSZW values for these systems were around 10 °C. It can be seen that the time needed for crystals to appear is not well defined

at the used 1 mL scale. The crystal growth rates of RDX were normal for a cooling crystallization process.

References

[1]   N. S. Tavare *Chemical Engineering Communications* 1987, 61, 259-318.

[2]   D. L. Freedman, K. W. Sutherland *Water Science and Technology* 1998, 38, 33-40.

[3]   R. M. Doherty, D. S. Watt *Propellants, Explosives, Pyrotechnics* 2008, 33, 4.

[4]   S. Budavari, M. J. O'Neil, A. Smith, P. E. Heckelman *The Merck Index,* 11th Edition Merck & Co.: Rahway, New Jersey, 1989.

[5]   J. E. F. Reynolds *Martindale: The Extra Pharmacopoeia*, 31st Edition The Royal Pharmaceutical Society: London, 1996.

[6]   I. S. Ahuja, I. Prasad *Inorganic and Nuclear Chemistry Letters* 1976, 12, 777.

[7]   K. S. Eccles, R. E. Deasy, L. Fábián, Doris E. Braun, Anita R. Maguire, S. E. Lawrence *CrystEngComm*, 2011, 13, 6923-6925.

[8]   J. W. Mullin *Crystallisation,* 4th Edition Butterworth-Heinemann Ltd.: Oxford, 2001.

[9]   P. Barrett, B. Smith, J. Worlitschek, V. Bracken, B. O'Sullivan, D. O'Grady *Organic Process Research & Development* 2005, 9, 348-355.

[10]   D. Kashchiev, G. M. van Rosmalen *Crystal Research and Technology* 2003, 38, 555-574.

[11]   M. Elwenspoek *Applied Physics A.* 1986, 41, 123.

[12]   N. A. Mitchell, P. J. Frawley, C. T. Ó'Ciardhá *Journal of Crystal Growth* 2011, 321, 91-99.

3 Electrospray crystallization for high quality submicron-sized crystals[1]

Nano- and submicron sized crystals are too small to contain inclusions and are therefore expected to have a higher internal quality compared to conventionally sized particles (several tens to hundreds of microns). Using electrospray crystallization, nano- and submicron-sized crystals can be easily produced. With the aid of electrospray crystallization a mist of ultra-fine solution droplets is generated and the subsequent solvent evaporation leads to crystallization of submicron-sized crystals. Using RDX solutions in acetone the conditions for a stable and continuous jet were established. At relatively small nozzle diameters and relatively low potential differences hollow spheres of RDX crystals were observed. At higher nozzle diameter and potential difference and in the region of a continuous jet, RDX crystals with an average size of around 400 nm could be produced. In order to test the quality of the submicron sized energetic material, impact and friction sensitivity tests were carried out. The test results show that the submicron-sized product had reduced friction sensitivity, indicating a higher internal quality of the crystalline product.

3.1 Introduction

The product quality of crystalline materials is determined by the crystallization process applied to produce these materials. The crystalline product quality is in turn determined by the crystal size distribution, kind of solid state, morphology, purity and internal defects. There are several methods to optimize the crystallization conditions in conventional crystallization processes in order to arrive at a certain quality of the crystalline product. Like using specific geometry with low cooling rate can end up in producing 1 mm crystals with narrow crystal size distribution [1].

Inclusions, dislocations and point, line or surface defects are internal defects [1]. For energetic materials it is thought that the initiation of an explosion can be caused by an unintentional shock wave hitting a defect upon its propagation through a crystal. It has been demonstrated that the higher the product quality of a solid energetic material, the less sensitive a plastic bonded explosive containing this energetic material becomes [2]. A reduced sensitivity means that the detonation threshold is higher, which would prevent unintentional detonations, therefore these explosives are safer to handle. For the energetic material RDX, for instance, a reduced cooling rate in batch cooling crystallizations resulted in RDX crystals with decreased inclusion content [3]. Therefore, optimizing conventional crystallization conditions is a good approach to achieve lower internal defect densities and thus less sensitive energetic materials.

Another approach is to greatly reduce the crystal size. Since inclusions are relatively large, submicron-sized crystals are believed to contain a smaller amount of inclusions. Crystal defects like dislocations usually originate from inclusions and therefore a much lower overall defect content is expected in nano- and submicron-sized crystals. Due to the relation of sensitivity and defect content of energetic compounds, the product quality can be easily quantified with the help of sensitivity tests.

This chapter presents an electrospray crystallization method for producing submicron-sized crystals of the energetic compound RDX. The method combines electrospraying of an undersaturated solution and solvent evaporation from the created droplets. The extent to which submicron particles can be produced with electrospray crystallization as well as their sensitivity performance as energetic material were investigated.

3.2 Electrospray Crystallization

There are several techniques for producing nanoparticles. Conventional methods like milling or pyrolysis and advanced methods like using thermal plasma [4], rapid expansion of supercritical solutions [5], or spray drying [6] are often used for nanoparticle production.

Electrospray crystallization is one of the advanced methods to achieve nano- and submicron-sized crystals [7]. A constant potential difference is applied between a grounded plate and a metal capillary (the nozzle) through which a conductive solution is pumped. If the potential difference is sufficiently high, electrostatic forces overcome the surface tension and any flow arriving at the tip of the nozzle is directly emitted as a jet of liquid droplets from a Taylor-cone formed at the nozzle as a jet of liquid droplets [8]. Due to the potential difference and the use of a conducting solution the surface of the droplets is charged. The surface charge density is mainly determined by the potential difference.

The jet contains small droplets which are accelerated towards the grounded plate by the electric field. Upon using a sufficiently volatile solvent such as acetone, solvent evaporation occurs which increases the surface charge because of the decrease in droplet volume. As the surface charge reaches a critical value (Rayleigh limit [9]) electrostatic forces overcome the surface tension and the droplet disrupts into smaller droplets to reduce the surface charge density by creating more surface area. This disruption process is called Coulomb fission [10].

The solute concentration increases as the solvent evaporates from the droplet. At some point during this process of droplet evaporation and disruption the driving force for crystallization becomes sufficiently large for crystal nucleation and growth to occur. It is assumed that crystallization is confined to the volume of the droplet [11]. Therefore, if the droplets are sufficiently small, typically one crystal per droplet is formed. Aggregation of droplets is prevented because the droplets have surface charges of equal sign. Thus, submicron or even nano-sized crystals can be formed. These submicron crystals accumulate at the grounded surface loosing their surface charge. Figure 3-1 shows the scheme of the electrospray crystallization process and the investigated process parameters (nozzle diameter d, flow rate φ, potential difference ΔU, solution concentration c and working distance D).
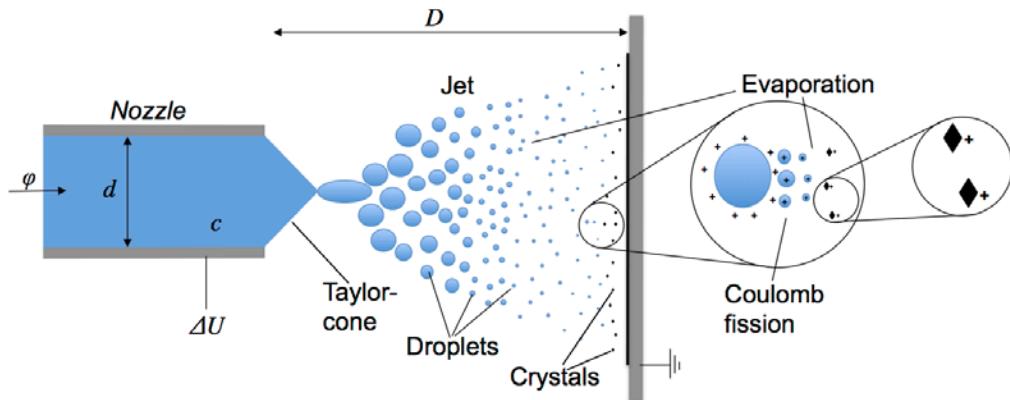
Figure 3-1. Process scheme of the electrospray crystallization. The varied operation conditions are the nozzle diameter (d), flow rate (φ), concentration (c), potential difference (ΔU) and working distance (D). During the process solvent evaporation, Coulomb fission and crystallization occur.

3.3 Experimental Methods

3.3.1 Materials

Class 2 RDX (cyclotrimethylene trinitramine) with an average size of around 400 µm was purchased from Chemring Nobel A. S., Norway. For the electrospray crystallization different solution concentrations were prepared with 99.8 % acetone purchased from Merck. Care was taken to choose materials in the device that withstand the exposure to acetone.

3.3.2 Single nozzle electrospray crystallization setup

The electrospray crystallization setup (see Figure 3-2) consisted of an Aitecs SEP-10S Syringe Pump with a 50 mL plastic syringe. A Wallis ±10 kV DC power supply was used to provide the potential difference ΔU between the tip of the nozzle and the grounded plate which were separated at a working distance D. The pump and a Festo 6x1 pneumatic tube were used to transport the solution with concentration c to the nozzle with a certain flow rate φ. Seven different nozzles (EFD, USA) were used for the experiments. All of them had the same length (25.4 mm) but the inner diameter d varied (0.1524, 0.254, 0.3302, 0.4064, 0.508, 0.5842 and 1.3716 mm, referred to in the text as respectively the 0.15,

0.25, 0.33, 0.4, 0.51, 0.58 and 1.37 mm nozzle for convenience). The experiments were performed at room temperature.

3.3.3 Multiple nozzle electrospray crystallization setup

Multiple nozzles have the advantage that higher production rates can be achieved. An eight-nozzle system was used with a Meredos TL-EAD peristaltic pump in order to have an equal distribution of the solution flow over the nozzles (Figure 3-2). The rest of the setup was similar to the single nozzle setup. The experiments were performed at room temperature.
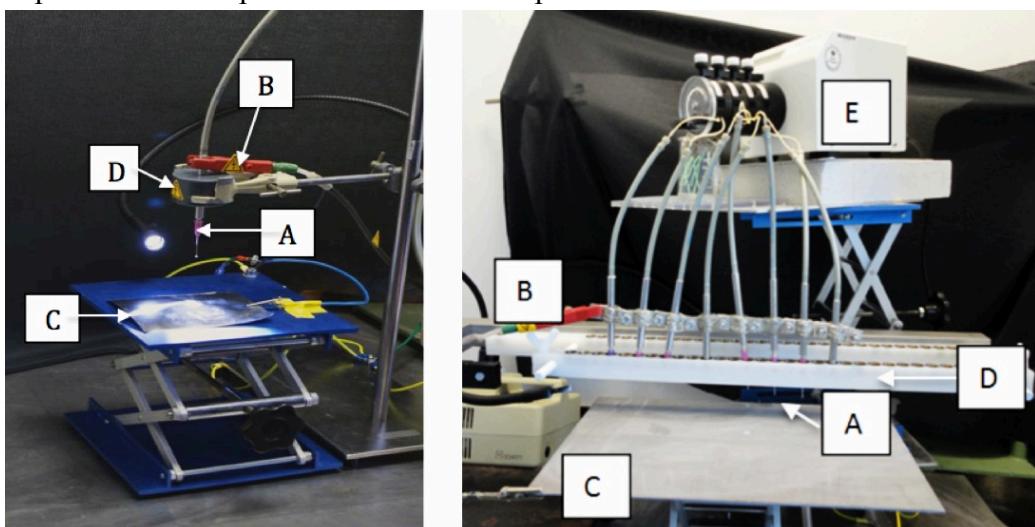
Figure 3-2. The single nozzle electrospray crystallization setup on the left and the eight-nozzle experimental set-up on the right showing the capillary nozzle (A), high voltage connectors (B), metal grounded plate on which the particles are collected (C), the nozzle holders (D) and the Meredos TL-EAD peristaltic pump (E).

3.3.4 Characterization tests

For morphological and size characterization of the crystalline samples a Philips XL30 FEG scanning electron microscope was applied. Typical instrument settings of the electron beam were 2 kV. Samples were investigated "as is", without any further treatment. Only low electron beam energies were used since energies higher than 2 kV at higher magnifications resulted in decomposition of the energetic materials.

The BAM Fallhammer and Friction Apparatus tests are the recommended test methods in the UN-recommendations for the transport of dangerous goods [12]. For the impact sensitivity test a BAM Fallhammer device was used (according to the international guidelines EC A.14 and UN 3(a)(ii)) [12]. The temperature during the test was 23 °C. The volume of the submicron RDX sample was approximately 40 mm^3 and the drop weight was 5 kg. During the test the drop height was decreased from 50 cm until initiation of the sample did not occur for 6 times in series.

The sensitivity to friction was determined by a BAM Friction Apparatus (according to the international guidelines EC A.14 and UN 3(b)(i) [12]. The sample is placed on a roughened porcelain plate, which is rigidly attached to the sliding carriage of the friction apparatus. A cylindrical porcelain peg is placed on top of the sample. The porcelain plate can move forward and backward under the porcelain peg. The smallest load of the peg, which causes deflagration, crackling or explosion of the test sample at least once in six consecutive trials is the outcome of the friction sensitivity test. The quantity of the test sample is 10 mm^3.

3.4 Results and Discussion

3.4.1 Single nozzle electrospray crystallization operation conditions

For RDX, acetone is a favorable solvent to use since RDX crystals from acetone have a compact shape [13]. Moreover, acetone is a (slightly) conductive solvent, which allows to electrospray the solution. Furthermore, acetone has a high vapor pressure, resulting in a relatively high evaporation rate during electrospray crystallization.

The first goal was to find the process conditions leading to the formation of a continuous jet in the single nozzle setup. A continuous jet is established when there is a stationary droplet emission from the nozzle without any interruption. Then, the effect of the five process variables was studied: the flow rate φ, potential difference ΔU, working distance D, nozzle diameter d and the solution concentration c.

Using a solution with a concentration of 20.8 mg mL^{-1} RDX a continuous jet was observed at a potential difference of +4.8 kV, a nozzle diameter of 0.58 mm, a working distance of 25 mm and a flow rate of 2.8 mL h^{-1}. This is taken as

our reference experiment for studying the operation conditions as well as the crystalline product characteristics.

Flow rate

A continuous jet was observed at flow rates between 1 mL h^{-1} and 5 mL h^{-1} and otherwise equal settings compared to the standard experiment. At flow rates below 1 mL h^{-1} the solution was only intermittently sprayed from the nozzle. Apparently the flow rate then is too small to achieve a steady-state electrospray of droplets from the tip. Flow rates higher than 5 mL h^{-1} resulted in formation of an unwanted continuous flow of solution from the tip without jet formation: The electrospraying cannot keep up with the accumulation of solution at the tip due to the relatively high flow rate.

Potential difference

A continuous jet is obtained when the potential difference is varied between 3.8 and 4.9 kV while using the standard settings for the other variables. Applying a potential difference above 4.9 kV resulted in formation of multiple jets. Three jets were observed when using a potential difference of 6.2 kV with an RDX solution of 20.8 mg mL^{-1}, a working distance of 25 mm and a flow rate of 2.8 mL h^{-1}. Multiple jets are caused by the formation of multiple Taylor cones. These multiple Taylor cones form because of the extremely high charge density at the nozzle tip.

Figure 3-3 shows the minimum and maximum potential difference for obtaining a continuous jet for different working distances using a RDX solution concentration of 20.8 mg mL^{-1}, a flow rate of 2.8 mL h^{-1} and a nozzle diameter of 0.58 mm. The area between the two lines indicates the region for obtaining a continuous jet.

Working distance

Figure 3-3 also shows that at larger working distances, a higher potential difference is needed to obtain a continuous jet. The working distance between the nozzle tip and the grounded plate was varied between 5 and 70 mm. Working distances smaller than 5 mm were not tested since unwanted sparks might occur. At working distances smaller than 10 mm solvent evaporation of the droplets travelling from tip to grounded plate was only partial and the remaining acetone evaporated on the grounded plate. That is unwanted since crystallization then partly occurs at the grounded plate. At working distances above 35 mm, the developed jet was continuous but the droplets were not

homogeneously distributed in time and space within the jet, i. e., it was observed that after a time intervals of several seconds a part of the flow was emitted in relatively large droplets from the nozzle tip, which travelled at the outer side of the jet to the ground plate. These droplets often partly evaporated on the collector plate.
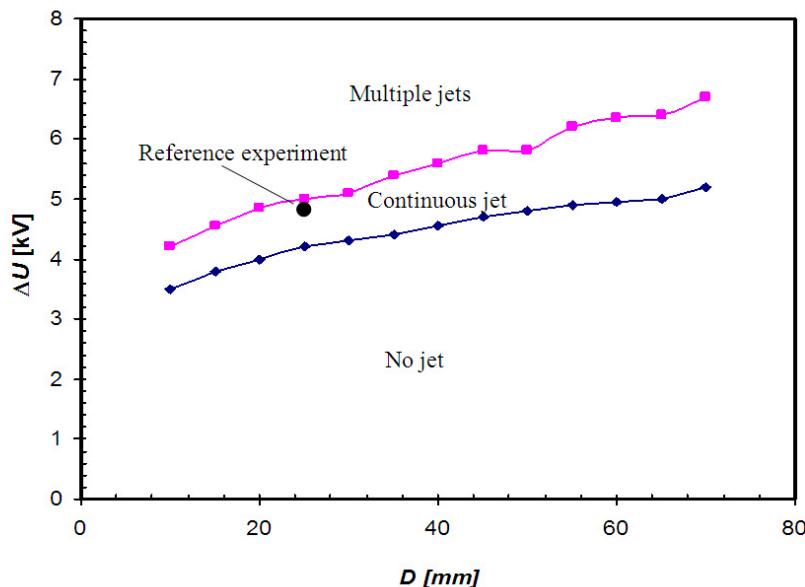
Figure 3-3. The potential difference ΔU and working distance D to obtain a stable and continuous single jet using a c=20.8 mg mL^{-1} RDX solution in acetone, a nozzle diameter d=0.4 mm, and a flow rate φ=2.8 mL h^{-1}. The upper line indicates the potential difference above which multiple jets were obtained; the lower line indicates the potential difference below which intermittently sprays were emitted from the nozzle tip. The area between the lines: region for continuous jet formation. Black point: conditions of the reference experiment.

Nozzle diameter
The minimum and maximum potential difference for the formation of a single continuous jet were determined for seven different nozzle diameters (Figure 3-4). For the concentration and flow rate the standard values were used, while 35 mm was chosen for the working distance since that was the upper limit below which no dripping occurred. A larger nozzle diameter demanded a higher potential difference in order to obtain a continuous jet.
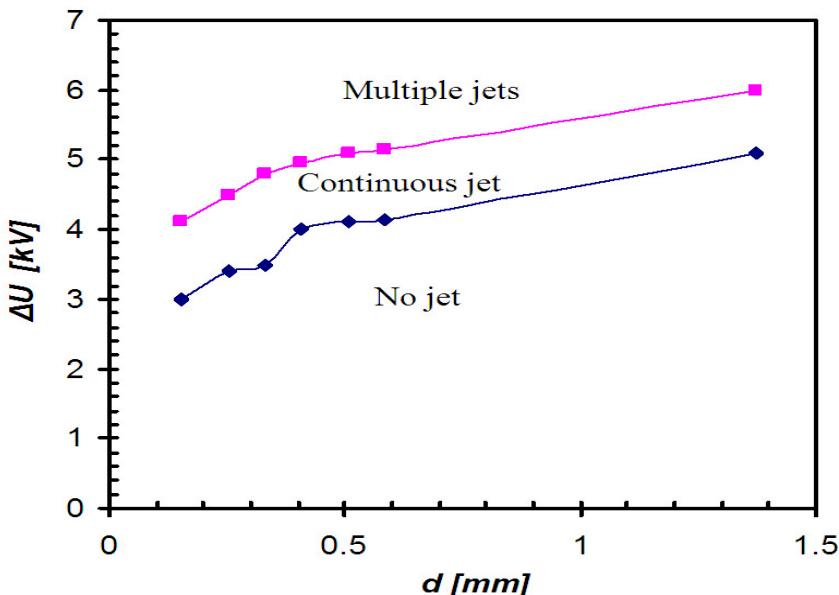
Figure 3-4. The minimum and maximum potential differences ΔU for obtaining a single continuous jet as a function of the nozzle diameter d at a working distance D=35 mm, concentration c=20.8 mg mL^{-1} and flow rate φ=2.8 mL h^{-1}. In the region between the lines a continuous jet was formed.

Concentration

While using the standard settings for the other variables, decreasing the RDX concentration did not affect the continuous jet formation: For concentrations between 2 and 20.8 mg mL^{-1} a continuous jet was formed. However, increasing the concentration led to unwanted crystallization at the nozzle tip. This eventually led to blocking of the nozzle. Using a concentration of 24.9 mg mL^{-1}, crystals were growing on the nozzle tip, which blocked the flow within 15 minutes. Using a solution close to the supersaturated concentration (41.6 mg mL^{-1} RDX) caused the blocking to occur within 40 s.

3.4.2 Product characterization

For checking the product size and shape, scanning electron microscopy was used. The resulting submicron-sized crystals of the standard experiment are shown in Figure 3-5. The produced crystals have a spherical shape and a size ranging from 200 to 600 nm. No extensive agglomeration was observed, which indicates that under these conditions droplets are not aggregating and the small

droplet volume causes the nucleation of only a single RDX crystal per droplet. This single crystal per droplet then consumes the dissolved RDX by growth upon further evaporation of the acetone in the droplet. A crystal size of 400 nm indicates that the solution droplet from which the crystal is formed is around 1.77 μm. These experiments show that electrospray crystallization can be used to obtain submicron crystals of RDX.
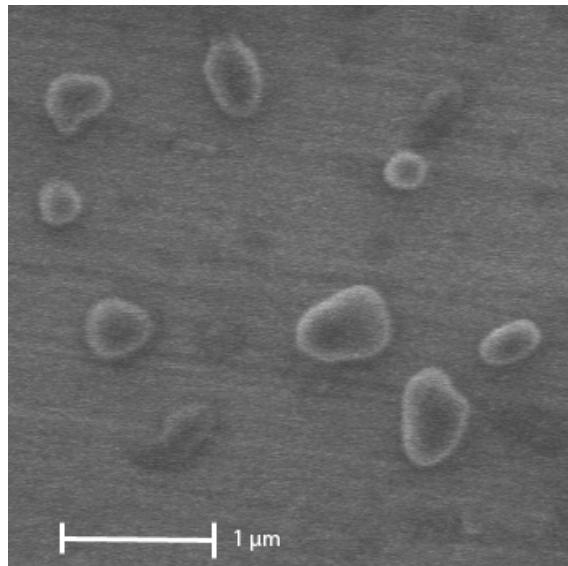
Figure 3-5. 200-600 nm sized RDX crystals from the standard electrospray crystallization experiment using the 0.58 mm nozzle at a potential difference of +4.8 kV, a working distance of 25 mm, a solution concentration of 20.8 mg mL^{-1} and a flow rate of 2.8 mL h^{-1}.

3.4.2.1 Hollow-sphere agglomerates

When the potential difference was decreased to below 4.5 kV or lower compared to the standard experiment, a considerable amount of hollow spheres of multiple agglomerated RDX crystals were observed in the crystalline material (Figure 3-6). These hollow spheres probably develop due to the combination of a relatively low potential difference and a relatively high RDX concentration. Under these conditions relatively large droplets might form due to a decreased surface charge, less coulomb fission and more aggregation of droplets. Due to the large concentration these droplets become supersaturated relatively soon after being sprayed from the nozzle. Then multiple crystals can form at the surface of the droplet, which develop in a shell of connected elongated crystals

of which the internal is empty. An alternative explanation for forming similar particles can be found elsewhere [14].
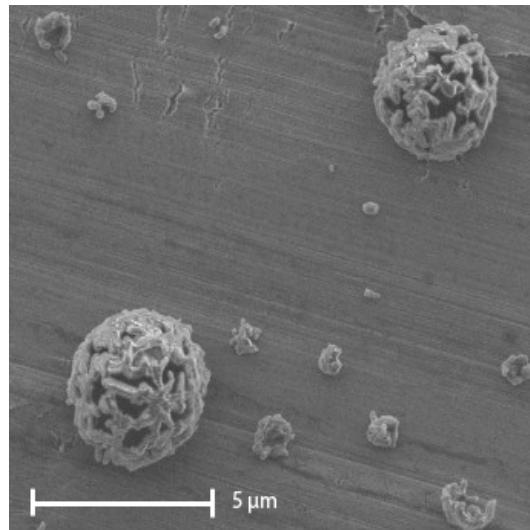
Figure 3-6. Hollow spheres of RDX crystals produced with the 0.58 mm nozzle at a potential difference of 4.2 kV, 25 mm working distance, a solution concentration of 20.8 mg mL^{-1} and a flow rate of 2.8 mL h^{-1}. Typically the size of these spheres was around 4 μm.

At a RDX concentration c = 20.8 mg mL^{-1}, these hollow-sphere agglomerates could be prevented by using a combination of a high potential difference ($\Delta U \geq$+4.5kV) and a large nozzle diameter ($d \geq$0.58 mm). These boundary values for nozzle diameter and potential difference decrease when lower concentrations are used. This indicates that also decreasing the solution concentration can prevent the presence of these hollow-sphere agglomerates in the product.

In case the potential difference is higher than +4.5kV, the hollow spheres were not observed, also above the potential difference threshold for a continuous single jet. At higher potential differences the charge density on the droplet surface is larger, which might result in smaller droplet sizes after Coulomb fission. In smaller droplets the chance of forming only one crystal is higher. Moreover, at higher surface charges the aggregation of droplets is decreased.

With 20.8 mg mL^{-1} concentration, hollow spheres and agglomerates can be observed in case the potential difference is rather low. In Figure 3-3 it can be seen that the operation window for potential difference is around 1 kV for obtaining a continuous jet. According to our measurements with this relatively high concentration hollow spheres can be observed in the lower region of this window.

The formation of these hollow-sphere agglomerates makes the operation window for submicron-sized RDX production without agglomerates produced from a continuous jet rather small. To obtain submicron-sized RDX crystals from a continuous jet, a low concentration ($c{\leq}20.8$ mg mL^{-1}) and a high potential difference ($\Delta U{\geq}+4.5$kV) are recommended with a nozzle diameter of $d{\geq}0.58$ mm at a working distance of $D{\leq}35$mm and a flow rate of 2.8 mL h^{-1}.

3.4.2.2 Crystal growth rate during electrospray crystallization

The average growth rate in the electrospray crystallization process was calculated by dividing the product crystal size (400 nm) with the estimated time the solvent needed for evaporation. From the experiments with different working distances it was observed that working distances below 10 mm resulted in acetone evaporation partly on the collector plate. Therefore 10 mm was chosen as the working distance for calculating the time for solvent evaporation. The actual time of growth of the nanoparticle is smaller since the nanoparticle is formed somewhere along the path from nozzle to plate. In order to calculate the time the droplet velocity is also needed. At a voltage of 5 kV in an electrospraying process the droplet velocity of acetone was reported to be 10.8 m s^{-1} [15]. The time the droplet is travelling was thus estimated to be 1.08 ms. Thus, the estimated growth rate was 370 µm s^{-1}. Compared with the growth rate of RDX in cooling crystallization (see Figure 2-7), electrospray crystallization results in at least 6000 times higher growth rates, which seems very large.

3.4.3 Multiple nozzle electrospray crystallization: product sensitivity

To check the expected product quality improvement, impact and friction sensitivity tests were performed. For these tests at least 1 g of material was needed, and therefore the multiple nozzle setup was used to increase the production rate. The production rate with the eight-nozzle setup was 84 mg h^{-1} using 24.9 mg mL^{-1} RDX at a flow rate of 1.8 mL h^{-1}.

With the produced samples impact sensitivity tests were carried out. When the drop height was set at 15 cm with a 5 kg drop weight (7.5 J impact energy) there was no ignition using the produced submicron-sized RDX. Ignition only occurred when the height was set to 20 cm (10 J). The conventional RDX needed 5 J energy for ignition which is half the energy measured for the submicron-sized RDX.

Friction sensitivity tests were performed as well with the submicron-sized RDX. Tests were carried out first at the highest possible load (360 N) to check the friction sensitivity of the 400 nm RDX. For this energetic material even with this high load no ignition occurred. The conventional RDX needed 144 N load for ignition. Apparently, the friction sensitivity is much lower for the submicron-sized energetic particles than for the conventionally sized explosive crystals. These sensitivity tests might indicate that the submicron-sized crystals contain fewer defects and therefore have higher internal quality.

Table 1. Impact and the friction sensitivity of 400 nm RDX compared with conventionally sized RDX

	Impact sensitivity (J)	Friction sensitivity (N)
Conventional RDX	**5**	**144**
Submicron sized RDX	**10**	**>360**

3.5 Conclusions

Submicron-sized crystals of RDX can be produced using electrospray crystallization. The sensitivity of samples having an average size of around 400 nm for RDX was tested. The samples were remarkably insensitive to friction stimuli while an insignificant difference for the impact sensitivity was observed. The operation window to establish a continuous jet and produce submicron-sized crystals is relatively narrow, but experimentally feasible. A new process design could optimize this process to obtain higher yields and offer improved process control.

References

[1]   J. W. Mullin *Crystallisation,* 4th Edition Butterworth-Heinemann Ltd.: Oxford, 2001.

[2]   A. E. D. M. van der Heijden, Y. L. M. Creyghton, E. Marino, R. H. B. Bouma, J. H. G. Scholtes, W. Duvalois *Propellants, Explosives, Pyrotechnics* 2008, 33, 25-32.

[3]   J.-W. Kim, J.-K. Kim, H.-S. Kim, K.-K. Koo *Crystal Growth & Design* 2009, 9, 2700-2706.

[4]   N. Rao, S. Girshick, J. Heberlein, P. McMurry, S. Jones, D. Hansen, B. Micheel *Plasma Chemistry and Plasma Processing* 1995, 15, 581-606.

[5]   V. Stepanov, L. N. Krasnoperov, I. B. Elkina, X. Zhang *Propellants, Explosives, Pyrotechnics* 2005, 30, 178-183.

[6]   H. Qiu, V. Stepanov, A. R. Di Stasio, T. Chou, W. Y. Lee *Journal of Hazardous Materials* 2011, 185, 489–493.

[7]   A. Jaworek *Powder Technology* 2007, 176, 18-35.

[8]   G. I. Taylor *Proceedings of the Royal Society of London Series A* 1964, 280, 383.

[9]   L. Rayleigh *Philosophical Magazine* 1882, 14, 184–186.

[10]   K. Suzuki, H. Matsumoto, M. Minagawa, M. Kimura, A. Tanioka *Polymer Journal* 2007, 39, 1128-1134.

[11]   E. Revalor, Z. Hammadi, J. P. Astier, R. Grossier, E. Garcia, C. Hoff, K. Furuta, T. Okutsu, R. Morin, S. Veesler *Journal of Crystal Growth* 2010, 312, 939-946.

[12]   R. Meyer, J. Köhler, A. Homburg *Explosives,* 6th Edition Wiley-VCH: Weinheim, 2007.

[13]   J. H. ter Horst, R. M. Geertman, A. E. D. M. van der Heijden, G. M. van Rosmalen *Journal of Crystal Growth* 1999, 198/199, 773-779.

[14]   Y. Jiang *Journal of The Electrochemical Society* 2007, 154, E107-E111.

[15]   H. Oh, K. Kim, S. Kim *Journal of Aerosol Science* 2008, 39, 801-813.

4 Electrospray crystallization for nano-sized pharmaceuticals with improved properties[2]

Many new pharmaceuticals have low water solubility, hampering their pharmaceutical activity upon administering. One approach to increase solution concentrations during drug administration is to increase the surface-to-volume ratio by decreasing the crystal product size. Submicron-sized niflumic acid crystals were produced by electrospray crystallization. Electrospray crystallization uses a high potential difference to create a mist of ultrafine charged solution droplets. The subsequent total solvent evaporation and droplet disruption process lead to crystallization of submicron-sized crystals. For concentrations well below the solubility concentration while using small nozzle diameters, niflumic acid crystals with a size of 200-800 nm were produced. In the absence of excipients, for the submicron-sized niflumic acid no significantly different dissolution profile compared to the conventional one was measured. However, if excipients were added, the dissolution rate for the submicron-sized product increases substantially in stimulated gastric juice, while that of the conventional product increased slightly. Probably the excipients avoid the aggregation of the hydrophobic submicron particles in the low pH environment.

4.1 Introduction

The interest in submicron-sized particles has emerged both in industry and scientific research in the last decade [1-3]. Nano- and submicron-sized crystals may have different chemical and physical properties, because the particle surface properties dominate those of the particle volume. However, they can also have beneficial properties because of their small volume. Submicron-sized crystals are too small to contain inclusions of which the size is usually in the micron size range. It was shown previously that submicron-sized crystals have improved properties that indicate a higher internal quality (less inclusions and reduced dislocations) compared to conventionally sized particles of several tens to hundreds of microns [4].

Since nearly half of the new active pharmaceutical ingredients (APIs) being identified are either insoluble or poorly soluble in water, solving bioavailability problems is a major challenge for the pharmaceutical industry [5]. Previously, the focus of this field was on the solution complexation [6] and amorphization [7] possibilities to increase the dissolution rate [8-11]. Since smaller particles have a much higher specific surface area, an increase in the dissolution rate (the amount of drug substance that dissolves per unit time) is expected at the same driving force for dissolution. An increase in the solubility might be expected as well, since according to the Ostwald-Freundlich relation, smaller particles have increased solubility [12]. However, an efficient, cost-effective and simple technique to produce submicron particles of organic pharmaceutical compounds is still lacking.

Niflumic acid (NIF) is an important anti-inflammatory drug and also has a weak analgesic effect [13]. It is primarily used to treat different forms of rheumatism, like rheumatoid arthritis or arthrosis, and to cure other inflammatory diseases [14]. However, its poor aqueous solubility [15] and dissolution rate [16] are disadvantages. To achieve optimal pharmacodynamic properties such as a rapid onset of the drug effect, fast dissolution is important for this type of drug.

The focus of this chapter is therefore the preparation of submicron-sized NIF crystals in order to achieve fast dissolution. Electrospray crystallization is introduced as a potentially efficient, cost-effective and simple method for the production of such submicron-sized NIF crystals. The changes in dissolution profile as well as the product morphology and structural properties of the produced crystals are investigated in this chapter.

4.2 Experimental Methods

4.2.1 Materials

Niflumic acid (2-[[3-(trifluoromethyl)phenyl]amino]-3-pyridinecarboxylic acid) with a mean size of around 80 μm (G. Richter Pharmaceutical Factory, Budapest, Hungary), β-D-Mannitol (Hungaropharma Plc., Budapest, Hungary) and Poloxamer 188 (Polyethylene-Polypropylene Glycol, Fluka, Ljubljana, Slovenia) were used as received. For the electrospray crystallization process different solution concentrations were prepared with 99.8 % acetone purchased from Merck. During the experiments only acetone was used as a solvent, thus the solvent effects were not investigated. Care was taken to choose materials in the device that withstand the exposure to acetone.

4.2.2 Single nozzle electrospray crystallization setup

The single nozzle electrospray crystallization setup was used to investigate the effect of the operating conditions and process parameters. This setup (see Figure 3-2) consisted of an Aitecs SEP-10S Syringe Pump with a 50 mL plastic syringe. A Wallis ±10 kV DC power supply was used in positive DC mode to provide the potential difference ΔU between the tip of the nozzle and the grounded plate, which were separated at a working distance D. The pump and a Festo 6x1 pneumatic tube were used to transport the solution with concentration c to the nozzle with a certain flow rate φ. Nozzles (EFD, USA) with a length of 25.4 mm varied in the inner diameter d (0.1524, 0.254, 0.3302, 0.4064, 0.508, 0.5842 and 1.3716 mm, referred to in the text as respectively the 0.15, 0.25, 0.33, 0.4, 0.51, 0.58 and 1.37 mm nozzle for convenience). It was visually checked whether the electrospray setup was operated in cone-jet mode at specific sets of process parameters.

4.2.3 Multiple nozzle electrospray crystallization setup

The use of multiple nozzle setup has the advantage of higher production rates. An eight-nozzle system was used with a Meredos TL-EAD peristaltic pump in order to have an equal distribution of the solution flow over the nozzles (Figure 3-2). Otherwise the setup was similar to the single nozzle setup.

4.2.4 Characterization of the product

For morphological and size characterization of the crystalline samples a Philips XL30 FEG and a FEI Nova NanoSEM 650 scanning electron microscopes (SEM) were applied. Typical settings of instrument were 1-2 kV electron beam and 3-10 mm working distance. The samples were investigated without applying a conductive coating. A relatively low acceleration voltage was used in order to prevent extensive charging of the particles.

Differential scanning calorimetry (DSC) was employed to investigate the melting behavior of the NIF samples and the crystallinity as well. A thermal analysis system with the STAR^e thermal analysis program V9.1 (Mettler Inc., Schwerzenbach, Switzerland) was applied to characterize the thermal behavior of the products. The DSC measurements were done with 2–5 mg of NIF in the temperature range between 25 °C and 300 °C. The heating rate was 5 °C min^{-1}. Argon was used as carrier gas at a flow rate of 10 L h^{-1} during the DSC investigation.

X-ray diffraction (XRD) was carried out in order to determine the crystalline form of the produced materials and to examine the transition between amorphous and crystalline phase. Samples were measured with a Bruker D8 Advance diffractometer. The XRD patterns were recorded in Bragg-Brentano geometry. Data collection was carried out at room temperature using monochromatic Cu Kα1 radiation (λ = 0.154060 nm) in the 2θ region between 10° and 120°, step size 0.02 degrees 2θ. The sample of about 10 milligrams was directly deposited on a zero background holder (Si single crystal <510> wafer) and placed into the XRD directly after production. The record program of the pattern was relatively fast, it lasted for 160 seconds. Diffraction patterns were recorded 5 minutes, 20 minutes and 75 minutes after production. Data evaluation was done with the Bruker program "EVA".

Solubility and dissolution rate measurements
The solubility measurements were performed in a phosphate buffer solution (pH 1.2 ± 0.1) at 37 ± 0.5 ºC. 25 mg of NIF was dispersed in 5 mL medium and stirred for 12 hours at 37 °C. After filtration the dissolved drug amount in the medium was determined by an ATI-Unicam UV2-100 UV/Vis spectrophotometer.

The dissolution profile of product samples containing equal amounts of drug (14 mg of NIF according to its therapeutic dose) was determined according to the paddle method [17]. A phosphate buffer solution (50 mL, pH 1.2 ± 0.1) at 37

± 0.5 ºC was used as a dissolution medium and the rotation speed of the paddles was 100 rpm. At time intervals 2 mL solution samples were withdrawn and filtered (cut-off 0.2 μm, Minisart SRP 25, Sartorius, Germany) and the amount of dissolved drug was determined by an ATI-Unicam UV2-100 UV/Vis spectrophotometer. It is common practice to replace the withdrawn samples with fresh medium.   Dissolution behavior was determined in the presence and absence of excipients both for conventional and submicron-sized NIF. D-Mannitol and Poloxamer 188 were used as excipients to help the de-aggregation and increase the wettability of the NIF crystals. D-Mannitol acts as a carrier, which provides the homogeneous distribution of the NIF crystals, while Poloxamer 188 helps as a stabilizer by wetting to arrest the aggregation of the drug. Table 4-1 shows the ratio of the excipients added to the drug. The physical mixtures were prepared using a Turbula mixer for 10 minutes as suggested by the manufacturer (Willy A. Bachofen Machinenfabrik, Switzerland). A homogeneous distribution of the NIF and the excipients was achieved by this mixing method without kneading or hard mechanical effects.

Table 4-1. The ratio of the niflumic acid (NIF) and the additives in the samples based on weight.

Product	NIF	Mannitol	Poloxamer
Conventional NIF	**1**	**-**	**-**
Conventional NIF with excipients	**1**	**2.5**	**0.25**
Submicron-sized NIF	**1**	**-**	**-**
Submicron-sized NIF with excipients	**1**	**2.5**	**0.25**

4.3 Results and Discussion

First, the electrospray crystallization process parameters are investigated for operation in a cone-jet mode. Next, the process parameters for the desired submicron product are determined using the single nozzle electrospray setup. In the last part the product is characterized and its dissolution profile is determined.

4.3.1 Electrospray Crystallization

To exploit the relations between the process parameters and the crystalline product quality (e.g., size), we need to understand the crystallization process during electrospray crystallization (Figure 3-1). A constant potential difference is applied between a grounded plate and a metal capillary (the nozzle), through which a conductive solution is pumped at a certain flow rate. If the potential difference is sufficiently high, electrostatic forces overcome the surface tension and a jet of liquid is emitted from the Taylor cone, formed at the nozzle [18]. After some distance from the nozzle, the jet becomes unstable and breaks into droplets, which are accelerated towards the grounded plate by the electric field. Due to the potential difference and the use of a conducting solution the surface of the droplets is charged. The surface charge density is mainly determined by the potential difference, the conductivity of the solution and the nozzle diameter. Coalescence of droplets is prevented because of the unipolar charge [19], which is important for preventing agglomeration and enables production of submicron crystals. Upon using a sufficiently volatile solvent such as acetone, solvent evaporation from the droplet occurs, which increases the surface charge density because of the decrease in droplet volume and area. As the surface charge reaches a critical value (Rayleigh limit [20]) electrostatic forces overcome the surface tension and the droplet disrupts into smaller droplets to reduce the surface charge density by creating more surface area. This disruption process is called Coulomb fission [21].

There are different operating modes of electrospray process depending on the potential difference and flow rate. When operated in the cone-jet mode, a stable jet is developed that consists of highly charged small solution droplets, from which monodisperse, and submicron-sized particles can be formed [22].

The solute concentration increases as the solvent evaporates from the droplet. At some point during this process of droplet evaporation and disruption, the driving force for crystallization becomes sufficiently large for crystal nucleation

and growth to occur. The micron-sized droplets contain a small quantity of solute, so the produced crystals are in the sub-micrometer range. Thus, submicron- or even nano-sized crystals can be formed upon total evaporation of the solvent. Aggregation of formed crystals during spraying is prevented since the crystals also have charges of equal sign. These charged submicron crystals accumulate at the grounded surface where they lose their surface charge.

Five exploitable process parameters were identified for this study: nozzle diameter (d), flow rate (φ), potential difference (ΔU), initial solute concentration (c) and working distance (D - the distance between the nozzle tip and the grounded plate). All the experiments were performed with solutions at room temperature, but the temperature of droplets in the jet could be lower due to the cooling effect of the evaporation of the acetone.

4.3.2 Effect of process parameters on jet formation

The first step was to find the process parameters for the cone-jet mode. For this purpose the single nozzle electrospray setup was used. The solubility of NIF in acetone was determined to be approximately 110 mg mL^{-1} at room temperature. Solute concentrations close to the solubility caused nozzle blockage by the encrustation of crystals on the nozzle tip. Therefore a low NIF concentration (20 mg mL^{-1}) was used.

Cone-jet mode is established if a stationary droplet emission from the nozzle takes place. This is a function of the nozzle diameter d, working distance D, flow rate φ, the potential difference ΔU and the solution properties (conductivity, surface tension and solute concentration c). There is a minimum threshold potential difference for establishing cone-jet mode (Figure 4-1). For example, using a NIF concentration of 20 mg mL^{-1} in acetone, a nozzle diameter of 0.33 mm and a flow rate of 1.8 mL h^{-1}, a minimum potential difference of 3.3 kV is needed to enter the cone-jet mode at 20 mm working distance. Below that threshold no jet or only an intermittent jet was formed.

Above the minimum threshold voltage, a single continuous jet is formed (cone-jet mode) up to a certain maximum threshold potential difference (+4.8 kV using of 20 mg mL^{-1} solution concentration in acetone, a nozzle diameter of 0.33 mm and a flow rate of 1.8 mL h^{-1} and 20 mm working distance). Above this maximum threshold, multiple Taylor-cones are formed due to the large surface charge density at the nozzle tip, and with it multiple jets are formed, each originating from an individual Taylor- cone.

Figure 4-1 shows the minimum and maximum potential difference, ΔU_{min} and ΔU_{max}, for obtaining a continuous, single jet as a function of the working distances using a NIF solution concentration of 20 mg mL^{-1}, a flow rate of 1.8 mL h^{-1} and a nozzle diameter of 0.33 mm. The width of the cone-jet mode operation window was increasing with the working distance. At 10 mm working distance the operation window was around 1 kV wide, while at a working distance of 20 and 75 mm a width of respectively 1.5 and 2 kV was observed.
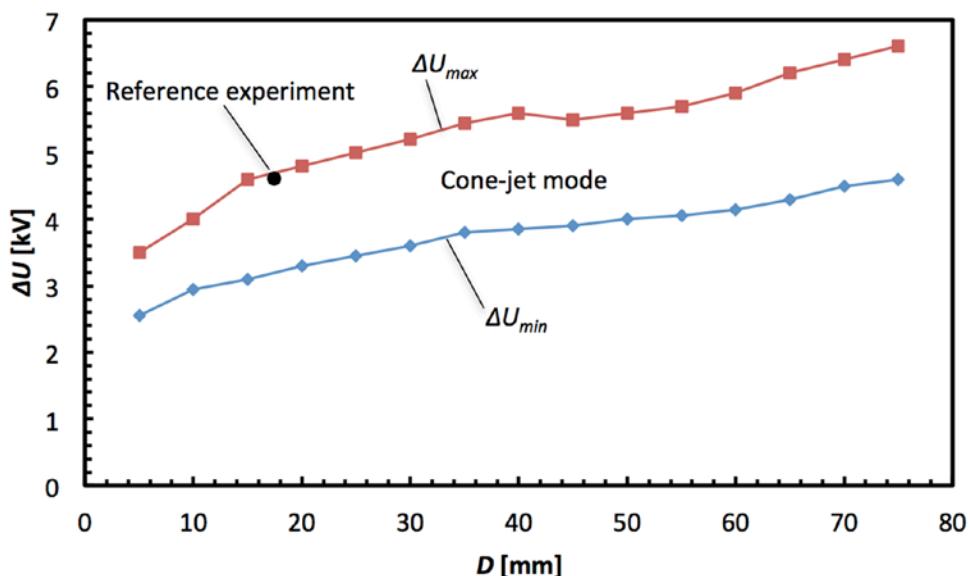
Figure 4-1. The minimum (ΔU_{min}) and maximum potential difference (ΔU_{max}) at different working distances to obtain a cone-jet mode using a NIF concentration of 20 mg mL^{-1} in acetone, a nozzle diameter of 0.33 mm and a flow rate of 1.8 mL h^{-1}. Above the upper line multiple jets were obtained, and below the lower line no jet or intermittent cone-jet mode was observed. The black point represents the reference experiment.

The solution flow rate also effects the jet formation. At a potential difference of +4.7 kV and a working distance of 17 mm a stable, single jet was observed only with a flow rate between 1.8 and 2.2 mL h^{-1}. It seems that only a very small operation window for the flow rate exists in electrospray crystallization of NIF from acetone.

Figure 4-2 shows the relation between nozzle diameter d and potential difference ΔU using a NIF concentration of 20 mg mL^{-1} in acetone at a working distance of 17 mm and a flow rate of 1.8 mL h^{-1} for cone-jet mode operation. A larger nozzle diameter demands a higher potential difference in order to obtain a

continuous jet. At a larger nozzle diameter the cone surface is larger, and thus, a higher potential difference is needed to overcome the increased total surface energy [22]. The width of the operation window for the potential difference to obtain a continuous jet was about 1.2-1.3 kV for all nozzle diameters used, except for the largest one, which was about 1.85 kV window for operation.
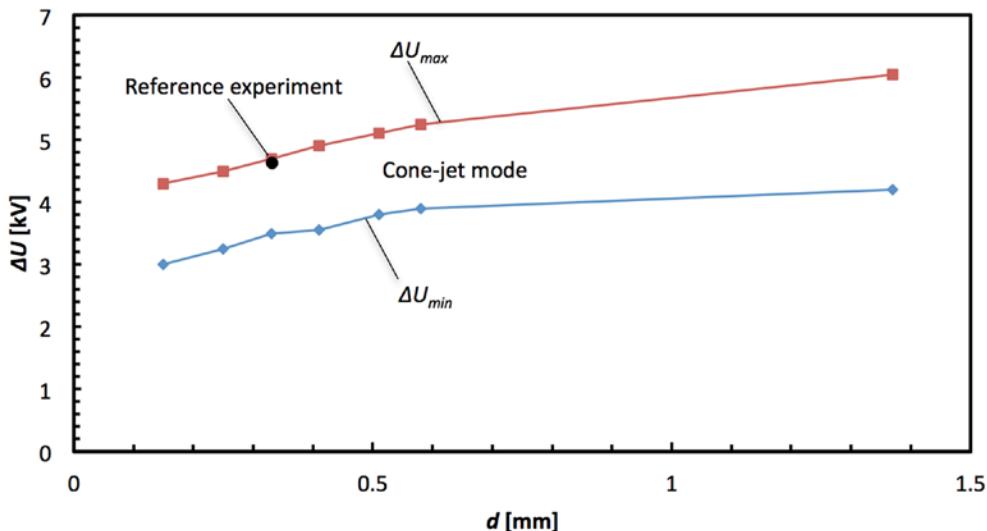
Figure 4-2. The minimum (ΔU_{min}) and maximum potential difference (ΔU_{max}) at different nozzle diameters to obtain a single jet using a concentration of 20 mg mL^{-1} NIF solution in acetone, a working distance of 17 mm and a flow rate of 1.8 mL h^{-1}. Above the upper line multiple jets were obtained, under the lower line no jets were obtained. Between the lines a single jet was obtained. The black point represents the reference experiment.

It can be concluded that the process parameters need a strict balance to obtain a cone-jet mode. The operation window is quite narrow for establishing the cone-jet mode using NIF-acetone solutions.

4.3.3 Effect of process parameters on particle characteristics

Using a solution with a NIF concentration of 20 mg mL^{-1} the cone-jet mode was observed at a potential difference of +4.7 kV, a nozzle diameter of 0.33 mm, a working distance of 17 mm and a flow rate of 1.8 mL h^{-1}. These process parameters were used to establish a reference experiment concerning product characteristics (Table 4-2).

Table 4-2. The process parameters for the reference electrospray crystallization experiment for NIF: potential difference (ΔU), working distance (D), nozzle diameter (d), concentration (c) and flow rate (φ). Using these parameters a continuous jet is formed.

ΔU [kV]	D [mm]	c [mg mL^{-1}]	d [mm]	φ [mL h^{-1}]
+4.7	17	20	0.33	1.8

The resulting submicron-sized crystals of the reference experiment are shown in Figure 4-3A. The produced crystals have a somewhat prismatic shape, while the size ranges from 200 to 800 nm and no extensive agglomeration is observed. Under these conditions, very small droplets are formed during the process and the small droplet volume causes the nucleation and growth of only a single NIF crystal per droplet. However, after the crystals were collected from the grounded plate into a petri dish, sometimes the submicron-sized crystals aggregated into 20-30 μm sized clusters (Figure 4-3B), possibly due to the strong interactions between the hydrophobic crystal surfaces of these submicron-sized crystals. After mixing the submicron-sized NIF with the excipients, these agglomerates are partially or totally disintegrated, as can be seen on Figure 4-3C of the submicron-NIF on the surface of a D-mannitol crystal. This reference experiments shows that electrospray crystallization can be used to obtain submicron-sized crystals of NIF.
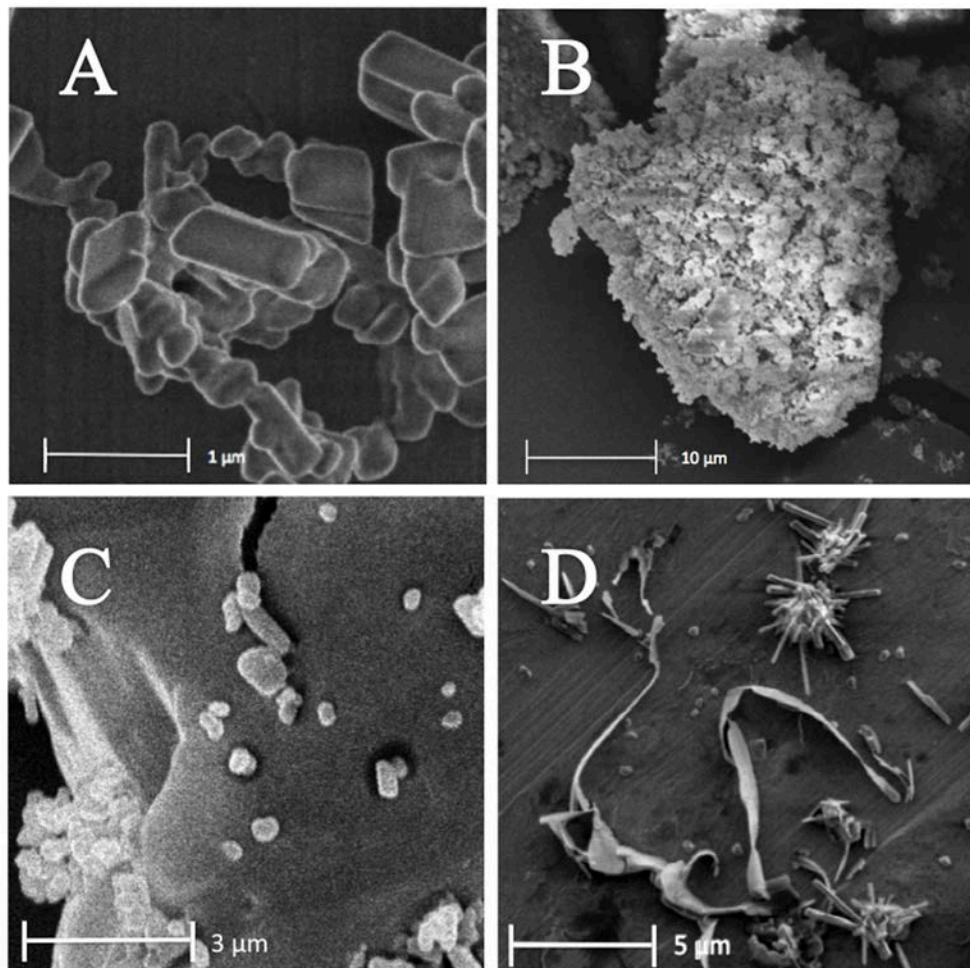
Figure 4-3. A. 200-800 nm sized NIF produced in the reference electrospray crystallization experiment (see Table 1 for the process conditions). The SEM image shows the crystals directly deposited on the grounded plate. **B.** A 30 μm NIF cluster created by the aggregation of the submicron-sized NIF crystals after removing the product from the grounded plate. **C.** Aggregated and individual submicron-sized NIF crystals on the surface of D-Mannitol after mixing. **D.** Ribbon-shaped and agglomerated needle-like crystals of NIF and agglomerates produced using the 0.41 mm nozzle at a potential difference of +4 kV, a working distance of 17 mm, a solution concentration of 25 mg mL^{-1} and a flow rate of 1.8 mL h^{-1}.

Three process parameters were identified in our system to have a major effect on the product size and tendency for agglomeration: solution concentration, nozzle diameter and the potential difference. Higher potential difference or

smaller nozzle diameter results in increased charge density of the droplets. Although it was reported that the flow rate has also significant effect on the product [22], probably due to the narrow operation window for the flow rate, in our system no significant difference was observed when the flow rate was varied within this operation window.

Concentration

The solution concentration is a main parameter in determination of the final product. It was found that at higher initial concentrations the average crystal size increased: the same droplet with a higher concentration contains more solute that can crystallize, resulting in larger crystals (Figure 4-4). This increasing size with increasing concentration coincides with previous findings of others [23].
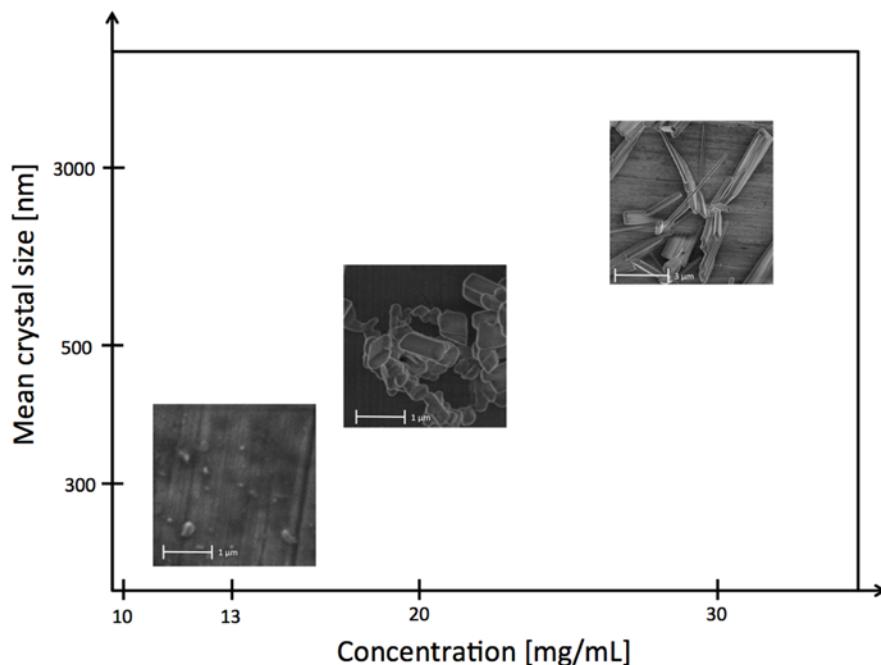
Figure 4-4. The relationship between the crystal size and shape and used solution concentration when NIF crystals are produced in electrospray crystallization. The crystal size increases with the increasing solution concentration, and the crystal shape becomes from somewhat spherical to needle-like.

The crystal morphology also depends on the initial concentration. At higher concentrations the obtained crystals were more needle-like, while at lower concentrations the crystals had somewhat spherical shape (Figure 4-4). At higher solution concentrations, crystallization occurs earlier after the droplets

have left the nozzle. In our view the most probable explanation is that crystallization occurs even before Coulomb fission of the droplets, resulting in even larger crystals. At lower concentrations, crystallization occurs later, possibly after the Coulomb fission of the droplets.

When crystallized conventionally, in general NIF has a needle-like shape [24], comparable to that in Figure 4-4 of an experiment at a higher concentration. The more compact and prismatically shaped crystals from the reference experiment indicate quite different growth behavior under these conditions.

Nozzle diameter and potential difference

Figure 4-3D shows ribbon-shaped and agglomerated needle-like crystals produced in cone-jet mode using a larger nozzle diameter of 0.41 mm and lower potential difference of 4 kV compared to the reference experiment. As it was shown in Figure 4-2, the nozzle diameter and potential difference are coupled with each other. Lower potential difference or larger diameter of the nozzle results in a lower charge density at the Taylor-cone, and therefore, at the droplet surface. At a lower surface charge Coulomb-fission is occurring later or is absent and crystallization might occur in larger droplets, resulting in these ribbon-shaped and agglomerated needle-like crystals. The optimal concentration in our system for producing submicron-sized crystals with a compact and prismatic shape was found to be around 20 mg mL^{-1}, when the proper process conditions were applied.

4.3.4 Structure analysis (DSC, XRD)

The melting point of the submicron-sized drug was measured to be 199 °C, slightly lower than the original material (204°C) and literature values [13] (see Figure 5-3 for DSC diagram). The lower melting point can be explained by the relatively large surface and thus increased total surface free energy compared to the original material [25]. The DSC results show that the normalized heat of melting for the electrosprayed material was 114 ±6 J g^{-1}, 85% of that for the conventional NIF. This would indicate that the electrosprayed NIF is at least 85% crystalline [26]. XRD patterns of both the spherical and elongated NIF crystals did not indicate other crystalline forms than the single reported form [24]. Diffraction patterns recorded directly after spraying did not show remarkable change in time, however, the powder pattern at 75 min shows more and sharper peaks than the others, which could indicate a change in crystallinity in the measured time frame (Figure 4-5). The product might be transformed

during the production or in the short time frame between the experiment and the first analysis.
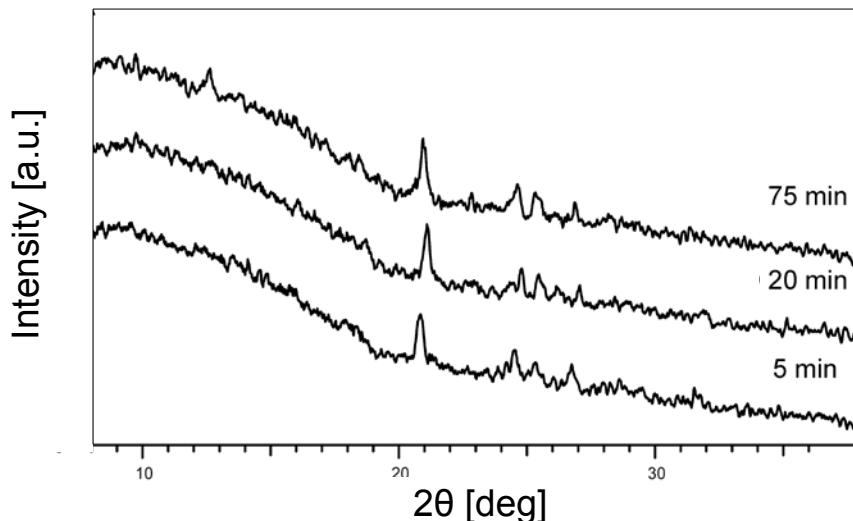
Figure 4-5. XRD patterns of the submicron-sized niflumic acid recorded 5 minutes, 20 minutes and 75 minutes after production. The diffraction patterns do not show remarkable change in time.

4.3.5 Solubility and dissolution rate measurements

For measuring the solubility and dissolution rate 1.7 g of submicron-sized NIF crystals were produced using the reference experiment conditions in the eight-nozzle setup. The eight-nozzle setup has under these conditions a production rate of 150 mg h^{-1} submicron-sized NIF.

Solubility and dissolution rate measurements of both the submicron-sized NIF and the raw material were performed. There were no significant differences measured between the solubility of the conventional (0.23 mg mL^{-1}) and the submicron-sized NIF samples (0.21 mg mL^{-1}). The submicron-sized and conventional NIF had also similar dissolution profiles at gastric pH. The explanation for this is that the nanoparticles tend to aggregate, and the advantage of the small size diminishes. The typical size of these aggregates was found to be around 30 μm (Figure 4-3B), which corresponds to the values found in literature [27]. Therefore, both solubility and dissolution rate measurements were performed in the presence of the excipients D-Mannitol and Poloxamer 188. These additives prevent aggregation of powders for both the conventional and submicron-sized NIF [28-29]. In the presence of the excipients the solubility of the submicron-sized NIF still did not increase. However, its dissolution

profile changed significantly. Figure 4-6 shows the measured dissolution profile with and without the excipients added to the conventionally sized and submicron-sized NIF. In the presence of the excipients the measured dissolution profile of the conventional NIF was not significantly different. However, when using the submicron-sized NIF in the presence of the excipients, significantly higher dissolution rates were achieved. Using the conventional NIF with the excipient D-Mannitol and Poloxamer 188 only 29% of the drug was dissolved after 30 min. When the submicron-sized NIF was applied with the same excipients the dissolution increased to 51% in the same amount of time. It seems that preparation of submicron-sized NIF with excipients preventing aggregation results in higher drug dissolution rates and therefore an improved absorption is possible.
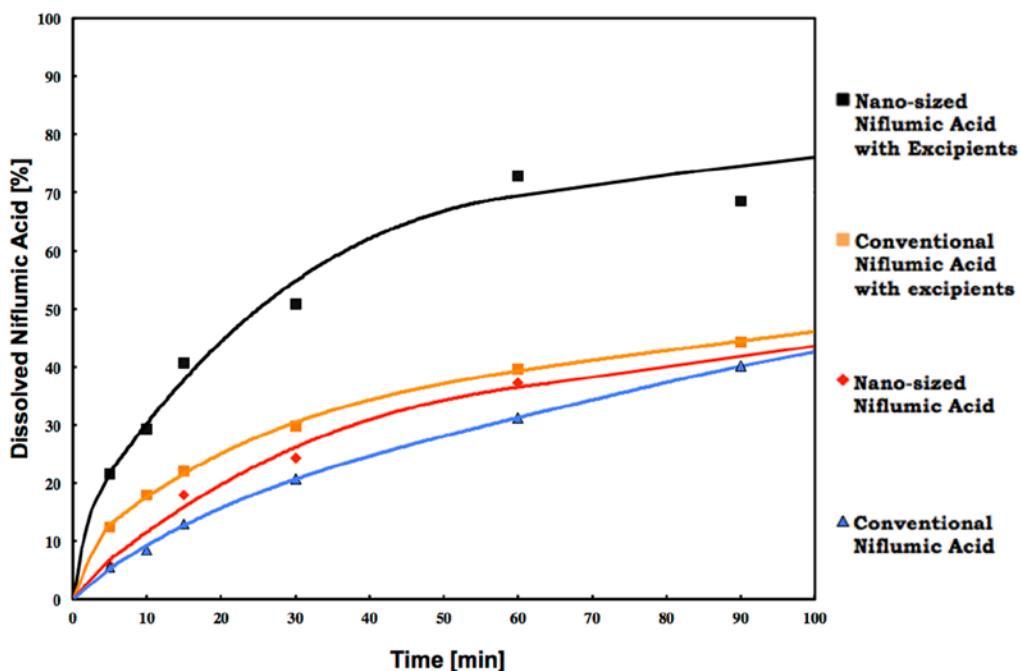
Figure 4-6. Dissolution profile of the conventional NIF without excipients (blue) and with excipients (orange) and the produced submicron-sized NIF without excipients (red) and with excipients (black). Using the conventional NIF with the excipient D-Mannitol and Poloxamer 188 only 22% of the drug was dissolved after 15 min and 39% in 1 h. When the submicron-sized NIF was applied with the same excipients the dissolution increased to 41% after 15 min and 73% in 1 h.

4.4 Conclusions

Submicron-sized niflumic acid crystals in the 200-800 nm size range can be produced by electrospray crystallization. However, the operation window for producing crystals in submicron-range without extensive agglomerations or ribbon formation is rather small. High solution concentrations in combination with large nozzle diameter resulted in ribbon-shaped and agglomerated needle-like crystals having the same crystal structure. When the excipients D-Mannitol and Poloxamer 188 were mixed with the submicron-sized niflumic acid the dissolution rate of the drug was enhanced. We can conclude that it is possible to increase the bioavailability of drugs by drastically reducing the crystal size of niflumic acid, while preventing their aggregation by applying the proper excipients.

References

[1]   Y. Xu, N. Al-Salim, J. M. Hodgkiss, R. D. Tilley *Crystal Growth & Design* 2011, 11, 2721-2723.

[2]   T. Naito, A. Kakizaki, T. Inabe, R. Sakai, E. Nishibori, H. Sawa *Crystal Growth & Design* 2011, 11, 501-506.

[3]   J.-W. Kim, M.-S. Shin, J.-K., Kim, H.-S. Kim, K.-K. Koo *Industrial & Engineering Chemistry Research* 2011, 50, 12186-12193.

[4]   N. Radacsi, A. I. Stankiewicz, Y. L. M. Creyghton, A. E. D. M. van der Heijden, J. H. ter Horst *Chemical Engineering & Technology* 2011, 34, 624-630.

[5]   V. A. Saharan, V. Kukkar, M. Kataria, M. Gera, P. M. Choudhury *International Journal of Health Research* 2009, 2, 107-124.

[6]   M. Kata, R. Ambrus. Z. Aigner *Journal of Inclusion Phenomena and Macrocyclic Chemistry* 2002, 44, 123-126.

[7]   R. Ambrus, Z. Aigner, C. Soica, C. Peev P. Szabó-Révész *Revista de Chimie* 2007, 58, 206-209.

[8]   F. Kesisoglou, S. Panmai, Y. Wu *Advanced Drug Delivery Reviews* 2007, 59, 631-644.

[9]   C. Leuner, J. Dressmann *European Journal of Pharmaceutics and Biopharmaceutics* 2000, 50, 47-60.

[10]   B. E. Rabinow *Nature Reviews Drug Discovery* 2004, 3, 785-796.

[11]   V. B. Patravale, A. A. Date, R. M. Kulkarni *Journal of Pharmacy and Pharmacology* 2004, 56, 827-840.

[12]   R. H. Müller, K. Peters *International Journal of Pharmaceutics* 1998, 160, 229-237.

[13]   S. Budavari, M. J. O'Neil, A. Smith, P. E. Heckelman *The Merck Index*, 11th Edition Merck & Co.: Rahway, New Jersey, 1989.

[14]   J. E. F. Reynolds *Martindale: The Extra Pharmacopoeia*, 31st Edition The Royal Pharmaceutical Society: London, 1996.

[15]   K. Takács-Novák, A. Avdeef, K. J. Box, B. Podányi, Gy. Szász *Journal of Pharmaceutical and Biomedical Analysis* 1994, 12, 1369-1377.

[16]   R. Ambrus, Z. Aigner, C. Dehelean, P. Szabó-Révész *Revista de Chimie* 2007, 58, 60-64.

[17]   *European Pharmacopoeia*, 3rd Edition Council of Europe: Strasbourg, 1996, 128-129.

[18]   G. I. Taylor *Proceedings of the Royal Society of London Series A* 1964, 280, 383.

[19]   C. U. Yurteri, R. P. A. Hartman, J. C. M. Marijnissen *KONA Powder and Particle Journal* 2010, 28, 91-115.

[20]   J. W. S. (Lord) Rayleigh *Philosophical Magazine* 1882, 14, 184-186.

[21]   K. Suzuki, H. Matsumoto, M. Minagawa, M. Kimura, A. Tanioka *Polymer Journal* 2007, 39, 1128-1134.

[22]   R. P. A. Hartman *Electrohydrodynamic Atomization in the Cone-Jet Mode,* Ph.D. Thesis, Delft University of Technology, The Netherlands, 1998.

[23]   E. Scholten, H. Dhamankar, L. Bromberg, G. C. Rutledge, T. A. Hatton *Langmuir* 2011, 27, 6683-6688.

[24]   H. M. Krishna Murthy, M. Vijayan *Acta Crystallographica* 1979, B35, 262-263.

[25]   G. C. Yang, F. D. Nie, H. Huang *Journal of Energetic Materials* 2007, 25, 35-47.

[26]   M. Wagner *Thermal analysis in practice – DSC evaluations* Mettler-Toledo AG: Schwerzenbach, 2009, 90-132.

[27]   J. R. van Ommen, C. U. Yurteri, N. Ellis, E. M. Kelder *Particuology* 2010, 8, 572-577.

[28]   P. Kocbek, S. Baumgartner, J. Kristl *International Journal of Pharmaceutics* 2006, 312, 179-186.

[29]   J. Hecq, M. Deleers, D. Fanara, H. Vranckx, K. Amighi *International Journal of Pharmaceutics* 2005, 299, 167-177.

5 Analysis and particle size reduction of niflumic acid crystals prepared by electrospray crystallization and other methods

Interest in submicron-sized drug particles has emerged from both laboratory and industrial perspectives in the last decade. Production of crystals in the nano scale range can serve as a formulation strategy to overcome the issue of poor solubility that many drugs suffer from, particularly those belonging to Classes II and IV in the Biopharmaceutical Classification System. In this work niflumic acid nanoparticles with a size range of 200-800 nm were produced by a novel crystallization method - electrospray crystallization. The properties of the niflumic acid particles were compared to those produced via evaporative and anti-solvent crystallization, using the same organic solvent, acetone. A remarkable difference in the product crystal size was shown depending on the applied method. The size and morphology of the crystals were analyzed by scanning electron microscopy and laser diffraction. The structure of the samples was investigated using differential scanning calorimetry, Fourier-transformed infrared spectroscopy and X-ray powder diffraction. The particles produced using the electrospray crystallization method were changing from amorphous to crystalline state after the procedure.

5.1 Introduction

Niflumic acid (NIF) is an important anti-inflammatory drug with a weak analgesic effect. It is primarily used to treat different forms of rheumatism, like rheumatoid arthritis or arthrosis, and to cure other inflammatory diseases [1]. However, its poor aqueous solubility and dissolution rate are disadvantages [2]. To achieve optimal pharmacodynamic properties such as a rapid onset of the drug effect, fast dissolution is critical. In our earlier studies, the aim was to improve the solubility and dissolution rate of the model substance via the preparation of ternary systems of NIF, cyclodextrin (CD) and polyvinylpirrolidone (PVP K-25) in different NIF to CD to PVP ratios by physical mixing, kneading, microwave irradiation and micronization [3-6].

The interest for nano/micron particles in pharmaceutical research has emerged recently since studies have proven that particle size reduction can influence the mechanisms of drug delivery in many ways [7-14]. The different methods used for particle size reduction can be divided into two main categories: top-down methods, where the raw material is subsequently broken down by using milling methods until micro- or nanosized particles are produced, and to bottom-up approaches (crystallization procedure), the basic principle of which involves the dissolution of the drug in a solvent, followed by the addition of the solution to a non-solvent which causes drug precipitation. The nanosuspension engineering processes currently used include precipitation using high-pressure homogenization in water, in mixtures of water and water-miscible liquids, or in non-aqueous media [15-19]. **Electrospray crystallization,** as a novel technique in bottom up procedures, has the potential to become an efficient, cost-effective method for the production of submicron-sized organic crystals [20], offering a simple formulation strategy to produce pharmaceutical ingredients with beneficial properties [21-23].

During electrospray crystallization, a high constant potential difference is applied to a nozzle, through which a conductive solution is pumped (Figure 3-1). If the potential difference is sufficiently high, electrostatic forces overcome the surface tension and a jet of liquid is emitted from the so-called Taylor-cone formed at the nozzle. At some distance from the nozzle, the jet becomes unstable and breaks into droplets, which are accelerated towards the grounded plate by the electric field. Coalescence of the droplets is prevented because of the unipolar charge [21] (which enables production of nano-sized crystals). Upon using a sufficiently volatile solvent such as acetone, solvent evaporation

occurs, which increases the specific surface charge density because of the decrease in droplet volume and surface area. As the surface charge density reaches a critical value, electrostatic forces overcome the surface tension and the droplet disrupts into smaller droplets to reduce the surface charge density by creating more surface area [24]. At some point during this process of droplet evaporation and disruption, the driving force for crystallization becomes sufficiently large for crystal nucleation and growth to occur. These charged submicron crystals accumulate at the grounded surface where they lose their surface charge.

Prior studies have shown that electrospray crystallization results in NIF particles with significantly improved dissolution rates [25 and *Chapter 4*], and this chapter focuses on the characterization of the produced submicron crystals. The goal of this research is to prepare and analyze submicron-sized NIF crystals. The effect of three different crystallization methods (electrospray crystallization, anti-solvent crystallization and evaporative crystallization) on the crystal structure, product and size micrometric properties is investigated and compared with the conventional NIF.

5.2 Materials and methods

5.2.1 Materials

Niflumic acid (2-[[3-(trifluoromethyl)phenyl]amino]-3-pyridinecarboxylic acid) with a mean size of around 80 μm was purchased from G. Richter Pharmaceutical Factory, Budapest, Hungary. For all the crystallization processes the solution was prepared with 99.8 % acetone, purchased from Merck.

5.2.2 Methods (Preparation procedures)

Electrospray crystallization
An eight-nozzle electrospray crystallization setup (Figure 3-2) with different NIF concentrations (10, 20 and 30 mg mL^{-1}) was used to produce the submicron-sized NIF. The setup consisted of eight nozzles, a nozzle holder, a grounded stainless steel collector plate, a Meredos TL-EAD peristaltic pump, which provided an equal distribution of the solution flow over the nozzles, and a Wallis ±10 kV DC power supply that was used in positive DC mode to provide the potential difference between the tip of the nozzles and the grounded plate.

The used nozzles had a length of 25.4 mm and the inner diameter of 0.33 mm. They were purchased from EFD, USA. The product is referred to in the text as **NIF-NANO** for the sample after 2 weeks storage.

Anti-solvent crystallization (AC)
In this method, a solution of 500 mg of NIF in 5 ml of acetone was added to 25 mL of an aqueous media at room temperature (25 °C) that was acting as an anti-solvent (Figure 5-1). Due to anti-solvent effect, the driving force for crystallization was reached rapidly, and a suspension of precipitated crystals was produced in water. This process was carried out by using a T-25 type of Ultra-Turrax disperser (IKA, Staufen, Germany) at 24000 rpm for 10 minutes, as the energy input for size reduction. This very high stirring rate in a slight temperature increase (up to 33 °C) and enhances the evaporation rate of the acetone from the mixture. The product was filtered and dried at room temperature. The product is labeled as **NIF-AC** in the text.
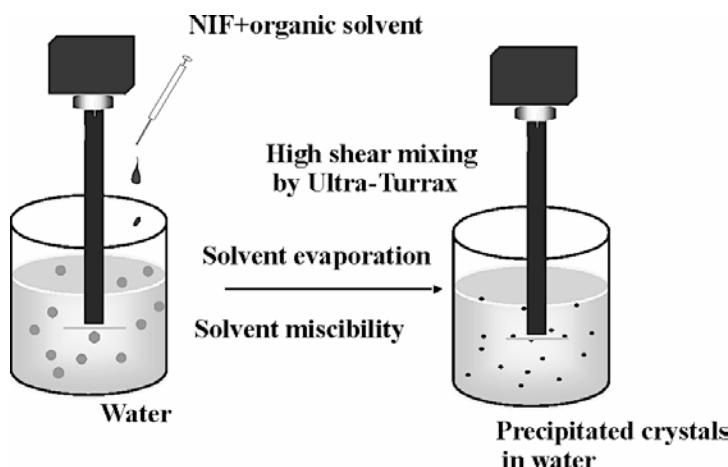
Figure 5-1. A Shematic of the solvent evaporation method.

Preparation of the sample by evaporative crystallization (SE)
250 mg of NIF was dissolved in 5 mL acetone, and then the solvent was evaporated with the help of a cold dryer (HM 3 Dryer, MH9150201, Siemens, Germany) until all the acetone evaporated. Then the dry powder was pulverized and homogenized manually in a mortar to ensure a narrow crystal size distribution. The NIF produced by evaporative crystallization is labeled in the text as **NIF-SE**.

5.2.3 Analysis

Scanning electron microscopy (SEM)

The crystal size and shape were examined by scanning electron microscopy (Hitachi S4700, Hitachi Scientific Ltd., Japan). A sputter coating apparatus (Bio-Rad SC 502, VG Microtech, England) was used to induce electric conductivity on the surface of the samples. The air pressure was 1.3–13.0 mPa. Samples were fixed onto a metallic stub with double-sided conductive tape (diameter 12 mm, Oxon, Oxford Instruments, UK). Images were taken in the secondary electron image mode at 10 kV acceleration voltage. The mean diameter of the particles was obtained by analyzing several SEM images within the ImageJ software environment [26]. Over 150 individual particle measurements were made using at least five different images in order to determine the particle size distribution.

Particle size analysis

The particle size distribution of the conventional NIF was measured by a laser diffractometer (Mastersizer S, Malvern Instruments Ltd, Worcestershire, UK) with the following parameters: 300RF lens, small volume dispersion unit rotated at 2000 rpm, 1.510 refractive index for dispersed particles, and 1.330 refractive index for the dispersion medium.

Differential scanning calorimetry (DSC)

DSC was employed to investigate the crystallization behavior and the melting behavior of the conventional and submicron-sized NIF. The DSC measurements were made with a Mettler Toledo DSC 821^e thermal analysis system with the STAR^e thermal analysis program V9.1 (Mettler Inc., Schwerzenbach, Switzerland). Approximately 2–5 mg of product was examined in the temperature range between 25 °C and 300 °C. The heating rate was 5 °C min^{-1}. Argon was used as the carrier gas at a flow rate of 10 L h^{-1}.

The crystallinity index of the different NIF samples was calculated from the heats of fusion: the ratio between the normalized enthalpy of the NIF samples and the normalized enthalpy of the conventional NIF indicates the product crystallinity [27].

X-ray powder diffraction (XRPD)

XRPD was carried out in order to determine the crystalline form and crystallinity of the produced materials. Samples were measured with a Bruker

D8 Advance diffractometer (Bruker AXS GmbH, Karlsruhe, Germany). Data collection was carried out at room temperature using monochromatic Cu K α1 radiation (α = 0.154060 nm) in the 2 theta region between 3° and 50°. For measurements directly after electrospray crystallization, about 10 milligrams of sample was directly deposited on a zero background holder (Si single crystal <510> wafer) and placed into the XRD directly after production. The recording of the pattern was relatively fast, it lasted 180 seconds. Diffraction patterns were recorded from 15 minutes till 20 hours after production at different time intervals.

Fourier transform infrared spectroscopy (FT-IR)

FT-IR spectroscopy was used to investigate the chemical stability of the drug. FT-IR spectra were measured on an AVATAR 330 FT-IR apparatus (Thermo Nicolet, USA), in the interval 400–4000 cm^{-1} and at 4 cm^{-1} optical resolution. Standard KBr pellets were prepared from 150 mg of KBr pressed with 10 ton and samples containing 0.5 mg of NIF were used.

5.3 Results and discussion

5.3.1 Electrospray crystallization process parameters

First, the electrospray crystallization process parameters were determined for the production of the desired submicron product. Three process parameters were identified to have a major effect on the product: initial solute concentration (c), potential difference (ΔU) and nozzle diameter (d), while the working distance (D) and flow rate (φ) were not investigated in this study.

When higher initial concentrations were used (30 mg mL^{-1}), the average crystal size increased: the same droplet with a higher concentration contains more solute that can crystallize, resulting in larger crystals (Figure 4-4). The crystal shape also depends on the initial concentration. At higher concentrations (30 mg mL^{-1}), the obtained crystals were more needle-like, while at lower concentrations (13 mg mL^{-1}), the crystals had a somewhat spherical shape (Figure 4-4).

A lower potential difference resulted in agglomeration of crystals. The increase of the nozzle diameter also resulted in agglomerate formation. A lower potential difference or larger nozzle diameter resulted in a lower charge density at the Taylor-cone and therefore at the droplet surface. At a lower surface charge

density Coulomb fission was occurring later or was absent and crystallization might have occurred in larger droplets, resulting in agglomerated crystals.

The optimal process parameters for producing submicron-sized NIF crystals (NIF-NANO) with a compact shape without agglomeration were found to be: solution concentration of 20 mg mL^{-1}, a potential difference of +4.7 kV, a nozzle diameter of 0.33 mm, a working distance of 17 mm and a flow rate of 1.8 mL h^{-1}. With these parameters somewhat prismatic shape NIF crystals with a mean size of around 500 nm were produced. The production rate under these conditions was 150 mg h^{-1}.

5.3.2 Product size and shape

The conventional NIF crystals had a smooth surface with prismatic shape with around 80 μm mean size and a broad crystal size distribution (Figure 5-2A). This shape was also seen for the NIF-SE crystals (Figure 5-2D). The crystal shape of NIF-SE was prismatic as well, and its size distribution was very broad with an estimated mean size of around 46 μm, probably due to the applied homogenization by manual pulverization. By using the anti-solvent crystallization method (NIF-AC), needle-like NIF crystals around 10 μm were produced (Figure 5-2C). This crystallization method combined with high shear mixing is an effective procedure for particle size reduction in the micron range. The electrospray crystallization procedure caused the most remarkable size and shape alterations from all the used crystallization methods. Somewhat spherical shaped NIF particles were found with a mean size of 500 nm (Figure 5-2B). These submicron particles were clustered into aggregates up to 20 μm in size, possibly due to the strong interactions between their hydrophobic crystal surfaces or due to static charging.

Table 1 presents the mean particle size of NIF determined using a SEM images analysis. It can be seen that the solvent evaporation with pulverization of the crystals (NIF-SE) decreased the crystal size to nearly half that of the conventional NIF size (80 μm). The crystals produced by the anti-solvent crystallization process (AC) were around 7 μm. Electrospray crystallization resulted in nano-sized particles around 500 nm. It seems that the increase in supersaturation in the anti-solvent crystallization process is not enough to obtain submicron crystals. Also the crystallization volume should be decreased. Similarly to electrospray crystallization, the main reason for size reduction is the

production of micron-sized droplets in the process, whereby crystallization can take place.
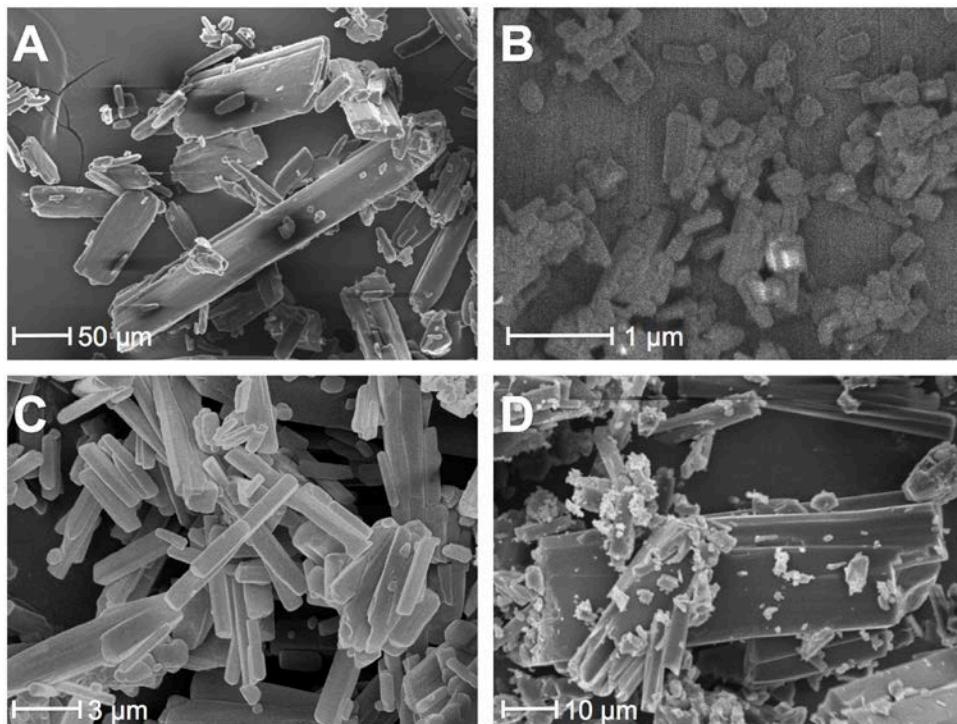
Figure 5-2. SEM images of **A**: NIF (manufacturer), B: NIF-NANO (after electrospraying), C: NIF-AC (using anti-solvent crystallization) and D: NIF-SE (with solvent evaporation)

Table 5-1 presents the mean particle size of the NIF particles determined from SEM image analysis. It can be seen that the solvent evaporation with pulverization of the crystals (NIF-SE) decreased the crystal size to nearly half that of the conventional NIF size (80 µm) determined. The product produced by the anti-solvent crystallization process (AC) resulted in crystals around 7 µm. Electrospray crystallization resulted in nano-sized particles, around 500 nm. It seems that the increase in supersaturation in the anti-solvent crystallization process is not enough to obtain submicron crystals. Also the crystallization volume should be decreased, as in electrospray crystallization the main reason of size reduction is that micron-sized droplets are created in the process, and crystallization commences in the small, confined volume offered by the droplets.

Table 5-1. The calculated mean crystal size of the conventional NIF and the produced crystals by SEM image analysis with the standard deviation (SD).

Sample	Mean size (µm)±SD
NIF	80±22.6
NIF-NANO	0.5±0.2
NIF-AC	7.4±3.9
NIF-SE	46.2±26

5.3.3 Structural analysis (XRPD, DSC and FT-IR)

The presence of amorphous fraction could be expected by spraying crystallization techniques, since the driving forces for crystallization are high [28, 29]. The presence of amorphous fraction has an effect on the stability of the samples as well. Due to the rapid evaporation of the solvent in electrospray crystallization, the crystal structure might not build up completely (kinetically formed more slowly) during the crystallization process [30]. Thus, structural characterizations were performed to check the crystalline state of the produced NIF crystals.

Differential scanning calorimetry
DSC was used to measure the melting point and the heat of melting of the NIF particles (Figure 5-3). A sharp endotherm at 203 °C reflected the melting point of the conventional NIF. The NIF-AC and NIF-SE samples presented similar DSC curves with a melting point at 203 °C. The submicron-sized NIF (NIF-NANO) had a well detectable melting point at a lower temperature (200 °C). The lower melting point and broader peak of the submicron-sized drug can be explained by the relatively large proportion of surface molecules compared to the bulk. The vibrational and positional enthalpy and entropy of surface molecules of submicron-sized materials are different from that of molecules inside the bulk of the crystals, which can alter physical properties, including the thermal properties [31].
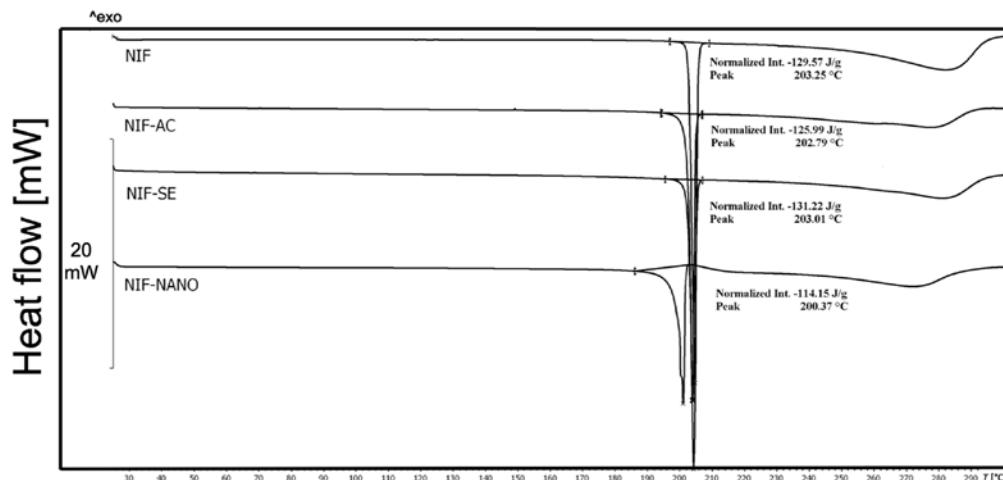
Figure 5-3. DSC curve of the conventional NIF compared with the recrystallized NIF obtained from the solvent evaporation (NIF-SE), the recrystallized NIF obtained from the solvent evaporation-antisolvent crystallization (NIF-AC) and the submicron-sized NIF from electrospray crystallization (NIF-NANO).

One way to test the crystallinity of the samples is to determine the normalized heat of melting. There is a relation between the heat of melting and the crystalline fraction of the sample. The crystallinity index of NIF was calculated from the normalized heat of melting of the samples (Table 5-2). The conventional NIF sample was assumed to have 100 % crystallinity. The sample produced by solvent evaporation (NIF-SE) showed higher heat of melting than the conventional NIF, probably due to the pulverization impact. The sample from the anti-solvent crystallization method (NIF-AC) showed 97 % crystallinity. The electrospray crystallization product (NIF-NANO) showed the lowest crystallinity from all the produced samples, 88 % of the material was measured to be crystalline, which implies that 12 % of the sample is amorphous. The crystallinity index was also calculated for a sample that was measured 15 minutes after the production by the electrospray crystallization process. Its crystallinity index was 81%; 7% less than the electrosprayed sample after 2 weeks (NIF-NANO). This shows that a part of NIF changed from amorphous phase to crystalline phase during the storage.

Table 5-2. The crystallinity index (CI) of the samples

Sample	Normalized Integral (J g^{-1})	CI (%)
NIF	129	98
NIF-SE	131	100
NIF-AC	125	95
NIF-NANO	114	87
Electrosprayed NIF (15 minutes after the procedure)	105	82

X-ray powder diffraction

XRPD analysis was used to examine the crystal structure and it was also used to assess the crystallinity of the products. The characteristic intensity values of the NIF can be found at 8.2, 12.9, 16.2, 23.2, 25.7 2θ values. All the produced samples showed peaks at the same positions as the conventional NIF, but their intensity was lower (Figure 5-4). When the three produced samples were compared with each other, it was shown that the NIF-SE sample had more intense peaks than the NIF-AC or NIF-NANO samples, indicating that the NIF-SE sample had higher crystallinity than the other two products. The peak intensity of the NIF-AC sample was in between the NIF-SE and the NIF-NANO samples. From the three produced materials, the NIF-NANO sample presents the lowest peak intensities, indicating the lowest crystalline fraction from the measured products. Since in general evaporative crystallization results in highly crystalline product, it was assumed that the NIF-AC and NIF-NANO samples are partially amorphous. The decrease in particle size of the NIF-AC and NIF-NANO samples can also be the reason for the measured lower intensities in the XRPD patterns.
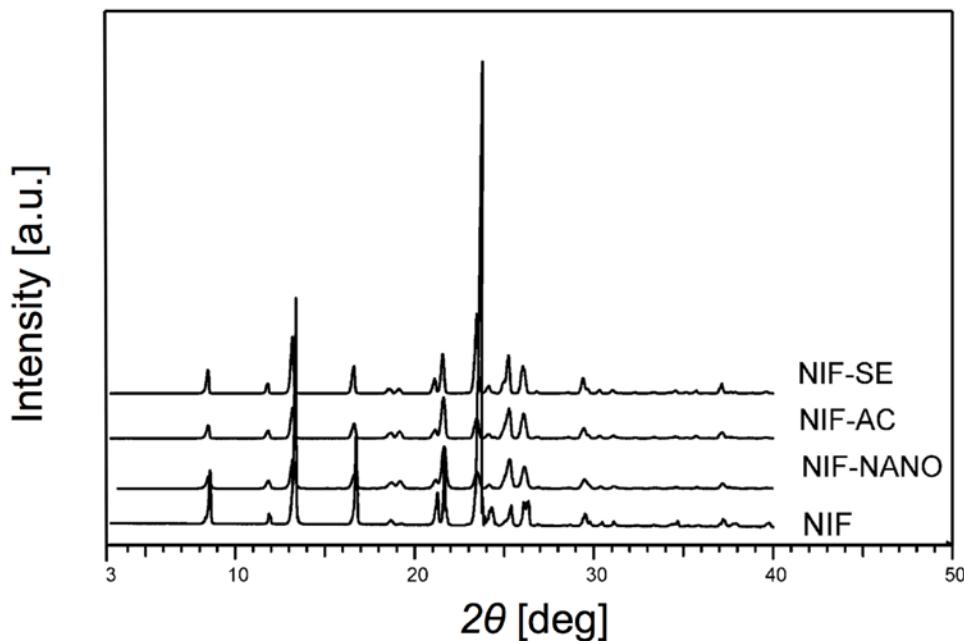
Figure 5-4. XRPD patterns of the NIF samples produced by solvent evaporation (NIF-SE), anti-solvent crystallization (NIF-AC) and electrospray crystallization (NIF-NANO), compared with the conventional NIF (NIF)

To investigate a possible transition between amorphous and crystalline state of the NIF-NANO sample, diffraction patterns of the sample were recorded directly after spraying for 20 h. The crystallinity did not change in the first 20 h (Figure 5-5). Since the XRPD pattern of the NIF-NANO sample (these are nanoparticles 2 weeks after electrospray crystallization) showed higher intensities than can be seen on the 20 h diffraction pattern, indicating a probable increase in the crystallinity in the following two weeks.
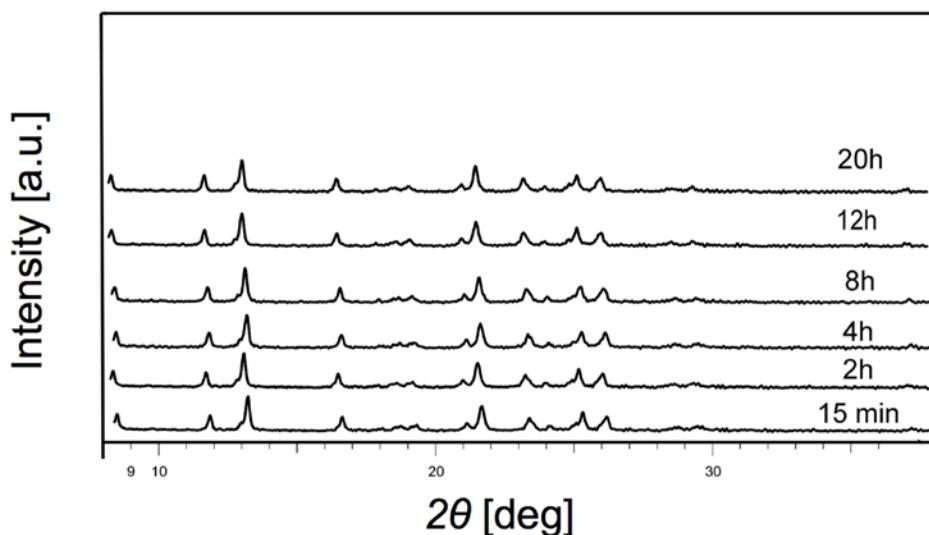
Figure 5-5. XRPD pattern of the produced NIF-NANO sample till 20 h after the procedure. No change in crystallinity can be observed.

FT-IR analysis

IR spectroscopy was used to study the chemical stability of the NIF samples. The IR spectrum of NIF displayed strong absorption at 1607 cm^{-1} that is due to the characteristic ν_{as} (COO) and ν_s (COO) stretching modes of carboxyl groups. A middle-strong peak at 3163 cm^{-1} could be ascribed to the N–H vibration of imine [32, 33] and the strong absorption peak at 1523 cm^{-1} is owing to the framework vibration of the phenyl and pyridine rings. The FT-IR spectra (Figure 5-6) of NIF-SE and NIF-NANO did not present differences compared with NIF. New bonds were not developed and old bonds did not disappear. According to the FT-IR analysis no chemical change in the structure was detected, which means that the produced samples did not show polymorphic transition or chemical decomposition. This implies that the produced NIF-NANO crystals were chemically stable before and after the procedure.
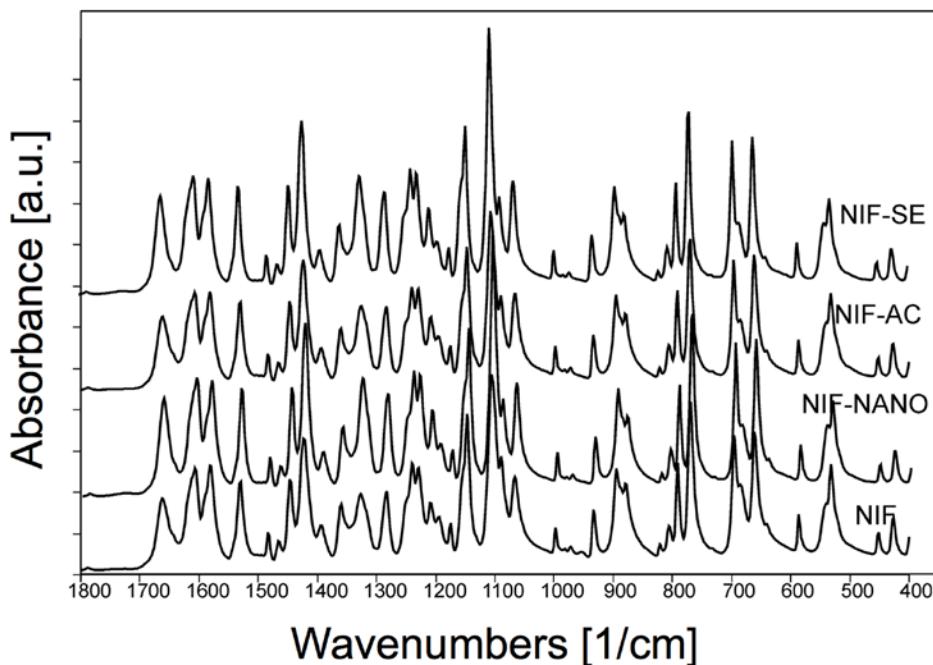
Figure 5-6. FT-IR spectra of NIF, NIF-NANO, NIF-AC and NIF-SE. No chemical change in the INA structure was detected.

5.4 Conclusions

This study has shown that electrospray crystallization as a non-conventional method can be used to formulate submicron-sized NIF crystals with a mean size of around 500 nm. Careful selection of the process parameters is critical to achieve the suitable size and shape. Lower initial solution concentrations lead to compact, somewhat spherical crystal shape, while higher concentrations result in needle-like crystals. The crystallization procedure was compared to two conventional crystallization methods, evaporative and anti-solvent crystallization, where macro- and micro-sized crystals were prepared. XRPD measurements of the NIF crystals showed that via evaporative and anti-solvent crystallization the products were highly crystalline right after their formation and also after 2 weeks. However, the electrosprayed product was partly amorphous right after the production, and only 81 % of the sample was crystalline. The crystallinity of the electrosprayed sample increased during storage, according to the DSC results the two-week-old electrosprayed NIF samples were 88% crystalline. According to the FT-IR measurements the NIF crystals were chemically stable before and after the procedure.

References

[1]   S. Budavari, M. J. O'Neil, A. Smith, P. E. Heckelman *The Merck Index,* 11th Edition Merck & Co.: Rahway, New Jersey, 1989.

[2]   J. E. F. Reynolds *Martindale: The Extra Pharmacopoeia*, 31st Edition The Royal Pharmaceutical Society: London, 1996.

[3]   R. Ambrus, Z. Aigner, C. Dehelean, C. Soica, P. Szabó-Révész *Revista de Chimie* 2007, 58, 60-64.

[4]   R. Ambrus, Z. Aigner, C. Soica, C. Peev, P. Szabó-Révész *Revista de Chimie* 2007, 58, 206-209.

[5]   M. Kata, R. Ambrus, Z. Aigner *Journal of Inclusion Phenomena and Macrocyclic Chemistry* 2002, 44, 123-126.

[6]   T. Szunyogh, R. Ambrus, P. Szabó-Révész *Acta pharmaceutica Hungarica* 2011, 81, 29-36.

[7]   J. Kanzer, S. Hupfeld, T. Vasskog, I. Tho, P. Hölig, M. Mägerlein, G. Fricker, M. Brandl *Journal of Pharmaceutical and Biomedical Analysis* 2010, 53, 359-365.

[8]   J. Zhang, H. Lv, K. Jiang, Y. Gao *International Journal of Pharmaceutics* 2011, 420, 180-188.

[9]   T. W. Prow, J. E. Grice, L. L. Lin, R. Faye, M. Butler, W. Becker, E. M.T. Wurm, C. Yoong, T. A. Robertson, H. P. Soyer, M. S. Roberts *Advanced Drug Delivery Reviews* 2011, 63, 470-491.

[10]   H. Chen, X. Kou, Z. Yang, W. Ni, J. Wang *Langmuir* 2008, 24, 5233-5237.

[11]   D. Missirlis, N. Tirelli, J. A. Hubbel *Langmuir* 2005, 21, 2605-2613.

[12]   J.-W. Kim, M.-S. Shin, J.-K. Kim, H.-S. Kim, K.-K. Koo *Industrial & Engineering Chemistry Research* 2011, 50, 12186-12193.

[13]   R. Ambrus, P. Kocbek, J. Kristl, R. Sibanc, R. Rajkó, P. Szabó-Révész *International Journal of Pharmaceutics* 2009, 318, 153-159.

[14]   V. A. Saharan, V. Kukkar, M. Kataria, M. Gera, P. M. Choudhury *International Journal of Health Research* 2009, 2, 107-124.

[15]   G. G. Liversidge, P. Conzentino *International Journal of Pharmaceutics* 1995, 125, 309-313.

[16]   P. Liu, X. Rong, J. Laru, B. von Veen, J. Kiesvaara, J. Hiruonen, T. Laaksonen, L. Peltonen *International Journal of Pharmaceutics* 2011, 411, 215-222.

[17]   R. H. Müller, A. Akkar *Encyclopedia of Nanoscience and Nanotechnology* 2004, 2, 627-638.

[18]   P. Kocbek, S. Baumgartner, J. Kristl *International Journal of Pharmaceutics* 2006, 312, 179-186.

[19]   T. Yasuji, H. Takeuchi, Y. Kawashima *Advanced Drug Delivery Reviews* 2008, 60, 388-398.

[20]   N. Radacsi, A. I. Stankiewicz, Y. L. M. Creyghton, A. E. D. M. van der Heijden, J. H. ter Horst *Chemical Engineering & Technology* 2011, 34, 624-630.

[21]   C. U. Yurteri, R. P. A. Hartman, J. C. M. Marijnissen *KONA Powder and Particle Journal* 2010, 28, 91-115.

[22]   A. Jaworek *Powder Technology* 2007, 176, 18-35.

[23]   B. Almería, W. Deng, T. M. Fahmy, A. Gomez *Journal of Colloid and Interface Science* 2010, 343, 125-133.

[24]   J. W. S. (Lord) Rayleigh *Philosophical Magazine* 1882, 14, 184-186.

[25]   N. Radacsi, R. Ambrus, T. Szunyogh, P. Szabó-Révész, A. I. Stankiewicz, A. E. D. M. van der Heijden, J. H. ter Horst *Crystal Growth & Design* 2012, 12, 3514-3520.

[26]   M. D. Abramoff, P. J. Magelhaes, S. J. Ram *Biophotonics International* 2004, 11, 36-42.

[27]   M. Wagner *Thermal analysis in practice – DSC evaluations* Mettler Toledo: Schwerzenbach, 2009.

[28]   M. J. Arias-Blanco, J. R. Moyano, J. I. Perez-Martinez, J. M. Gines *Journal of Pharmaceutical and Biomedical Analysis* 1998, 18, 275-279.

[29]   H. A. Crisp, J. C. Clayton, L. G. Elliott, E. M. Wilson *U.S. Patent* 4,820,1833, 1989.

[30]   S. Nakayama, T. Watanabe, M. Senna *Journal of Alloys and Compounds* 2009, 483 217-221.

[31]   G. C. Yang, F. D. Nie, J. S. Li *Journal of Energetic Materials* 2007, 25, 35-47.

[32]   K. Takács-Novák, A. Avdeef, K. J. Box, B. Podányi, Gy. Szász *Journal of Pharmaceutical and Biomedical Analysis* 1994, 12, 1369-1377.

[33]   H. M. K. Murthy, M. Vijayan *Acta Crystallographica* 1979, 35, 262-263.

6   Cold plasma synthesis of high quality organic nanoparticles at atmospheric pressure[3]

Atmospheric pressure cold Surface Dielectric Barrier Discharge (SDBD) plasma was used for the first time to produce nano-sized organic crystals. Nano-sized particles can have beneficial product properties, such as improved internal quality and dissolution rate, compared to conventionally sized crystalline products. In cold plasma crystallization a nebulizer system sprays the solution aerosol into the plasma with the help of a carrier gas. The plasma heats and charges the droplets causing solvent evaporation and Coulomb fission to occur, after which nucleation and crystal growth commence within the small, confined volume offered by the small droplets. As a result nano-sized crystals are produced. The operation conditions of SDBD plasma to produce nano-sized crystals of the energetic material RDX were determined by scanning electron microscopy, and the product was investigated with X-ray powder diffraction and sensitivity tests. The sensitivity tests indicated that the nano-sized product had reduced sensitivity for friction, indicating a higher internal quality of the crystalline product.

6.1 Introduction

The interest in nanoparticle synthesis has emerged both in industry and scientific research in the last decade [1-4]. Nano-sized crystals can have strikingly different chemical and physical properties, because the particle surface properties dominate those of the bulk. Since smaller particles have a much higher specific surface area, an increase in the overall dissolution rate is expected at the same driving force for dissolution. Nano-sized crystals are furthermore too small to contain inclusions of which the size is usually in the micron size range. These inclusions of pockets of mother liquor are generally causing other crystalline defects, like dislocations [5]. Therefore the internal quality of nano-sized crystals is considered to be higher than the conventional, micron-sized (100-400 μm) crystals. There are several techniques using for instance rapid expansion of supercritical solutions [6], electrospray crystallization [7] or thermal plasmas [8] to produce nanoparticles. However, none of these methods offer the possibility to produce nano-sized organic crystals at industrial scale with low operation costs. Rapid expansion of supercritical solutions is a complex and costly technique, while electrospray crystallization has limitations on scaling-up. Thermal plasmas offer an effective, cost efficient way of nanoparticle production [8]. However, thermal plasmas are not suitable for organic compounds because the high temperature causes decomposition reactions.

Cold plasmas are operated at temperatures close to ambient temperature, which would prevent the decomposition of organic compounds, while they can be scaled up to industrial level. However, cold plasmas are often operated in vacuum that can make the process rather difficult and expensive, mainly at larger scales [9-10]. The atmospheric pressure plasma systems are of interest for reducing equipment and processing costs when relatively high production rates are required. In this study a specific type of plasma, the surface dielectric barrier discharge (SDBD), which is a cold plasma applicable at atmospheric pressure, was used. The opportunity offered by atmospheric pressure cold plasma is the synthesis of organic materials with the capability of scaling up and low operating costs [9].

In this study SDBD plasma was used for the synthesis of high quality nano-sized crystals of the energetic organic compound RDX. The operation conditions and boundary limits of the process at laboratory scale were

determined. Then, the produced nano-sized energetic crystals were analyzed by X-ray diffraction and tested for their sensitivity.

6.2 Atmospheric pressure cold plasma

Plasma consists of electrons, ions and neutral species, which are in an excited or ground state. A plasma can be characterized by the degree of ionization. In a thermal plasma the gas is generally fully ionized and the electrons and the ions have equivalent temperature [11]. If a small fraction of gas is ionized and the concentration of energetic electrons is too small to heat up the gas, the plasma is referred to as a non-thermal or cold plasma [12]. In cold plasma the temperature of the ionized gas as a whole (ions and molecules) remains relatively low. The electron temperature, however, is typically several thousands of degrees since the electrons are more easily excited due to their smaller mass compared to the heavier ions and thermal equilibrium is not reached [11]. In our research the focus was on using a cold plasma.

SDBD is a type of cold plasma that can be operated at atmospheric pressure. The plasma is generated on top of the surface of an SDBD plate. The plate is made of a dielectric material in which an electrode system is embedded. There are discharge electrodes on one side that consist of line-shaped conductors that are deposited on or are partly embedded in the dielectric material. A plate-shaped counter-electrode is embedded in the dielectric on the opposite side of the plate (Figure 6-1). This configuration results in a strong electric field close to the discharge electrodes. The plasma then is a result of discharges caused by a pulsed high voltage between the discharge- and the counter-electrodes [13]. This produces a stable, high-frequency surface discharge starting from both side edges of each line-shaped discharge electrode, and covering uniformly the ceramic surface [14]. SDBD is generally used as a new and efficient ozone generator [15].
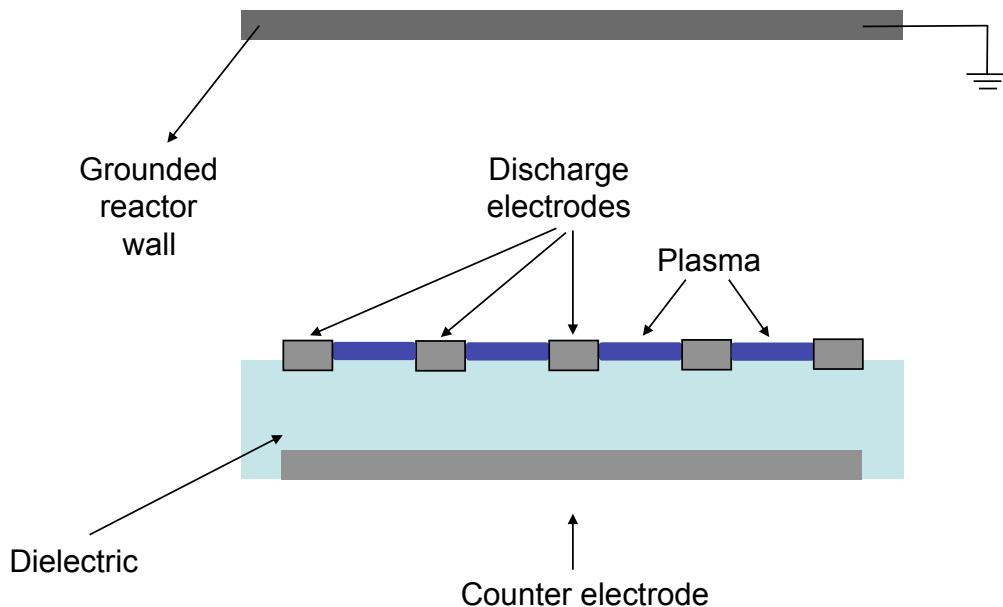
Figure 6-1. Schematic cross section of an SDBD plate with the grounded reactor wall above, which was used for electrostatic collection of the charged particles.

6.3 Experimental

6.3.1 Materials

Class 2 RDX (cyclotrimethylene trinitramine) with an average size of around 350 μm was purchased from Chemring Nobel AS, Norway. For the plasma crystallization process different solution concentrations were prepared with 99.8 % acetone purchased from Merck.

6.3.2 Plasma aided crystallization setup

Figure 6-2 represents the schematics of the plasma aided crystallization experimental setup. The setup consists of a gas and nebulizer system, a reactor chamber containing the SDBD plate and the optional nozzle, the high voltage system for plasma generation and particle collection and devices for electrical and thermal measurements.
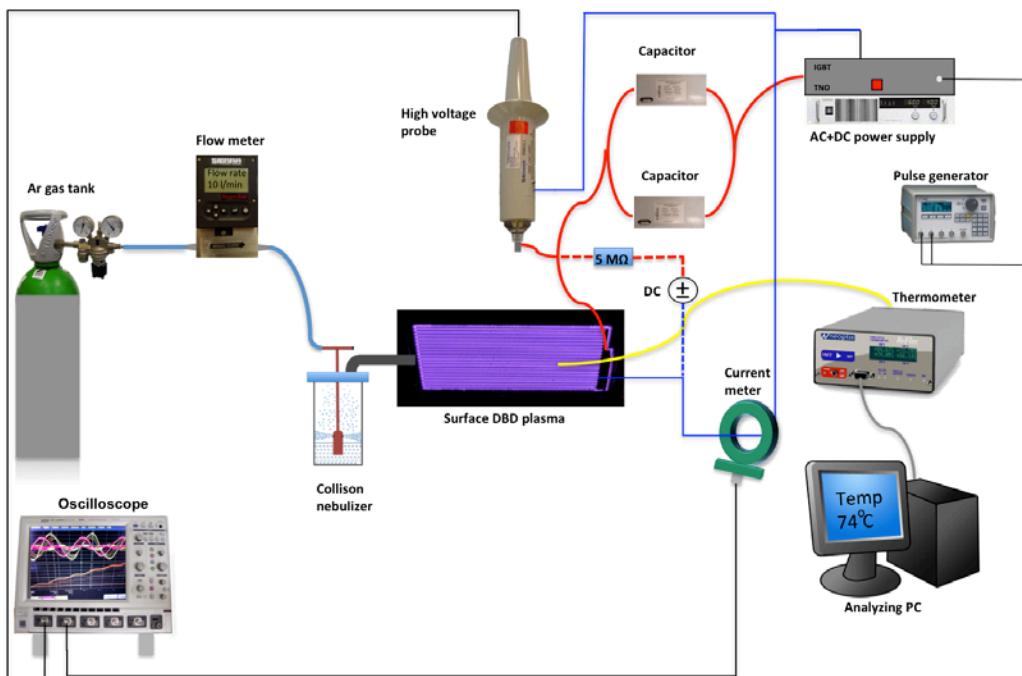
Figure 6-2. Schematic diagram of the experimental setup for SDBD plasma crystallization.

Gas and nebulizer system

A Sierra Smart-Track flow meter was used to control the argon flow rate. A Dräger X-am 3000 gas detector was used to measure the oxygen content of the reactor chamber. The argon gas was transported through the Collison nebulizer (BGI Inc., USA) and carried the RDX-acetone solution as an aerosol spray into the plasma chamber (Figure 6-3). The Collison nebulizer is a well-known technique for efficient aerosolization of various liquids [16]. High pressure gas (2 bars) is introduced into a glass jar, which contains 4-120 ml liquid at the bottom. The lower part of the nozzle head stays in the liquid. Micro-channels are present at the bottom of the nozzle head and at the side of the nozzle-head as well. The high-pressure gas going through the side-holes sucks the fluid up to the tube. Via the side-holes the fluid is broken up into a fine aerosol jet. Most of this jet is blown to the internal wall of the glass jar, which refluxes into the bottom liquid. The rest of the jet, containing the smaller particles can escape the jar, which is carried to the plasma reactor by the high pressure argon gas.

According to the manufacturer an aerosol of 0.4 to 16 μm droplets of a non-volatile liquid can be produced.

Plasma reactor chamber and SDBD plate

The plasma experiments were carried out at atmospheric pressure in a tube-shaped plasma reactor chamber, placed horizontally with the dimensions: 300 mm length, 130 mm diameter and 2.8 mm wall thickness. The reactor chamber is made of stainless steel on one end closed with a 14 mm diameter hole in the middle, where the nebulizer is attached. The other end is closed by a transparent 8 mm thick PMMA disk, which is 1 mm smaller in diameter than the inner diameter of the tube. A slit between the reactor tube and the PMMA disk is needed to maintain a constant area of the inlet and outlet of the chamber in order to keep out the air. During the experiments the plasma is visually observed through this transparent plate.

The SDBD plate is placed in the middle of the reactor tube facing upwards with the help of a rail system made of PTFE (Figure 6-3). Two different sizes of SDBD plates were used: 200 x 100 mm and 100 x 100 mm. The plates are made of 96% alumina ceramics (Al_2O_3) and are 1 mm in thickness. The electrode system of the SDBD plate consists of 20 interconnected 1 mm wide, 50 µm thick strips of platinum deposited on the ceramic plate. The gap between the electrode strips is 3 mm. The length of the electrodes is 80 mm on the 100 x 100 mm plate and 180 mm on the 200 x 100 mm plate. In order to direct the entire aerosol above the plasma a stainless steel nozzle was used with an 8 mm slit. The length of the nozzle is 70 mm. Two strong neodymium magnets held the nozzle in place and made it easy to remove.
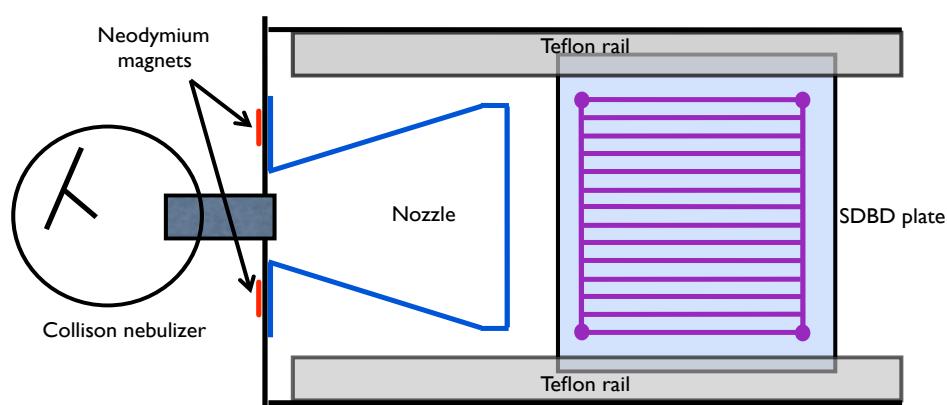
Figure 6-3. The schematic representation of the SDBD plasma reactor with the nozzle and the 100 x 100 mm SDBD plate

Electrical power system

A pulsed high voltage of peak-to-peak 5-8 kV, with a frequency of 25 or 10 kHz was used to generate the plasma. A Xantrex XFR 600-4 DC power supply connected to a home-made AC power supply containing an insulated gate bipolar transistor (IGBT) was used to create the AC voltage. The pulsed voltage was generated by a BNC 565 pulse/delay generator. To ensure that most of the current flows through the SDBD plate two 15 pF capacitors were connected in parallel between the high voltage electrode and the discharge electrode of the SDBD plate.

By applying a DC bias voltage superposed on the AC voltage, the plasma can be used as a charger and the uniformly charged particles can be collected on the grounded plasma reactor chamber wall (Figure 6-1). To use the plasma as a charger an additional DC power supply (Spellman SL1200 +10 kV, USA) was added to the setup, which was connected between the SDBD plate electrodes with a 5 MΩ resistor (added with a dashed line on Figure 6-2). The resistor was needed to protect the additional DC power supply. Care was taken to apply a lower DC bias voltage than the amplitude of the plasma exciting AC voltage. If the DC bias voltage were higher than the amplitude of AC voltage, sparking would occur, which could lead to the damage of the electrical power system.

Equipment for electrical and thermal measurements

The high voltage was measured by a Tektronix P6015A high voltage probe and the current was measured by a Pearson 2877 current monitor. Both were connected to a LeCroy WaveSurfer 44Xs oscilloscope.

A Neoptix ReFlex 4-channel fiber optic temperature thermometer (Neolink, USA) was used to measure the temperature surrounding the plasma with a PTFE-coated Neoptix T1 optical temperature probe. The optical sensor was placed 8 mm above the centre of the SDBD plate during the experiments. The step-response time of the system was 250 ms.

6.3.3 Characterization Tests

For morphological and size characterization of the crystalline samples, Philips XL30 FEG and FEI NovaSEM 560 environmental scanning electron microscopes were applied. Samples were investigated without applying a conductive coating. Only low electron beam energies were used since energies higher than 2 kV resulted in decomposition of the energetic materials at higher magnifications.

X-ray powder diffraction (XRPD) pattern was recorded in Bragg-Brentano geometry in a Bruker D8 Advance diffractometer. Data collection was carried out at room temperature using monochromatic Cu Kα radiation in the 2θ region between 10° and 60°, step size 0.034 degrees 2θ. The sample is placed on a Si {510} substrate and rotated during the measurement. Data evaluation has been done with the Bruker program EVA.

The BAM Fallhammer and Friction Apparatus tests are the recommended test methods in the UN recommendations on the transport of dangerous goods [17]. For the impact sensitivity test a BAM Fallhammer device was used (according to the international guidelines EC A.14 and UN 3(a)(ii)) [17]. The temperature during the test was 23 °C. The volume of both the conventional and nano-sized RDX sample was approximately 40 mm^3 and the drop weight was 1 kg. During the test the drop height was decreased from 50 cm until initiation of the sample did not occur. Each time a different sample was used.

The sensitivity to friction was determined by a BAM Friction Apparatus according to the international guidelines EC A.14 and UN 3(b)(i) [17]. The sample is placed on a roughened porcelain plate, which is rigidly attached to the sliding carriage of the friction apparatus. A cylindrical porcelain peg is placed on top of the sample. The porcelain plate moves forward and backward under the porcelain peg, creating friction. The smallest load of the peg, which causes deflagration, crackling or explosion of the test sample at least once in six consecutive trials is the outcome of the friction sensitivity test. The quantity of the test sample is 10 mm^3.

6.4 Results and Discussion

SDBD plasma crystallization is a new technique for synthesis of organic nano-sized crystals. In this process solution droplets are created by a nebulizer and sprayed into the plasma. To exploit the relations between the process parameters and the product properties, the understanding of the crystallization process during SDBD plasma crystallization is essential. The plasma has two functions.

First, the plasma acts as a heat source and enhances the evaporation rate of the solvent droplets. Upon evaporation, supersaturation is created [18] and nucleation and crystal growth commence within the small, confined volume offered by the small droplets.

Secondly, the plasma discharges electrically charge the evaporating solution droplets. As the surface charge density of a droplet reaches a critical value

(Rayleigh limit), electrostatic forces overcome the surface tension and the droplet disrupts into smaller droplets to reduce the surface charge density by creating more surface area [19]. This disruption process is called Coulomb fission [20] and results in micron-sized droplets of solution.

As a result nucleation of the dissolved organic compound will start from the micron-sized solution droplets and nano- or submicron-sized crystals will be formed.

As a first step, the process parameters for supplying a flow of droplets to the reactor, creating a homogeneous, stationary plasma and collecting the formed particles were determined (section 6.4.1). Then, the properties of the produced particles are discussed in relation to the process conditions (section 4.2).

6.4.1 Determination of the process parameters

The gas composition, flow rate and electric power determine the plasma generation, while, next to the plasma, the discharge plate arrangement, DC bias potential difference and solution concentration have effect on the particle production.

Gas composition
The energy needed for plasma generation and the plasma structure depend on the gas composition. Exciting plasma in air costs a relatively large amount of energy, because the oxygen molecules in air dissociate and combine into ozone [21]. Noble gases, like helium or argon lead to lower energy consumption for plasma generation. It was already shown by Vons et al. that inorganic nanoparticle production by SDBD plasma is possible using argon gas, while in helium it was not [9]. This is due to the difference in plasma structure. When argon gas is applied the plasma is a mixture of filamentary and glow discharge, while in helium it has only a glow structure [9]. Argon gas was thus used to carry the RDX-acetone solution as an aerosol into the reactor in this study.

Gas flow
The gas flow rate needs to be sufficiently high in order to keep the air out, and offer low energy operation of the plasma. However, the side-holes of the nebulizer head restrict the gas flow, especially when a solution is transported.

Using an RDX-acetone solution concentration of 6.3 mg mL^{-1} with argon gas and the six-hole nebulizer head lead to a maximum flow rate of 11 L min^{-1}. This flow rate turned out to be sufficiently high to have a minimal oxygen content of

around 2.2 vol % in the reactor during a stationary state. When the 3-hole nebulizer head was used with the same solution and gas, the argon flow was limited to maximally 4 L min^{-1}, which resulted in an oxygen content of around 15%. Therefore, for plasma crystallization only the 6-hole nebulizer head was used and the gas flow rate was kept at 11 L min^{-1}.

Plasma generating power

There is a minimum power that is needed to be applied on the SDBD plate to excite a plasma. The total electrical power consumption (P) of the SDBD plate depends on the applied voltage, current and the pulse frequency. It can be calculated as equation 1 shows:

$$P = \frac{1}{T}\int_0^T U(t)I(t)\,dt \tag{6.1}$$

where T is the time period of the wave, U(t) is the measured potential difference between the discharge and the counter electrodes and I(t) is the measured current.

The minimum power for creating a homogeneous plasma also depends on the size and electrode arrangement of the SDBD plate. Table 6-1 shows the minimum power delivered into a plasma when different parameters were used. It can be seen that the power is proportional to the surface area. Operating the plasma with the 100 x 100 mm SDBD plate needs approximately half the energy than with the 200 x 100 mm plate.

Table 6-1. Calculated power delivered to the SDBD plate for exciting a homogeneous plasma.

Size [mm]	200 x 100	200 x 100	100 x 100	100 x 100
Pulse frequency [kHz]	25	10	25	10
Exciting voltage [kV]	7.8	8.3	4.6	5.1
Power [W]	118	70	55	35

Droplet charge and particle collection

A DC voltage was superposed on the plasma generator pulsed AC voltage. By applying the DC bias the charging effect of the process is enhanced [22]. Figure 6-4 shows the plasma exciting voltage with and without applying the +2 kV DC bias: the pulsed exciting voltage was shifted upwards by using a positive DC potential difference, which means that only positive charges are created by the

plasma and delivered to the droplets. Thus coalescence of the droplets and aggregation of the formed crystals is prevented because of their unipolar charges. Finally, with the application of the DC bias voltage the charged nanocrystals can be collected electrostatically with high efficiency using a grounded collector plate [23].
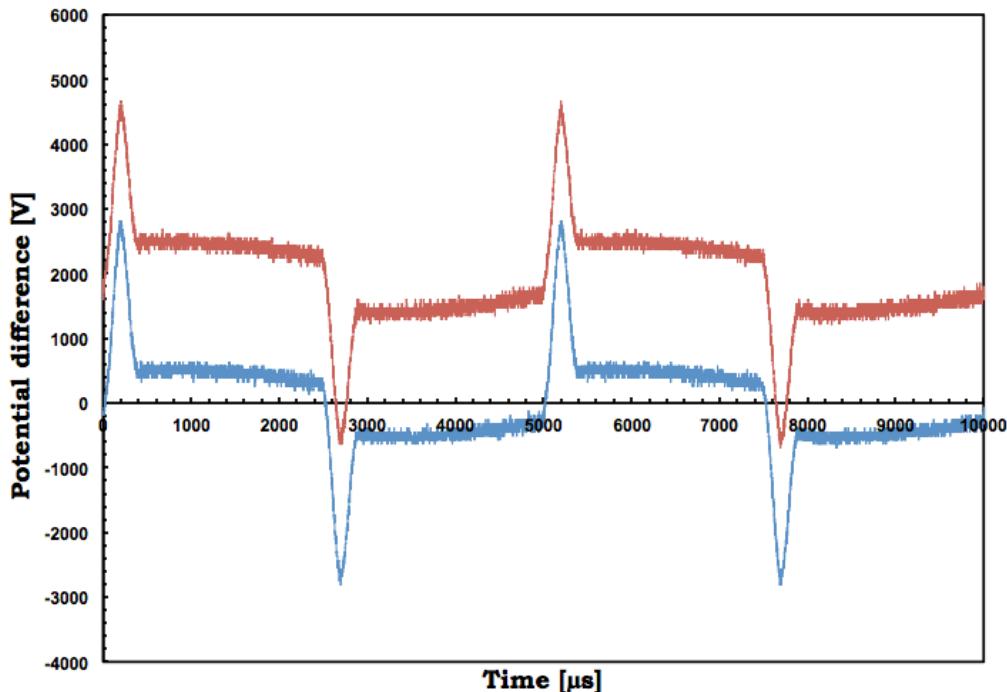
Figure 6-4. The pulsed voltage used for exciting plasma. The upper red curve is with +2 kV DC bias potential difference, the lower blue curve is without the DC bias.

Temperature

A fiber optics temperature measurement was used to assess the temperature of the gas surrounding of the SDBD plate. When the plasma was turned on, the average temperature above the SDBD plasma increased rapidly. The heating rate strongly depended on the power delivered to the plasma, which is related to the applied voltage and frequency. Figure 6-5 shows how the temperature profile developed 8 mm above the centre of the SDBD plate during the plasma crystallization process. The temperature at the plate surface might be higher. The temperature above the plasma was measured for both the 100 x 100 mm and 200 x 100 mm SDBD plates at 10 kHz and 25 kHz pulse frequencies. Since the larger plates need more energy for operation, the temperature during operation

with the 200 x 100 mm plate was higher than with the 100 x 100 mm plate. When the SDBD plates were excited with 25 kHz frequency, the temperature rapidly increased even for the 100 x 100 mm plate, because the very frequent excitation of the plasma discharges increase the temperature substantially. The aim of the temperature measurement was to find the operation conditions with the lowest possible temperature for nano-sized RDX production in order to avoid its decomposition. The lowest stationary temperature was achieved, when the 100 x 100 mm SDBD plate was used with an exciting voltage of 5.1 kV and a pulse frequency of 10 kHz. By using these settings, the stationary temperature measured 8 mm above the SDBD plate was around 70 °C. Since RDX has an autoignition temperature around 200 °C [24], it was assumed that the temperature in the process was sufficiently below the autoignition temperature, and the decomposition of RDX is sufficiently reduced.
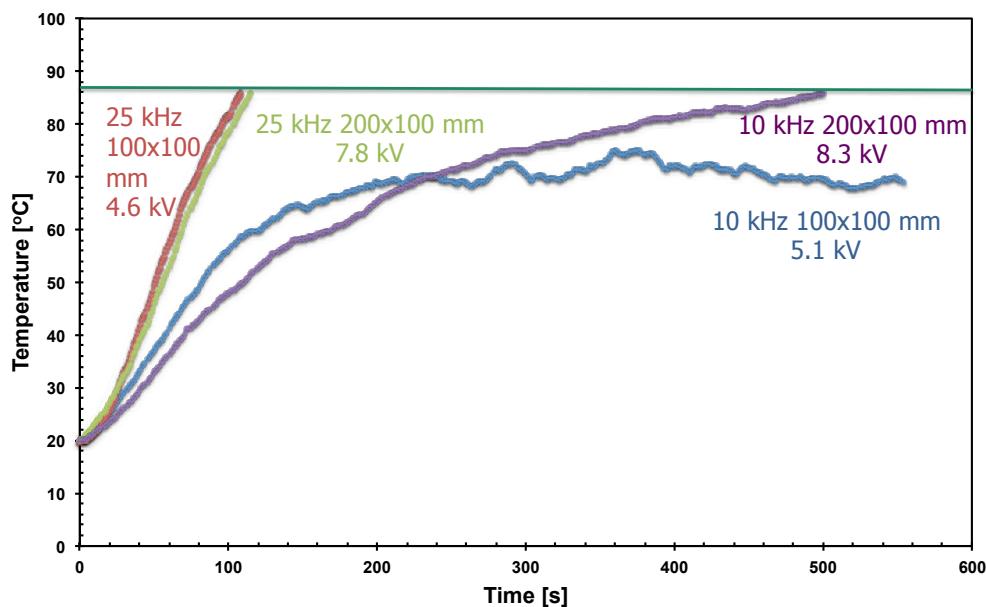
Figure 6-5. Temperature profiles measured 8 mm above the plasma surface for both the 100 x 100 mm and 200 x 100 mm SDBD plates. A stationary temperature below 90 °C can only be produced with the 100 x 100 mm discharge plate operating at 5.1 kV exciting voltage and 10 kHz pulse frequency.

6.4.2 Product properties

The process parameters determine the quality of the product. Table 6-2 shows the relation between the process parameters and the product properties. All the samples are from the same location, the top of the grounded reactor wall. The plasma crystallization process was operated for 3 minutes in all cases, except in the case, where plasma was not turned on.

RDX crystals in the size range of 200-900 nm (Figure 6-6 and Table 6-2, row 1) were produced using the 100 x 100 mm SDBD plate longitudinal to the flow, a solution concentration of 10 mg mL^{-1} RDX, an argon flow rate of 11 L min^{-1}, a 10 kHz pulse frequency over the 5.1 kV exciting AC potential difference and a DC bias voltage of +2 kV. These operating conditions define our reference experiment for comparison with results under other operating conditions. No extensive agglomeration was observed, which indicated that under these conditions droplets were not coalescing and the small droplet volume caused the formation of only a single RDX crystal per droplet [25]. This single crystal per droplet then completely consumed the dissolved RDX in the evaporating droplet.

XRPD patterns of the produced nano-sized RDX showed that the product is crystalline with the stable, α crystal structure [26].
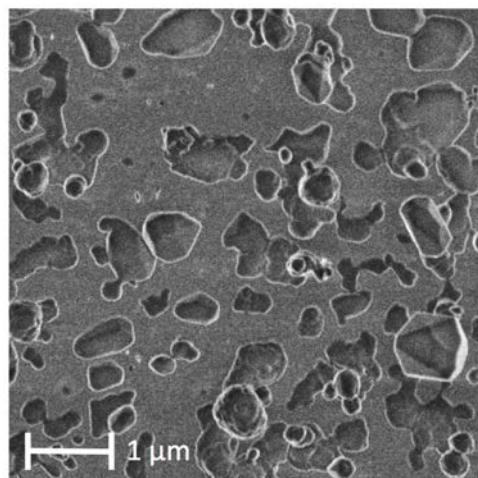
Figure 6-6. RDX crystals in the size range of 200-900 nm with prismatic and spherical shape created from 10 mg mL^{-1} solution concentration by applying 5.1 kV pulsed exciting voltage with 10 kHz frequency and a DC bias of 2 kV using the 100 x 100 mm SDBD plate longitudinal to the flow.
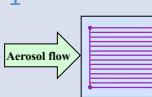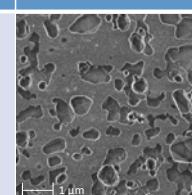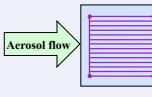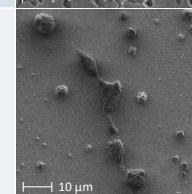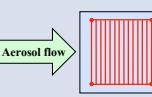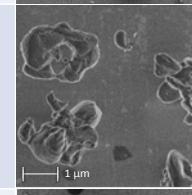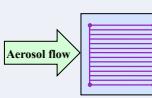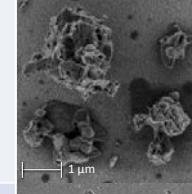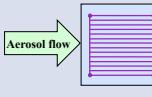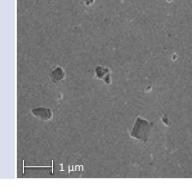
Changing the process parameters resulted in a product with different properties. The effects of the process parameters on the product properties are discussed below.

Effect of the plasma

In order to investigate the effect of the plasma on the crystals, the setup was also tested without plasma. When the plasma is not turned on, extensive agglomerates (> 4 µm) are created even at low, 6.3 mg mL^{-1} solution concentration (Table 6-2, row 2). Since the temperature is not increased by the plasma, the evaporation rate of the solution droplets are lower, and crystallization starts later. The lack of the charging effect due to the absence of the plasma results in the absence of the Coulomb disruption process. As a result, agglomerates are created even at relatively low RDX concentrations, because crystallization commences from a relatively large droplet that is produced by the Collison nebulizer and upon solvent evaporation multiple crystals are created from one droplet.

Table 6-2. The relation between the process parameters and the product size and shape. During all the experiments the argon flow rate was 11 L min^{-1}. By applying the parameters of row 1, 200-900 nm sized RDX crystals are produced. When the plasma is not turned on, extensive agglomerates are formed even at low solution concentrations (row 2). When the aerosol flow is transverse to the discharge plate, agglomerated crystals are formed (row 3). The increase in solution concentration results in larger crystals and agglomerations of around 2 µm (row 4). When the DC bias voltage is not applied, the number of collected crystals significantly decreases (row 5).

Plate configuration	Solution concentration [mg mL^{-1}]	Exciting voltage [kV]	Pulse frequency [kHz]	DC bias voltage [kV]	Product
1	10	5.1	10	+2	
2	6.3	0	0	0	
3	10	5.1	10	+2	
4	19.84	5.1	10	+2	
5	10	5.1	10	0	

SDBD plate configuration effect

Since the 100 x 100 mm SDBD plate is square-shaped it is possible to place it in the plasma reactor channel either longitudinal or transverse to the aerosol flow. Since plasma is not present above the discharge electrodes, the aerosol flow interacts differently with the plasma in the two configurations, which in turn has an effect on the product. When the SDBD plate was placed longitudinal to the incoming aerosol flow, individual, submicron crystals were produced, as shown in the reference experiment (Table 6-2, row 1). However, when the SDBD plate was placed transverse to the aerosol flow, agglomerates of RDX were formed (Table 6-2, row 3). In this transverse configuration the droplets travel perpendicular to the electrodes and experience an intermittent plasma, interrupted by the electrodes after every few millimeters. As a result, the droplets may not be charged sufficiently so that droplet coalescence and particle agglomeration occur.

When the plate is placed longitudinal to the flow and the droplets travel along the electrodes through the plasma, they experience more plasma interaction, than in the transverse arrangement. Therefore, the longitudinal configuration enhances the droplet charge and the subsequent Coulomb fission and particle formation. However, in this configuration part of the droplets that travel above the electrodes are probably not charged sufficiently. After solvent evaporation, the formed particles are not attracted by the grounded reactor wall and form a deposition layer on the surface of the electrodes or leave the reactor with the flow.

As a conclusion, it seems that the transverse configuration, which means an intermittent plasma, gives the same charging effect to all the droplets travelling at the same height above the SDBD plate, but the charging effect is not enough for nanoparticle formation without agglomeration. In the longitudinal arrangement, the charging effect is large enough for nanoparticle synthesis, but a large fraction of the droplets may not be affected by the plasma sufficiently for an efficient collection of the particles.

Solution concentration

It was found that with increasing initial solution concentrations compared to the reference experiment the chance for agglomeration increases. Using 12 mg mL^{-1} solution concentration resulted in the appearance of some 1 μm sized agglomerates, while at 15.8 mg mL^{-1} solution concentration nearly half of crystals were agglomerated with a size of around 1 μm. Relatively higher solution concentrations (19.8 mg mL^{-1}) resulted in formation of only

agglomerates of the produced crystals in the size range of 1-2 μm (Table 6-2, row 4).

If the initial concentration is higher, the chance for larger crystals or agglomerate formation increases. The same droplet with a higher concentration contains more solute that can crystallize, resulting in larger crystals. Furthermore, crystallization would occur earlier in the process, possibly even before extensive Coulomb fission occurred. Then several crystals can be formed from a single droplet, which might agglomerate.

Effect of DC bias potential difference
Experiments with and without the DC bias potential difference were performed to investigate the effect of the DC bias, which was superposed on the plasma generator pulsed voltage. Without the DC bias both negative and positive droplets are produced by the plasma, and these droplets attract, join and neutralize each other. With the help of the applied DC bias only positively or only negatively charged droplets can be produced, which repel each other, and are attracted to the grounded reactor wall, where they loose their surface charge. It can be seen from the experiments that by applying a DC bias the number of collected crystals significantly increased (Table 6-2, row 5). Approximately ten times more crystals are collected on the grounded reactor wall in the same time frame when the DC bias is applied. The applied DC bias not only avoids aggregation of droplets, it is also necessary for efficient electrostatic collection of the produced nanoparticles.

6.4.3 Production rate

It is shown that atmospheric pressure cold plasma can be used for organic nanocrystal synthesis. By applying the parameters of the reference experiment, the nano-sized RDX production rate was 200 mg h^{-1}, while theoretically a production rate of around 2.6 g h^{-1} is possible under these conditions, showing significant product loss. In order for industrial application to be feasible the production loss should be diminished to acceptable levels.

The main factors that determine the production rate in the plasma crystallization process are the amount of solute entering the reactor and the efficiency of the particle collection. The amount of solute is in turn determined by the solution concentration and the carrier gas flow rate. The DC bias voltage and the SDBD plate size, position and arrangement determine the particle collection process in which charged particles are attracted by the grounded plate.

Using high concentrations of RDX to achieve high production rates is not possible with the Collison nebulizer. Solution concentrations close to the saturation concentration led to unwanted crystallization and scaling in the micro-channels of the nebulizer, which resulted in full blockage after 1-2 minutes of operation. There is thus a strong relation between the clogging and the solution concentration. Therefore it is important to know the temperature dependent solubility of the used material in the solvent and use only solution concentrations that are substantially lower than the solubility at room temperature. In the case of RDX around 20% of the saturation concentration can be used without clogging.

The gas flow rate and thus the aerosol injection into the reactor are limited by the micro-channels of the nebulizer. The 11 L min^{-1} gas flow rate that was achieved with the 6-hole nebulizer head corresponds to 4.3 mL min^{-1} solution sprayed by the nebulizer. However, significant scaling occurs within the nozzle, in the tube between the reactor and the nebulizer, in the knee tube of the nebulizer and on the discharge electrodes of the SDBD plate. Approximately 10% of the solute cannot reach the plasma because of this scaling. This amount of scaling in the current system cannot be avoided.

The efficiency of the particle collection is determined by the DC bias. As mentioned in the experimental part, the DC bias potential difference has a limit. If the DC bias voltage exceeded the amplitude of the plasma exciting AC voltage, sparking could occur between the SDBD plate and the reactor wall. Thus in the current system the theoretical maximum of the DC bias voltage is 2.55 kV.

In principle, when using electrostatic collection, around 75 % collection efficiency can be achieved for particles in the size of around 500 nm [23]. To investigate the particle collection efficiency, the outflowing gas was studied on the content of crystals by applying a metal sheet above the gas outlet for 3 minutes during operation of the reference experiment. The sheet was investigated with SEM, and particles were observed on it. These particles had an amorphous appearance, and were likely not RDX. This indicates that the RDX that is not collected is either decomposed, or deposited within the reactor. Indications for decomposition of organic materials were observed as very small amounts of carbon deposition (less than 1 % of the injected solute) on the SDBD plate between the electrodes. Probably the organic molecules that have too much plasma exposure were decomposed and escaped the reactor chamber with the outflowing gas.

The product loss can be reduced by applying a better geometry that minimizes scaling and decomposition of the solute. If the carrier gas would bring the aerosol at a proper distance above the plasma as a thin gas layer, the plasma treatment could be optimal for the production of nano-sized particles without decomposition.

An increase in the production rate could be achieved by applying a larger SDBD plate, however, then also cooling should be introduced, because as shown in Figure 6-5, temperature increases with the increasing plate size. If the gas or solution were cooled, it would have a cooling effect directly on the gas above the plasma. However, this would decrease the solubility of the RDX in the solution resulting in clogging of the micro-channels of the nebulizer head. It might be better to apply an air- or water-cooling system or a Peltier element on the counter-electrode of the SDBD plate, which could supply an indirect cooling effect.

An improved SDBD geometry could be a vertically placed SDBD cylinder instead of a plate, with the length of around 30 cm and the discharge electrodes on the inner surface. By this design, the plasma geometry could be optimized. By applying the plasma generating electrodes as a spiral, the advantage of the longitudinal and transverse arrangement could be combined. The solution droplets would have increased plasma exposure, more or less for the same time, resulting in increased collection efficiency and reduced product loss. At the bottom of the setup, a modified nebulizer could produce the solution droplets by applying a reversed cone at the top of the nebulizer to direct the aerosol to the plasma. An extra carrier gas that is present as a thin layer above the discharge electrodes could bring the aerosol to a proper distance from the inner surface, to charge the droplets equally and avoid the decomposition. The top part of the setup could be a grounded metal cap, where the crystals would be collected electrostatically.

6.4.4 Product sensitivity

To check the expected product quality improvement, impact and friction sensitivity tests were performed. For these tests 1 gram of material was produced using the conditions of the reference experiment.

In the impact sensitivity test ignition occurred when the height was set to 50 cm (5 J) in the impact test (Table 6-3). The conventional RDX also needed 5 J energy for ignition. Therefore, the impact sensitivity test showed no difference in impact sensitivity for the nano-sized RDX.

In the friction sensitivity tests, even at the highest possible load (360 N), no ignition occurred. The conventional RDX needed 144 N load for ignition (Table 6-3). Apparently, the friction sensitivity is much lower for the nano-sized energetic particles than for the conventionally sized explosive crystals. The friction sensitivity tests might indicate that the nano-sized crystals contain less defects and therefore have a higher internal quality. However, impact sensitivity does not show this reduced sensitivity.

These results correspond with our previous findings, where nano-RDX produced by electrospray crystallization was investigated and the difference in impact sensitivity was negligible, while the friction sensitivity decrease was significant [7].

Table 6-3. Impact and friction sensitivity of 500 nm RDX compared with conventionally sized RDX

	Impact sensitivity (J)	Friction sensitivity (N)
Conventional RDX	**5**	**144**
Nano-sized RDX	**5**	**>360**

6.5 Conclusions

A homogeneous plasma was generated by surface dielectric barrier discharge (SDBD). The process parameters were identified and stationary operation conditions for organic nanocrystal production were achieved. It seems that only by spraying the solution droplets longitudinal the SDBD plate results in nanoparticle formation without agglomeration. By using the longitudinal configuration, energetic RDX crystals in the range of 200-900 nm were produced from a low concentration RDX-acetone solution. When the process was operated at relatively higher solution concentrations, the crystals agglomerated into >1μm clusters. The sensitivity of the nano-sized samples was tested to investigate the internal quality of the RDX crystals. The nano-sized RDX samples showed a remarkable insensitivity towards friction stimuli, indicating that the internal quality of the nano-sized RDX crystals is higher than that of conventionally sized RDX. A disadvantage of the current process design is that the production rate is relatively low and the product loss is also significant. Plasma aided crystallization is a new process for the production of organic nano-sized crystals. It can be scaled up relatively easily, but more investigation is needed in order to optimize the process.

References

[1]   J.-W. Kim, M.-S. Shin, J.-K. Kim H.-S., Kim K.-K., Koo *Industrial & Engineering Chemistry Research* 2011, 50, 12186-12193.

[2]   A. Pancholi, V. G. Stoleru, C. D. Kell *Nanotechnology* 2007, 18, 215607.

[3]   T.-J. Park, G. C. Papaefthymiou, A. R. Moodenbaugh, Y. Mao, S. S. Wong *Journal of Materials Chemistry* 2005, 15, 2099-2105.

[4]   A. K. Sugih, D. Shukia, H. J. Heeres, A. Mehra *Nanotechnology* 2007, 18, 035607.

[5]   T. Kobayashi, Y. Fujiyoshi, N. Ueda *Acta Crystallographica* 1982, A38, 356-362.

[6]   V. Stepanov, L. N. Krasnoperov, I. B. Elkina, X. Zhang *Propellants, Explosives, Pyrotechnics* 2005, 30, 178-183.

[7]   N. Radacsi, A. I. Stankiewicz, Y. L. M. Creyghton, A. E. D. M. van der Heijden, J. H. ter Horst *Chemical Engineering & Technology* 2011, 34, 624-630.

[8]   N. Rao, B. Micheel, D. Hansen, C. Fandrey, M. Bench, S. Girshick, J. Heberlein, P. McMurry *Chemistry and Plasma Processing* 1995, 15, 581-606.

[9]   V. Vons, Y. Creyghton, A. Schmidt-Ott *Journal of Nanoparticle Research* 2006, 8, 721-728.

[10]   A. Schutze, J. Y. Jeong, S. E. Babayan, J. Park, G. S. Selwyn, R. F. Hicks *IEEE Transactions on Plasma Science* 1998, 26, 1685-1694.

[11]   B. Eliasson, U. Kogelschatz *IEEE Transactions on Plasma Science* 1991, 19, 1063-1077.

[12]   R. Morent, N. De Geyter, J. Verschuren, K. De Clerck, P. Kiekens, C. Leys *Surface and Coatings Technology* 2008, 202, 3427-3449.

[13]   J. Salge *Surface and Coatings Technology* 1996, 80, 1-7.

[14]   J. Rahel, M. Simor, M. Cernak, M. Stefecka, Y. Imahori, M. Kando *Surface and Coatings Technology* 2003, 169, 604-608.

[15]   S. Masuda, K. Akutsu, M. Kuroda, Y. Awatsu, Y. Shibuya *IEEE Transactions on Industry Applications* 1988, 24, 223-231.

[16]   K. R. May *Journal of Aerosol Science* 1973, 4, 235-241.

[17]   *UN Recommendations on the Transport of Dangerous Goods, Manual of Tests and Criteria,* 4th Revised Edition New York and Geneva: United Nations, 2004.

[18]   J. W. Mullin *Crystallisation,* 4th Edition Butterworth-Heinemann Ltd.: Oxford, 2001.

[19]   J. W. S. (Lord) Rayleigh *Philosophical Magazine* 1882, 14, 184-186.

[20]   K. Suzuki, H. Matsumoto, M. Minagawa, M. Kimura, A. Tanioka *Polymer Journal* 2007, 39, 1128-1134.

[21]   U. Kogelschatz, B. Eliasson, W. Egli *Pure and Applied Chemistry* 1999, 71, 1819-1828.

[22]   R. W. Gundlach *DC biased AC corona charging* U.S. Patent 6,349,024. February 19, 2002.

[23]   M. Rhodes *Introduction to Particle Technology,* 2nd Edition West Sussex: John Wiley & Sons Ltd. 2008.

[24]   J. Harris *Thermochimica Acta* 1976, 14, 183-199.

[25]   E. Revalor, Z. Hammadi, J. P. Astier, R. Grossier, E. Garcia, C. Hoff, K. Furuta, T. Okutsu, R. Morin, S. Veesler *Journal of Crystal Growth* 2010, 312, 939-946.

[26]   R. J. Karpowicz, S. T. Sergio, T. B. Brill *Industrial and Engineering Chemistry Product Research and Development* 1983, 22, 363-365.

7 Atmospheric pressure cold plasma synthesis of submicron-sized pharmaceuticals with improved physico-chemical properties[4]

A reduction in particle size is one of the strategies to enhance the dissolution behavior of low water-soluble drugs such as niflumic acid. Atmospheric pressure cold plasma crystallization is a novel technique to achieve such sub-micrometer particles. This technique uses a surface dielectric barrier discharge (SDBD) plasma that both charges and heats solution droplets. Atmospheric pressure cold plasma crystallization was used to produce niflumic acid crystals and its excipient, Poloxamer 188, with a significant decrease in size compared to the conventional products. A substantial increase in dissolution rate of the submicron niflumic acid was observed in the presence of the plasma-made excipient.

7.1 Introduction

Solving bioavailability problems of new pharmaceutical products is a major challenge for the pharmaceutical industry, since nearly half of the new active substances in the pipeline are either insoluble or poorly soluble in water [1-3]. Studies with poorly water-soluble drugs have demonstrated that particle size reduction to the sub-micron range can lead to an increase in the dissolution rate (the total amount of drug substance that dissolves per unit time) and a higher bioavailability [4-7].

By decreasing the crystal product size the surface-to-volume ratio is increased. Due to the relatively larger surface area the dissolution rate is enhanced so that a higher concentration can be reached in shorter time frames. Since, according to the Ostwald-Freundlich relation, smaller particles have increased solubility [8], an increase in the solubility might be expected as well, possibly further increasing the dissolution rate. Thus, a substantial particle size reduction can offer a solution for bioavailability problems of a specific drug.

There are several techniques to produce nanoparticles. The nano-suspension engineering processes currently used are pearl milling and high-pressure homogenization, either in water or in mixtures of water and water-miscible liquids or non-aqueous media [9-13]. However, milling changes the crystal shape and often results in formation of (partially) amorphous materials because of the high energy input [14]. High pressure homogenization can also produce amorphous materials and sometimes causes decomposition of the crystals, again because of the relatively high energy input. A more advanced method is electrospray crystallization [15], but the low production rate is a limiting factor. Cold plasma technology offers the possibility to produce a wide range of nanoparticles, and to coat them in the same process or to change their hydrophobic properties to hydrophilic or to increase their mechanical stability [16]. Plasma processing is relatively inexpensive, energy efficient and easily scalable to industrial levels [17]. Furthermore, plasma processes are considered as an environmentally benign technology [18].

Niflumic acid (NIF) is an important anti-inflammatory drug with a weak analgesic effect [19]. It is primarily used to treat different forms of rheumatism, like rheumatoid arthritis or arthrosis [20]. However, its poor aqueous solubility [21] and dissolution rate [22] are disadvantages. To achieve optimal pharmacodynamic properties such as a rapid onset of the drug effect, fast dissolution is critical. In practice, certain excipients, such as Poloxamer 188, are

added to NIF the crystalline product to improve its physical and chemical properties.

The aim of this study is to prepare submicron-sized crystals of NIF as well as of its excipient Poloxamer 188 in order to achieve fast dissolution and rapid onset of the drug effect. Atmospheric pressure cold plasma crystallization is introduced as a potential method for the production of sub-micrometer-sized drug crystals with the possibility of scaling up the process. The differences in dissolution rate as well as the product morphology and crystal form of the produced crystals are also investigated.

7.2 Experimental Methods

7.2.1 Materials

Niflumic acid (2-[[3-(trifluoromethyl)phenyl]amino]-3-pyridinecarboxylic acid) with a median particle size of around 80 μm (see Figure 5-2 for the SEM images of the original product) was purchased from Sigma-Aldrich, USA, *β-D-Mannitol* with a median particle size of around 86 μm was purchased from Hungaropharma Plc., Hungary), and *Poloxamer 188* (Polyethylene-Polypropylene Glycol) with a median particle size of around 122 μm was purchased from Fluka, Slovenia. For the plasma crystallization process different solution concentrations were prepared with 99.8 % acetone purchased from Merck.

7.2.2 Plasma crystallization setup

Surface dielectric barrier discharge (SDBD) plasma crystallization is a new technique for the synthesis of organic submicron-sized crystals. SDBD is a type of cold plasma that can be operated at atmospheric pressure. The plasma is generated on top of the surface of an SDBD plate. The plate is made of 96% alumina ceramics (Al_2O_3) and is 1 mm in thickness. An electrode system is deposited onto the SDBD plate. There are discharge electrodes on one side that consist of line-shaped conductors that are deposited on or are partly embedded in the dielectric material. This electrode system consists of 20 interconnected 1 mm wide, 80 mm long and 50 μm thick strips of platinum deposited on the ceramic plate. The gap between the electrode strips is 3 mm. A plate-shaped counter-electrode is embedded in the dielectric on the opposite side of the plate

(Figure 6-1). This configuration results in a strong electric field close to the discharge electrodes. The plasma then is a result of discharges caused by a pulsed high voltage between the discharge- and the counter-electrodes [23]. A Xantrex XFR 600-4 DC power supply connected to a home-made AC power supply and a BNC 565 pulse/delay generator was used to create the pulsed AC voltage.

Argon gas at 2 bar pressure was transported through a Collison nebulizer (BGI Inc., USA) and carried the solution as an aerosol spray into the plasma chamber. A Sierra Smart-Track flow meter was used to control the argon flow rate. In order to direct the entire aerosol above the plasma, a stainless steel nozzle was used with an 8 mm slit (Figure 6-1). The length of the nozzle is 70 mm. Two strong neodymium magnets held the nozzle in place and made it easy to remove. By applying a DC bias voltage superposed on the AC voltage, the plasma can be used as a charger and the uniformly charged particles can be collected on the grounded plasma reactor chamber wall (Figure 6-1). To use the plasma as a charger an additional DC power supply (Spellman SL1200 +10 kV, USA) was added to the setup, which was connected between the SDBD plate electrodes with a 5 MΩ resistor.

Equipment for electrical and thermal measurements
The high voltage was measured by a Tektronix P6015A high voltage probe and the current was measured by a Pearson 2877 current monitor. Both were connected to a LeCroy WaveSurfer 44Xs oscilloscope. A Neoptix ReFlex 4-channel fiber optic temperature thermometer (Neolink, USA) was used to measure the temperature surrounding the plasma with a PTFE-coated Neoptix T1 optical temperature probe. The optical sensor was placed 8 mm above the centre of the SDBD plate during the experiments. The step-response time of the system was 250 ms.

7.2.3 Characterization of the product

Scanning electron microscopy (SEM) was used to investigate the particles by a Hitachi S4700 electron microscope (Hitachi Scientific Ltd., Japan). A sputter coating apparatus (Bio-Rad SC 502, VG Microtech, England) was applied to induce electric conductivity on the surface of the samples. The air pressure was 1.3–13.0 mPa. NIF particle diameter distributions were obtained by analyzing several SEM images with the ImageJ software environment [24, 25]. Over 150

individual particle measurements were made in at least five different images in order to determine the particle size distribution.

X-ray powder diffraction (XRPD) was carried out in order to determine the crystalline form of the produced materials. Samples were measured with a Bruker D8 Advance diffractometer (Bruker AXS GmbH, Karlsruhe, Germany). Data collection was carried out at room temperature using monochromatic Cu K α1 radiation (α = 0.154060 nm) in the 2 theta region between 3° and 50°, step size 0.02 degrees 2θ. Data evaluation was done with the Bruker program EVA.

Differential scanning calorimetry (DSC) was employed to investigate the melting behavior of the NIF samples. The Mettler Toledo thermal analysis system with the STAR^e thermal analysis program V9.1 (Mettler Inc., Schwerzenbach, Switzerland) was applied to characterize the thermal behavior of the products. The DSC measurements were done with 2–5 mg of NIF in the temperature range between 25 °C and 300 °C. The heating rate was 5 °C min^{-1}. Argon was used as carrier gas at a flow rate of 10 L h^{-1} during the DSC investigation.

FT-IR spectroscopy was used to investigate the chemical stability of the drug. FT-IR spectra were measured on an AVATAR 330 FT-IR apparatus (Thermo Nicolet, USA), in the interval 400–4000 cm^{-1}, at 4 cm^{-1} optical resolution. Standard KBr pellets were prepared from 150 mg of KBr pressed with 10 ton and the calculated amount of the samples containing 0.5 mg of NIF.

Dissolution rate measurements

The dissolution of different powder samples, containing the same amount of drug (14 mg according to the dose), was determined according to the paddle method [26]. A phosphate buffer solution (50 mL, pH 1.2 ± 0.1) at 37 ± 0.5 ºC was used as a dissolution medium and the rotation speed of the paddles was set at 100 rpm. At certain time intervals 2 mL solution samples were withdrawn and filtered (cut-off 0.2 μm, Minisart SRP 25, Sartorius, Germany) and the amount of dissolved drug was determined by an ATI-Unicam UV2-100 UV/Vis spectrophotometer. The withdrawn samples were replaced by fresh medium as it is done in common practice. The dissolution behavior was determined in the presence and absence of excipients both for conventional and submicron-sized NIF. D-Mannitol and Poloxamer 188 were used as excipients to help the de-aggregation and increase the wettability of the NIF crystals. D-Mannitol acts as a carrier, which provides the homogeneous distribution of the NIF crystals, Poloxamer 188 helps as a stabilizer by wetting the particles to minimize (or inhibit) the aggregation of the drug [27]. Table 4-1 shows the ratio of the

excipients added to the drug. The physical mixtures were prepared using a Turbula mixer for 10 minutes as suggested by the manufacturer (Willy A. Bachofen Machinenfabrik, Switzerland). A homogeneous distribution of the NIF and the excipients was achieved by this mixing method without kneading or hard mechanical effects.

7.3 Results and Discussion

First, the plasma crystallization process is described, and its parameters are investigated for producing the desired products at a low temperature. Next, the produced NIF and Poloxamer 188 particles are characterized and their dissolution profiles are determined.

7.3.1 Plasma crystallization

SDBD plasma crystallization is a new process for drug synthesis in the submicron size range. Plasma is an ionized gas that consists of electrons, ions and neutral species, which are in an excited or ground state [28]. In the SDBD plasma, a large number of filamentary discharges (microdischarges) is produced. These microdischarges can ionize for instance aerosol droplets, and dissociate them into smaller droplets, or functionalize the surface of materials by adding or removing chemical groups without changing bulk properties or appearance [29]. During plasma crystallization, solution droplets, created by a nebulizer are sprayed into the plasma. The plasma has two functions. First, the plasma acts as a heat source and thus enhances the evaporation rate of the solvent droplets. Secondly, the plasma electrically charges the solution droplets. As the surface charge of a droplet reaches a critical value (Rayleigh-limit), electrostatic forces overcome the surface tension and the droplet disrupts into a myriad of smaller droplets to reduce the surface charge density by creating more droplet surface area [30]. This disruption process is called Coulomb fission and results in micron-sized droplets of solution [31].

Upon solvent evaporation, supersaturation for crystallization is created in the solution droplets [32]. At some point the driving force for crystallization becomes sufficiently large for crystal nucleation and growth to occur. At sufficiently low concentrations nucleation of the dissolved organic compound will only start after the formation of the micron-sized solution droplets. Nano- or

submicron-sized crystals will then be formed upon evaporation of all solvent from the micron-sized droplets. Figure 7-1 shows the schematics of the process.

By applying a DC bias voltage superposed on the AC voltage, coalescence of the droplets is avoided while the particles can be collected on a specific location (Figure 7-1). By applying the DC bias the charging effect of the droplets within the process is enhanced as described in a patent by Gundlach [33]. By this way coalescence of the droplets and aggregation of the formed crystals is prevented because of their unipolar charges. Furthermore, by the application of the DC bias voltage, the charged crystals can be collected electrostatically with high efficiency using a grounded collector plate [34], where they loose their surface charge.
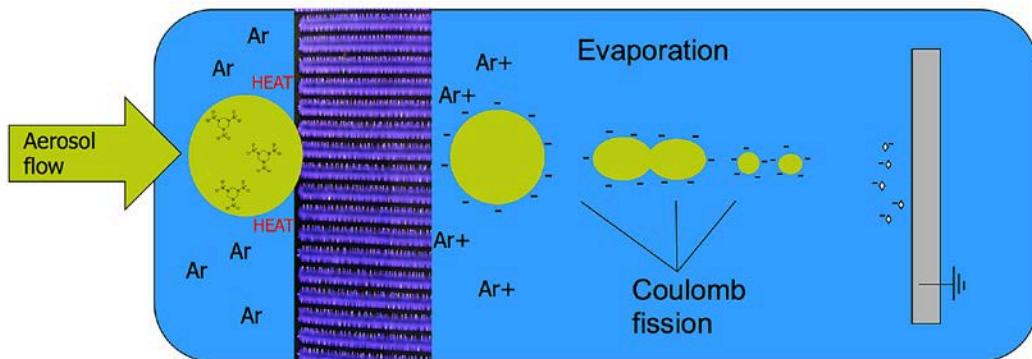
Figure 7-1. Process scheme of plasma aided crystallization. The NIF-acetone aerosol is carried by argon gas above the SDBD plate and interacts with the plasma. The plasma heats and charges the droplets, which results in enhanced evaporation of the solvent and probably Coulomb-fission of the droplets. At some point the driving force for crystallization becomes sufficiently large for crystal nucleation and growth to occur. After the solvent is evaporated completely, the charged crystals are collected on the grounded reactor wall, where they loose their surface charge.

7.3.2 Plasma process parameters

Table 7-1 shows the process parameters used for submicron-sized NIF production. Using a solution concentration of 20 mg mL^{-1} NIF in acetone, an argon flow rate of 11 L min^{-1}, a 10 kHz pulse excitation over the 3.7 kV potential difference and a DC bias voltage of +2 kV, submicron-sized NIF crystals were produced. The 11 L min^{-1} argon flow rate through the micro-channels of the nebulizer results in approx. 4.5 mL min^{-1} solution sprayed into the plasma reactor chamber with a solution concentration of 20 mg mL^{-1} NIF in

acetone is used. The process parameters for submicron-sized organic crystal production are investigated in detail in *Chapter 6*.

Table 7-1. The process parameters for the reference plasma crystallization experiment for NIF: AC peak-to-peak potential difference (ΔU), DC bias potential difference (ΔU_{bias}), solution concentration (c), frequency (f) and argon gas flow rate (φ). Using these parameters, a homogeneous surface plasma is formed on the SDBD plate.

ΔU [kV]	ΔU_{bias} [kV]	c [mg mL^{-1}]	f [kHz]	φ [L m^{-1}]
3.7	+2	20	10	11

Plasma temperature

Figure 7-2 shows how the temperature profile developed 8 mm above the centre of the SDBD plate during the plasma crystallization process. The average temperature above the SDBD plasma increased rapidly until 42 °C. Then the temperature decreased to around 40 °C and became stationary at that temperature. The temperature at the plate surface might be higher.
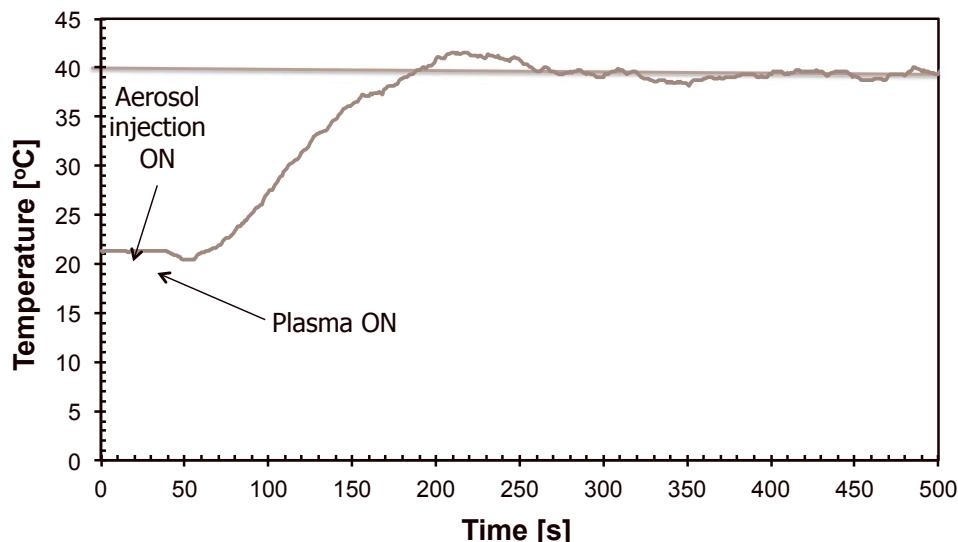
Figure 7-2. Temperature profiles measured 8 mm above the plasma surface. A stationary temperature around 40 °C was present during the submicron-sized particle generation.

CHAPTER 7

7.3.3 Product characterization

The produced NIF crystals are somewhat spherical, with a mean size of 700 nm (Figure 7-3). The submicron-sized NIF crystals are aggregated into 5-6 µm sized clusters, which can be seen by the clearly visible border lines of the individual NIF crystals. The submicron NIF crystals possibly stick together due to the strong interactions between the hydrophobic crystal surfaces or due to static charging of these small crystals.
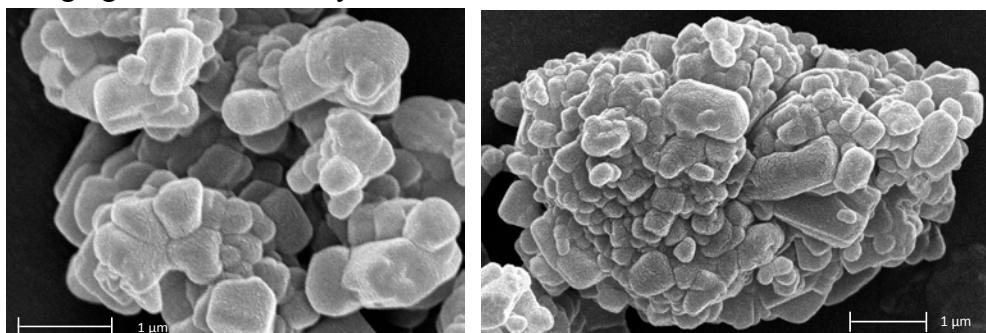
Figure 7-3. Left: NIF crystals in the size range of 400-1000 nm Right: A 6 µm aggregate of the submicron NIF crystals.

Excipient

The Poloxamer 188 was also produced by plasma crystallization, with the same process parameters used for NIF (Table 7-1). The product is from spherical to irregular shape in the size range of 1-3 µm in diameter (Figure 7-4), which is larger than the NIF made by plasma crystallization. The Poloxamer 188 formed a large amount of irregular shaped large crystals that are probably agglomerates. Possible explanation for the relatively large size and tendency for agglomeration can be the semi-crystalline nature and the macromolecular structure of the Poloxamer 188, which leads to a viscous solution. In case the initial solution is highly viscous in the plasma crystallization process, the product is generally larger, and agglomerates can be present.
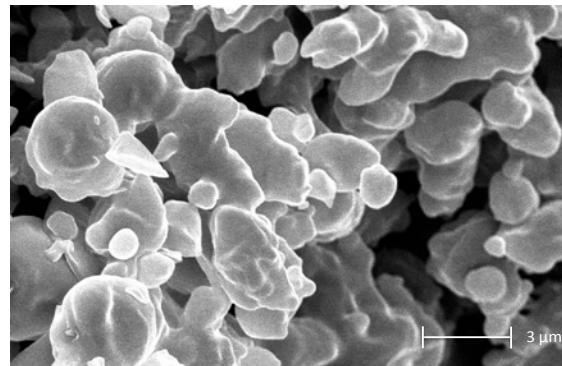
Figure 7-4. Poloxamer 188 in the micron size range produced by cold plasma technology.

7.3.4 Solid state analysis (DSC, XRPD, FT-IR)

Structural characterizations were performed to check the crystallinity of the produced NIF crystals and Poloxamer 188. The melting point of the submicron-sized NIF was measured to be 202.9 °C, slightly lower than the original material (203.4 °C) and than the literature values [19] (Figure7-5). The lower melting point could be explained by the relatively large surface area and thus increased total surface free energy compared to the original material [35]. Poloxamer is a semi-cyrstalline material with melting point around 56 °C. The melting point decreased slightly to 53.6 °C, probably again due to the size reduction of the material.

There is a relation between the crystallinity and normalized heat of melting of the samples [36]. The DSC results show that the normalized heat of melting for the submicron-sized NIF was 113.6 J g^{-1}, 80% of that for the conventional NIF (140.4 J g^{-1}). This indicates that the plasma-made NIF is 80% crystalline and 20% amorphous. The heat of melting for the plasma-made Poloxamer 188 is 93% of that for the conventional material, indicating a 7% decrease in crystallinity due to the plasma process.
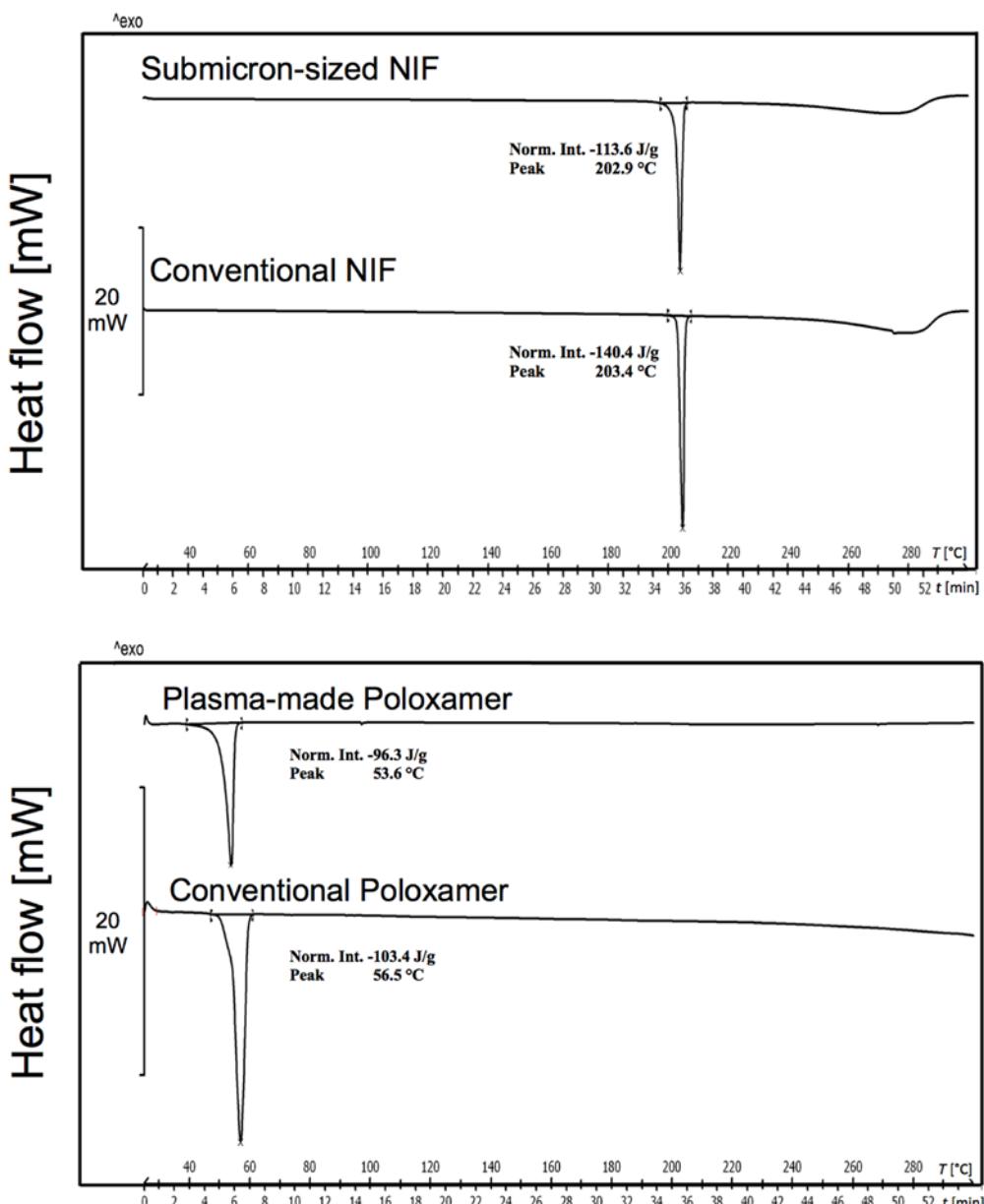
Figure 7-5. DSC curves of the conventional NIF and the submicron-sized NIF (top) and of the conventional Poloxamer 188 and plasma-made Poloxamer 188. The melting points of both produced materials are slightly lower than the conventional ones.

The XRPD patterns of the submicron-sized NIF crystals showed the single known crystal form for both NIF [37] and Poloxamer 188 (Figure 7-6).
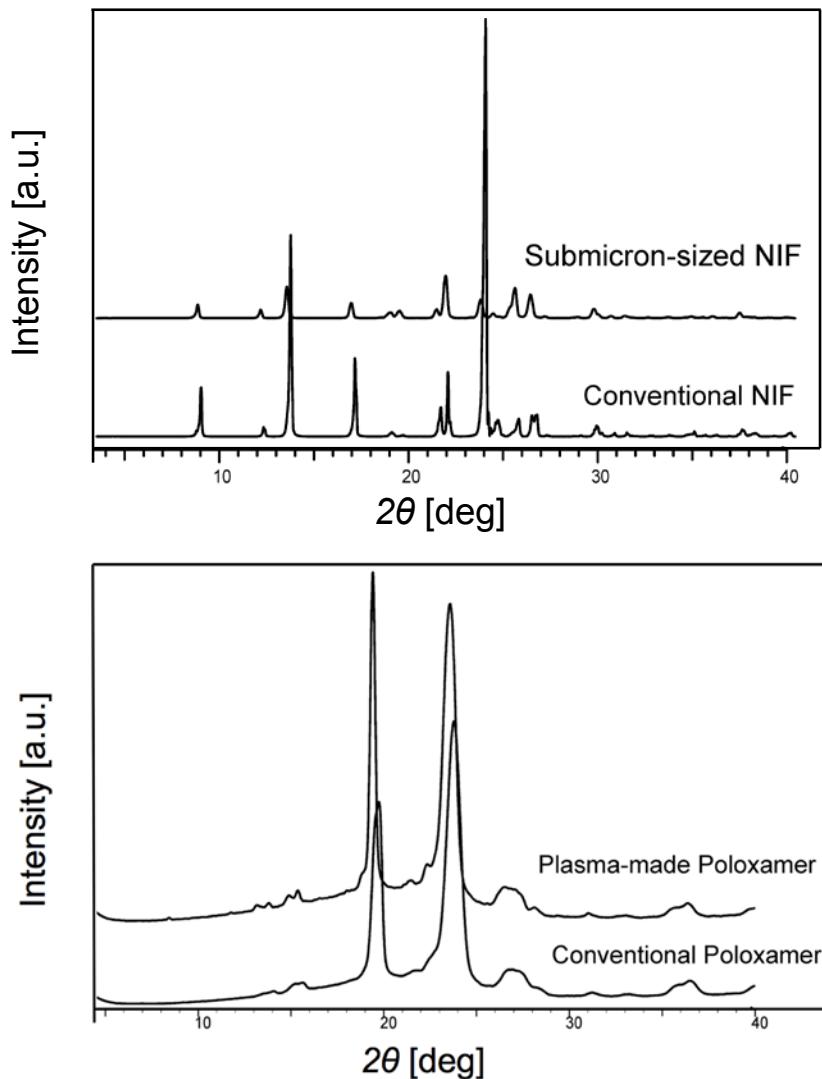
Figure 7-6. XRD pattern of the conventional and submicron NIF crystals (top) and of the conventional and plasma-made Poloxamer 188 (bottom).

FT-IR spectroscopy was performed to investigate the possible changes in the molecular structure. The IR spectra showed that both the produced NIF and Poloxamer 188 did not alter chemically in the process, since no physical transition or decomposition was observed (Figure 7-7).
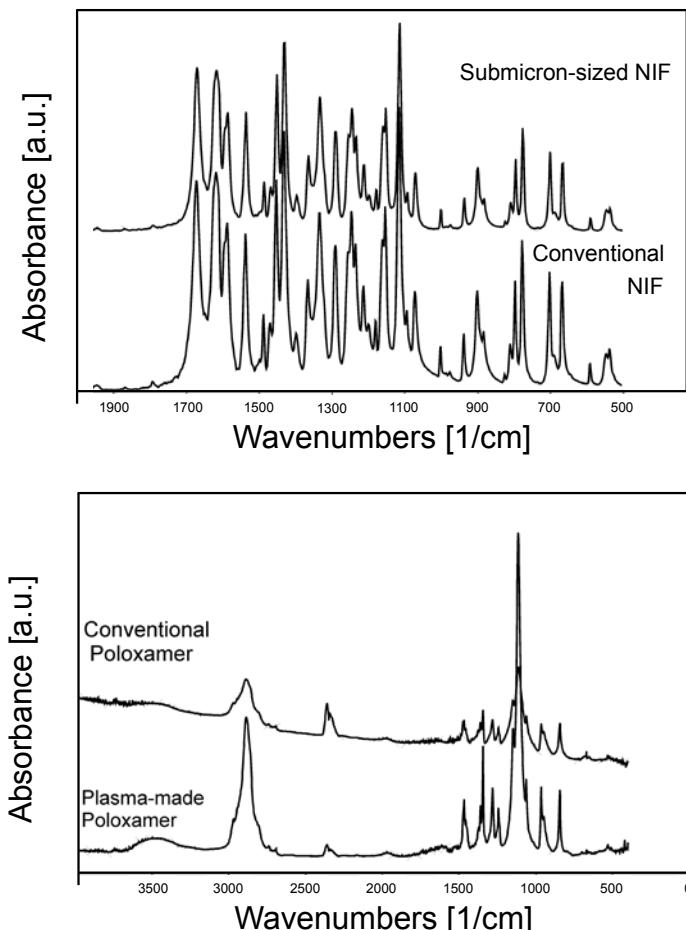
Figure 7-7. FT-IR spectra of the conventional and submicron-sized NIF crystals (top) and the conventional and plasma-made Poloxamer 188 (bottom). No change was observed in the molecular structure of the produced NIF and Poloxamer 188.

7.3.5 Dissolution rate measurements

Dissolution rate measurements were performed at gastric pH (pH 1.2). While the conventional NIF has a low dissolution rate (31% of the drug dissolving in the first hour), that of the conventional NIF in presence of the conventional excipients D-Mannitol and Poloxamer 188 is already somewhat higher with

40% of the drug dissolving in the first hour (Figure 7-8). The submicron-sized NIF without the excipients had a slightly higher dissolution rate, with around 50% dissolving in 1 h. Interestingly, by mixing the conventional NIF with the plasma-made Poloxamer 188 and conventional D-Mannitol, the dissolution rate increased significantly: 81% of the NIF was dissolved within 1 h due to the increased efficiency of the plasma-made Poloxamer 188. The dissolution rate further increased upon using the submicron-sized NIF with the plasma-made Poloxamer 188 and conventional D-Mannitol: 76% of NIF was already dissolved after 15 min while as much as 96% was dissolved in 1 h. Within 90 min the NIF was completely dissolved.

In general, the excipient, Poloxamer 188, de-aggregates and increases the wettability of the NIF crystals, which helps the dissolution behavior of the NIF crystals [38, 39]. Apparently, the Poloxamer 188 helps the dissolution of the hydrophobic NIF crystals more efficiently when its size is reduced. Via size reduction, significantly higher surface area can be achieved that leads to an increased interaction between the drug and excipient sites, which results in more efficient de-aggregation of the NIF.

When the micron-sized, plasma-made Poloxamer 188 is used with the submicron NIF, it can very rapidly and effectively disintegrate the aggregated NIF clusters, and due to the extremely high surface area of NIF crystals, rapid dissolution can occur. Thus preparation of submicron-sized NIF and few micron-sized Poloxamer 188 can result in substantially higher drug liberation and absorption than can be achieved by the conventional compounds. The synergy between the aggregation prevention of the excipients and the increased surface area of the submicron-sized NIF result in a substantially increased dissolution rate of NIF.
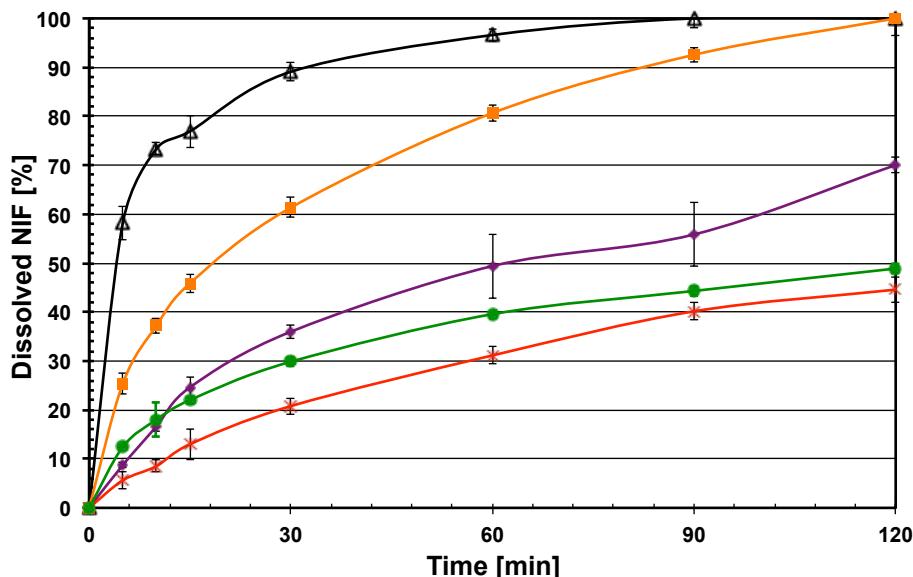
Figure 7-8. Dissolution profiles of the conventional NIF and the submicron NIF with and without the excipient D-Mannitol and Poloxamer 188 at pH 1.2. Only 20 % of the conventional NIF (×) was dissolved into the solution after 30 min. Using the conventional NIF with the conventionally sized excipients (●), 30% of the drug was dissolved after 30 min. The dissolution of the submicron-NIF (◆) was slightly higher, 36 % of the drug was dissolved in the same time. By adding the plasma-made Poloxamer 188 and conventional D-Mannitol to the conventional NIF (■), 61% of the drug was dissolved in 30 min. When the submicron-sized NIF was applied with the plasma-made Poloxamer 188 and conventional D-Mannitol (Δ), the dissolution increased to 89% after 30 min.

7.4 Conclusions

Via the size reduction of the drug particles and/or excipient particles, it is possible to enhance the dissolution profile of poorly soluble active pharmaceutical ingredients and therefore increase their bioavailability. Submicron-sized niflumic acid crystals with a mean size of 700 nm were produced by atmospheric pressure cold plasma crystallization. The submicron crystals aggregated into 5-6 micron particle clusters due to the large specific surface area and/or static energy of the crystals. The product was highly crystalline and had a slightly lower melting point than the conventional niflumic acid. Its commonly used excipient, Poloxamer 188 in the size range of 1-3 µm

was also produced by atmospheric pressure cold plasma crystallization. Agglomeration of the Poloxamer 188 particles was observed, which was probably due to its macromolecular structure and semi-crystalline nature. Dissolution rate measurements showed that by using the produced few micron-sized Poloxamer 188 with the conventional niflumic acid already leads to a substantial increase in the dissolution rate. When the plasma-made Poloxamer 188 was applied with the produced submicron-sized niflumic acid crystals, the dissolution rate increased even more and the niflumic acid dissolved completely within 90 minutes. Atmospheric pressure cold plasma crystallization is an interesting crystallization technique that leads to submicron particles that can have significantly improved properties such as dissolution rate.

References

[1]   A. S. Myerson *Handbook of Industrial Crystallization* Butterworth-Heinemann Ltd.: Oxford, 1993.

[2]   N. J. Babu, A. Nangia *Crystal Growth & Design 10th Anniversary Perspective* 2011, 2662-2679.

[3]   M. P. Patil, A. B, Pandit *Ultrasonics Sonochemistry* 2007, 14, 519-530.

[4]   C. Leuner, J. Dressmann *European Journal of Pharmaceutics and Biopharmaceutics* 2000, 50, 47-60.

[5]   B. E. Rabinow *Nature Reviews Drug Discovery* 2004, 3, 785-796.

[6]   V. B. Patravale, A. A. Date, R. M. Kulkarni *Journal of Pharmacy and Pharmacology* 2004, 56, 827-840.

[7]   F. Kesisoglou, S. Panmai, Y. Wu *Advanced Drug Delivery Reviews* 2007, 59, 631-644.

[8]   R. H. Müller, K. Peters *International Journal of Pharmaceutics* 1998, 160, 229-237.

[9]   G. G. Liversidge, P. Conzentino *International Journal of Pharmaceutics* 1995, 125, 309-313.

[10]   M. Trotta, M. Gallarete, F. Pattarino, S. Morel *Journal of Controlled Release* 2001, 76, 119-128.

[11]   K. Peters, S. Leitzke, J. E. Diederichs, K. Borner, H. Hahn, R. H. Müller, S. Ehlers *Journal of Antimicrobial Chemotherapy* 2000, 45, 77-83.

[12]   J. Hecq, M. Deleers, D. Fanara, H. Vranckx, K. Amighi *International Journal of Pharmaceutics* 2005, 299 167-177.

[13]   F. Debuigne, J. Cuisenaire, L. Jeunieau, B. Masereel, J. B. Nagy *Journal of Colloid and Interface Science* 2001, 243, 90-101.

[14]   C. Suryanarayana *Progress in Materials Science* 2001, 46, 1-184.

[15]   N. Radacsi, R. Ambrus, T. Szunyogh, P. Szabó-Révész, A. I. Stankiewicz, A. E. D. M. van der Heijden, J. H. ter Horst *Crystal Growth & Design* 2012, 12, 3514-3520.

[16]   M. Simor, A. Fiala, D. Kovacik, P. Hlidek, A. Wypkema, R. Kuipers *Surface and Coatings Technology* 2007, 201, 7802.

[17]   V. Vons, Y. Creyghton, A. Schmidt-Ott *Journal of Nanoparticle Research* 2006, 8, 721-728.

[18]   N. Carneiro, A.P. Souto, E. Silva, A. Marimba, B. Tena, H. Ferreira, V. Magalhaes *Coloration Technology* 2001, 117, 298.

[19]   S. Budavari, M. J. O'Neil, A. Smith, P. E. Heckelman *The Merck Index,* 11th Edition Merck & Co.: Rahway, New Jersey, 1989.

[20]   J. E. F. Reynolds *Martindale: The Extra Pharmacopoeia*, 31st Edition The Royal Pharmaceutical Society: London, 1996.

[21]   K. Takács-Novák, A. Avdeef, K.J. Box, B. Podányi, Gy. Szász *Journal of Pharmaceutical and Biomedical Analysis* 1994, 12, 1369-1377.

[22]   R. Ambrus, Z. Aigner, C. Dehelean, C. Soica, P. Szabó-Révész *Revista de Chimie* 2007, 58, 60-64.

[23]   J. Salge *Surface and Coatings Technology* 1996, 80, 1-7.

[24]   M. D. Abramoff, P. J. Magelhaes, S. J. Ram *Biophotonics International* 2004, 11, 36-42.

[25]   R. Remias, Á. Kukovecz, M. Daranyi, G. Kozma, S. Varga, Z. Kónya, I. Kiricsi *European Journal of Inorganic Chemistry* 2009, 24, 3622-3627.

[26]   *European Pharmacopoeia*, 3rd Edition Council of Europe: Strasbourg, 1996, 128-129.

[27]   J. K. Aronson *Meyler's Side Effects of Drugs: The international Encyclopedia of Adverse Drug Reactions and Interactions,* 15th Edition Oxford 2006, 2203-2204.

[28]   B. Eliasson, U. Kogelschatz *IEEE Transactions on Plasma Science* 1991, 19, 1063-1077.

[29]   J. Rahel, M. Simor, M. Cernak, M. Stefecka, Y. Imahori, M. Kando *Surface and Coatings Technology* 2003, 169 604-608.

[30]   J. W. S. (Lord) Rayleigh *Philosophical Magazine* 1882, 14, 184-186.

[31]   K. Suzuki, H. Matsumoto, M. Minagawa, M. Kimura, A. Tanioka *Polymer Journal* 2007, 39, 1128-1134.

[32]   J. W. Mullin *Crystallisation,* 4th Edition Butterworth-Heinemann Ltd.: Oxford, 2001.

[33]   R. W. Gundlach *DC biased AC corona charging* U.S. Patent 6,349,024. February 19, 2002.

[34]   M. Rhodes *Introduction to Particle Technology,* 2nd Edition John Wiley & Sons Ltd.: West Sussex, 2008.

[35]   G. C. Yang, F. D. Nie, H. Huang *Journal of Energetic Materials* 2007, 25, 35-47.

[36]   M. Wagner *Thermal analysis in practice – DSC evaluations* Mettler-Toledo AG: Schwerzenbach, 2009, 90-132.

[37]   H. M. Krishna Murthy, M. Vijayan *Acta Crystallographica* 1979, B35, 262-263.

[38]   I. Ghosh, S. Bose, R. Vippagunta, F. Harmon *International Journal of Pharmaceutics* 2011, 409, 260-268.

[39]   D. Myers *Surfaces, Interfaces and Colloids: Principles and Applications* 2nd Edition Weinheim: Wiley-VCH, 1999.

8 Crystallization of isonicotinamide in a strong electric field

This research investigates the effect of a strong DC electric field on the polymorphic control of a model pharmaceutical compound, isonicotinamide, during cooling crystallization from 1,4-dioxane. When an electric field as strong as 5.6×10^5 V m^{-1} was applied, crystals formed only on the anode. The crystal growth rate was measured to be significantly higher in the presence of the electric field than in its absence. In the absence of the electric field metastable form I of isonicotinamide was crystallized, while in the presence of the electric field the stable form II was obtained. In our view the localized formation of form II crystals on the anode and the increase in crystal growth rate are due to the substantial local supersaturation increase around the anode. It appears that the electric field has the potential to be used towards polymorphic control in a crystallization process.

8.1 Introduction

Polymorphism is the ability of a solid material to exist in more than one form or crystal structure [1]. It plays an important role in the crystallization of industrially important substances, such as pharmaceuticals, food, agrochemicals, dyes and explosives [2-6]. Polymorphism is especially important for the pharmaceutical industry, where often one particular polymorph is wanted [1, 7]. Different polymorph substances may exhibit great differences in chemical or physical properties (e.g. solubility, dissolution rate, bioavailability, density, melting point, and morphology) [8, 9]. Polymorphic formation is primarily determined by nucleation and crystal growth, which are governed by thermodynamics, kinetics, and fluid dynamics [10].

Electric field may influence thermodynamics, kinetics and fluid dynamics and thus also the crystallization behavior. Recently a number of studies appeared which investigated the effect of electric fields on these phenomena [11-13]. By changing the crystallization behavior of a compound, nucleation and growth can be influenced in such a way that a different polymorph can be obtained under the influence of an electric field. Aber et al. have reported that by applying a constant electric field of 6×10^5 V m^{-1} to supersaturated aqueous glycine solutions, the γ polymorph can be obtained, while in the absence of the electric field always the α form crystallizes [14].

Isonicotinamide (INA) was used as the model compound. INA is a pharmaceutical that possesses strong anti-tubercular, anti-pyretic, and anti-bacterial properties [15], and is commonly used as a co-former in co-crystallization for tuning the physical properties (e.g. bioavailability) of drug molecules [16]. INA possesses favorable properties for our research, such as a distinct polymorphic shape and a high dipole moment (3.68 D [17]). It was previously studied that self-association of INA in solution controls the polymorph crystallization [18].

In this chapter the effect of a strong DC electric field on the solution crystallization behavior of INA is investigated and discussed. Two experimental setups were used to investigate the electric field effects, and the crystallization behavior, fluid dynamics and crystalline product were analyzed.

8.2 Experimental methods

8.2.1 Materials

Isonicotinamide (pyridine-4-carboxamide) with ≥99% purity was purchased from Sigma-Aldrich. For the crystallization processes different solution concentrations were prepared with 99.8% pure 1,4-dioxane (1,4-dioxacyclohexane) purchased form Sigma-Aldrich.

8.2.2 Solution preparation

Different concentrations of INA (c = 17, 20, 25, 30 and 35 mg mL^{-1}) were dissolved in 1,4-dioxane, and heated up to 65 °C in a stirred vessel until a clear solution was obtained. Prevailing supersaturation ratios of S = 1, 1.1, 1.4, 1.7 and 2.05 were present in the crystallization system (respectively to the concentrations) at temperature T = 25°C.

8.2.3 Experimental setup for investigating the effects of the electric field

Two setups were used to study the effects of the electric field (Figure 8-1). The first was an 8 mL glass vial, with two copper rod electrodes (Ø 1 mm) present in parallel. The electrodes were going through a special PVC cap, which closed the glass vial. The electrodes had a length of 5 cm inside the glass vial, and almost reaching the bottom of the glass vial leaving a 3 mm gap. The distance between the electrodes was 6 mm. Within the solution contained in the setup, a constant but inhomogeneous electric field with a maximum of around 5.6 × 10^5 V m^{-1} could be generated by a DC power supply (FUG HCN 14, Germany). A Crystalline multiple reactor station (Avantium Phamatech BV, Amsterdam) was used to provide a controlled crystallization environment and visualization by an on-board camera system for the *in situ* investigation of the electrode and crystals forming on it. In the text this setup is referred to as the **inhomogeneous field setup**.

The other experimental setup was made of a glass cuvette (Labomed, 45 × 12.5 × 3.5 mm, 1.7 mL) with two copper plate electrodes (thickness 1 mm) mounted onto its smallest inside walls. The distance between the electrodes was 8 mm. The solution was between the two copper electrodes. The DC power supply was connected to the electrodes. Within the solution contained in the

setup, between the two electrode plates, a more or less homogeneous electric field up to 5.6×10^5 V m^{-1} could be generated. INA-1,4-dioxane solution ($c = 35$ mg mL^{-1}) was cooled down from 65 °C to room temperature by natural cooling, while the electric field was applied. Potential differences of 5, 7.5 and 10 kV were applied, which created a homogeneous electric field of 2.84×10^5, 4.26×10^5 and 5.6×10^5 V m^{-1} respectively. In the text this setup is referred to as the **homogeneous field setup**.

In order to reach as high as possible electric fields, the electrodes were inside the solution in both systems. Both experimental setups were operated without stirring during crystallization.
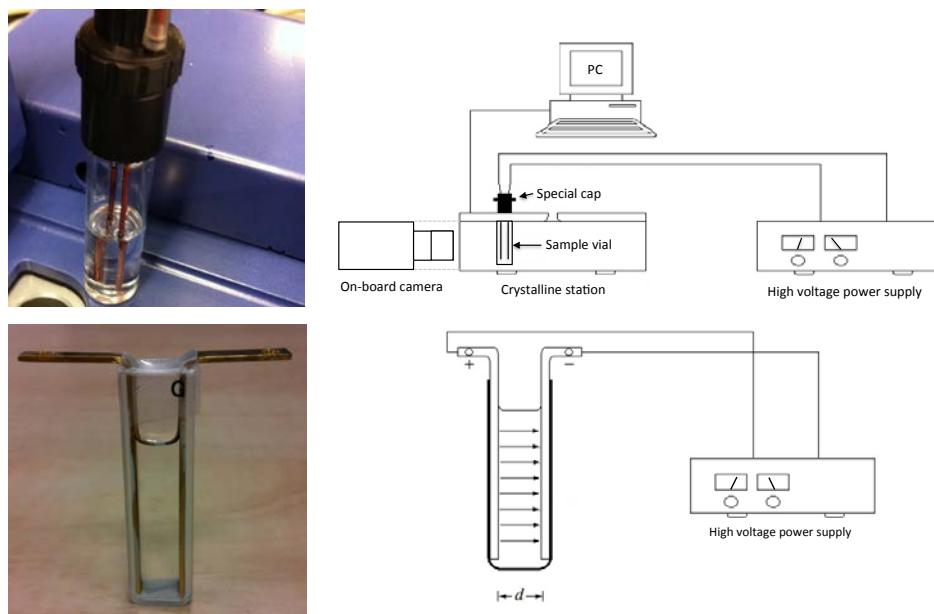
Figure 8-1. Top: The inhomogeneous field setup with the two copper electrodes going through a special PVC cap, and the schematics showing the sample placement in the Crystalline station for visualization experiments. The sample solution or suspension is placed in the glass vial, and the rod-shaped copper electrodes inside the solution are connected to the high voltage DC power supply. **Bottom:** The homogeneous field setup and a schematic drawing of the electrodes mounted onto the inside walls of a glass vial, and connected to the high voltage power supply.

8.2.4 Suspension visualization

The electric field effect on a suspension of INA-1,4-dioxane was studied in both experimental setups. Clear solutions of INA were prepared in 1,4-dioxane by heating the samples above their saturation temperature. Then, by natural cooling, the samples were allowed to cool down to 25 $^{\circ}$C, and a suspension was obtained. Then the electric field was applied, and its effects were recorded by a camera system. The initial solution concentration was 35 mg mL^{-1}.

8.2.5 Induction time measurements in the presence of the electric field

In the presence of a continuously applied 5.6×10^5 V m^{-1} electric field the induction times were measured in the Crystalline multiple reactor station for INA supersaturation ratio of $S = 2.05$. For the measurements a 100 mL solution was prepared by dissolving the INA crystals in the 1,4-dioxane. The solution was kept at 90 °C in a stirred vessel for at least 3 hours to make sure that the crystals were dissolved. A bottle-top dispenser was used to dispense 4 mL of clear solution into each vial. There was no stirrer applied in this case, since a magnetic stirrer could cause an electric breakdown between the electrodes. The clear solution was quickly cooled down in the Crystalline setup to 25 °C with a rate of 5 °C min^{-1}. The moment the solution reached a temperature of 25 °C was taken as time zero, after which a constant temperature of 25 °C was maintained. At some point in time, crystals grew on the anode, which was visualized by the on-board camera system of Crystalline. The difference between the time at which the first crystal appeared on the anode and time zero was taken as the induction time.

8.2.6 Induction time probability determination

The probability distribution of the induction time can be determined from a large number of induction time measurements at constant supersaturation, temperature, and volume [19]. For N isolated experiments, the probability $P(t)$ to measure an induction time between zero and time t is defined as

$$P(t) = \frac{N^+(t)}{N} \tag{8.1}$$

where $N^+(t)$ is the number of experiments in which crystals are detected at time t.

8.2.7 Crystal growth rate measurements

The crystal growth rate in the presence of the electric field was studied in an unstirred cooling crystallization process at a starting concentration of 35 mg mL^{-1} isonicotinamide in dioxane. For this, the Crystalline Particle Viewer station was used to visualize the crystals appearing on the electrode during the cooling crystallization of INA. This device is capable to take images every second and with the help of an integrated size scale, it is easy to follow the size development of the crystals growing on the electrode. The average crystal growth rate during the crystallization process can be estimated by dividing the size increase by the time period at which the growth occurred. 4 mL solutions of INA were prepared in 1,4-dioxane. The samples were heated above their saturation temperature in order to obtain a clear solution. Then the electric field was applied, and the solution was cooled down to 25 °C using a cooling rate of 5 °C min^{-1}.

The crystal growth rate in the absence of the electric field was determined after turning the electric field off. This was done at the moment the first crystals were visible on the anode surface. This procedure was necessary since crystals did not form on the electrode in the absence of an electric field, but rather formed in the bulk solution of which it is difficult to track individual crystals for crystal growth rate measurements.

8.2.8 Product characterization

Solid phase Raman spectroscopy was used to distinguish the stable form of INA from the metastable ones after each crystallization experiment [18]. The Raman spectra were recorded with a Hololab series 5000 Raman spectroscope (Kaiser Optical System Inc., USA) by excitation radiation at 785 nm using a NIR probe.

Thermogravimetric analysis (TGA) was used to characterize the thermal behavior of the produced crystals. A Perkin Elmer TGA7 was used to measure the thermal stability upon heating. The samples were measured in a nitrogen atmosphere, with a heating rate of 10 °C min^{-1} and a purge rate of 20 mL min^{-1}.

NMR spectroscopy was performed to investigate the molecular structure of the product. A clear solution of INA was made in DMSO-d6 for the solution NMR spectroscopy measurements. A Bruker Avance-400 NMR spectrometer at 400 MHz was used at 25 °C using 5 mm sample tubes.

X-ray powder diffraction (XRPD) was carried out afterwards in order to verify the crystalline form of the recrystallized materials. XRPD patterns were

recorded in a Bragg-Brentano geometry of a Bruker D8 Advance diffractometer equipped with a Vantec position sensitive detector and graphite monochromator. Data collection was carried out at room temperature using monochromatic Co Kα radiation (λ = 0.179026 nm) in the 2θ region between 10° and 60°, with a step size of 0.034 degrees 2θ and a step time of 1 s. The sample was placed on a Si {510} substrate and rotated during measurement. Data evaluation was done with the Bruker program 'EVA'.

8.3 Results

In this section the crystallization process in the presence and absence of the electric field is characterized. The effects of the electric field on cooling crystallization are investigated both theoretically and experimentally. The electric current is measured upon establishing an electric field in the homogeneous field setup. Then the effects of both a strong inhomogeneous and a strong homogeneous electric fields on the crystallization behavior of INA are investigated.

8.3.1 Model system

The INA-dioxane system was chosen to study the effect of an electric field on the polymorph crystallization behavior. One of the reasons for this is the ease of distinction between the stable form II and the metastable forms. The stable polymorph (form II) forms INA dimers and the metastable polymorph I, III, IV and V are arranged as chains (Figure 8-2) [18]. It can be seen from the figure that the pyridine group in the INA molecule does not participate in hydrogen bonding at the crystal structure of form II, contrary to all other currently known forms of INA. Another reason to choose this system is because of the weak hydrogen bonding capabilities of 1,4-dioxane. Therefore large effects of the solvent on the behavior of the INA solute in solution are not expected [18]. Furthermore, the non-polar solvent, 1,4-dioxane, as well as INA do not seem prone to undergo electrochemical reactions, and the solvent acts as an insulator. A last reason for choosing this system was the relatively large dipole moment of INA.
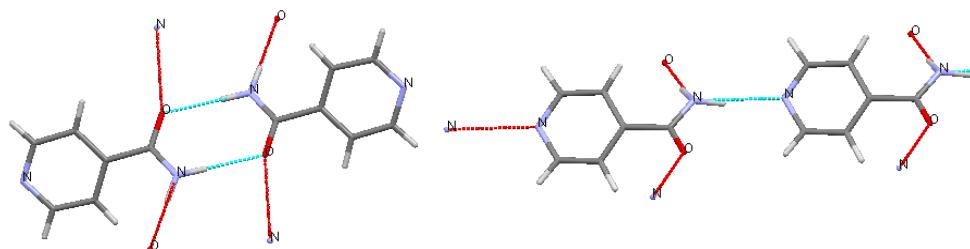
Figure 8-2. The hydrogen bonding motif in the stable form II of INA (left) and in the metastable forms I, III, IV and V (right).

8.3.2 Cooling crystallization in the presence of the electric field

During the cooling crystallization experiments in the presence of an inhomogeneous field (with a maximum of around 5.6×10^5 V m^{-1}) using a cooling rate of 5 $^{\circ}$C min^{-1}, crystals formed on the anode surface (Figure 8-3). There were no crystals visible at other locations or in the solution. Solid phase Raman spectroscopic and XRPD analysis showed that the crystalline material formed on the anode in the inhomogeneous field was a mixture of form II and I (Table 1).
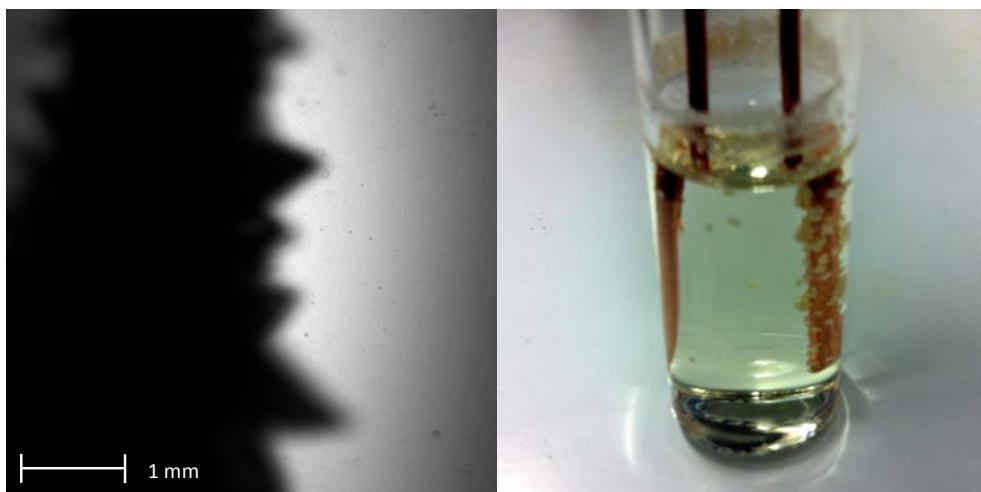
Figure 8-3. Left: Slightly out of focus faceted crystals growing on the surface of the anode in the presence of the inhomogeneous electric field. **Right:** Crystals on the anode in a vial after a solution crystallization in the presence of an electric field strength of 5.6×10^5 V m^{-1} (initial solution concentration of 35 mg mL^{-1}, a cooling rate 1 $^{\circ}$C min^{-1}).

Cooling crystallization experiments in the homogeneous field setup were performed at different electric field strengths (2.84×10^5, 4.26×10^5 and 5.6×10^5 V m^{-1}) under conditions of natural cooling. Also in the presence of a homogeneous field the crystals formed on the anode surface. The XRPD patterns of the recrystallized samples at an electric field strength of 2.84×10^5 and 4.26×10^5 V m^{-1} showed a mixture of INA form I and form II. When an electric field as strong as 5.6×10^5 V m^{-1} was applied, only the stable form II was crystallized on the anode. Using the same electric field strength in an inhomogeneous field still resulted in a mixture of polymorphs.

These results suggest that by applying a sufficiently high homogeneous electric field during the crystallization of the INA-1,4-dioxane system, the stable form II instead of form I can be obtained. A reason for obtaining a mixture of polymorphs in the presence of a strong inhomogeneous electric field may be due to the locally different electric field around the electrode. The two rod-shaped electrodes placed in parallel generate an electric field, which is the highest in between the two electrodes, and the field strength is decreasing towards the sides. The locations at the electrode with lower electric field strengths would result in mixtures of polymorphs while the locations with higher electric field strengths result in only form II.

Table 1. The parameters used during cooling crystallization in the absence and presence of the electric field E and the obtained polymorph of INA

Solution concentration [mg mL^{-1}]	Supersaturation ratio at 25 °C	Polymorph in the absence of the E	Polymorph in the homogeneous $<5.6 \times 10^5$ V m^{-1} E	Polymorph in the homogeneous $>5.6 \times 10^5$ V m^{-1} E	Polymorph in the inhomogeneous E
35	2.05	I	I+II	II	I+II

In the absence of the electric field crystallization took place in the bulk solution, even when the electrodes were in the solution. When the electric field was not applied, the metastable form I crystallized under all concentrations of 17-35 mg mL^{-1}. TGA validated that no solvates were present. The XRPD measurements confirmed that the recrystallized INA in the absence of the electric field was the metastable form I. Kulkarni et al. reported that the pure form II can be also achieved from solutions in dioxane without the electric field by using different crystallization conditions [18].

8.3.3 Effects of the electric field

In order to rule out the occurrence of reactions, the electric current of the INA-1,4-dioxane system was measured in the homogeneous field setup at a solution concentration of 35 mg mL^{-1}, at 65 °C. For the maximum electric field (5.6×10^5 V m^{-1}) applied at a potential difference of 9.7 kV (Figure 8-4, black line), the measured current was as low as 0.8 µA. When only 1,4-dioxane was used, no current could be measured (Figure 8-4, red line). Since the measured direct current in the presence of the solute molecules was very low (less than 1 µA), and there was no apparent gas generation in the crystallization vessel, redox reactions are not likely to occur [20]. If a reaction would occur, the measured current is too low to be able to convert a substantial amount of the present INA. The molecular structure of the crystallized product, furthermore, was confirmed by NMR spectroscopy to be INA.
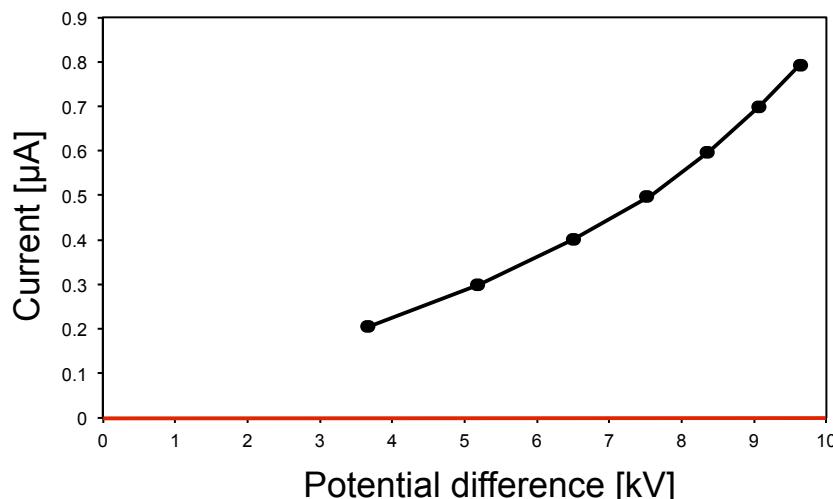
Figure 8-4. The measured current in the homogeneous field setup. In a clear solution of INA-1,4-dioxane ($c = 35$ mg mL^{-1}, $T = 65$ °C) a current of 0.3 µA is measured at a potential difference of 5.2 kV (black line). In case there is no solute in the solvent, and only the clear solution is present at the same temperature, no current was measured even at 10 kV potential difference (red line).

After ruling out the occurrence of a reaction, three possible effects of the electric field on the crystallization were identified. These effects will be discussed from the viewpoint of crystal nucleation.

The electric field can affect the nucleation thermodynamics and/or kinetics by changing the stationary nucleation rate [21]. The stationary nucleation rate J_s in the absence of the electric field is expressed by the following equation in the classical nucleation theory [21]:

$$J_s = zf^*C_0 \; exp \; (-B/\Delta\mu^2) \tag{8.2}$$

where z is the Zeldovich factor, f^* is the frequency of the monomer attachment to the nucleus, C_0 is the concentration of the nucleation sites, and B is a thermodynamic parameter.

The Zeldovich factor z in case of three-dimensional nucleation of a new phase is expressed by the following equation [21]:

$$z = 3\Delta\mu^2/4(\pi kTa^3\gamma^3)^{1/2} \tag{8.3}$$

where k is the Boltzmann-constant (1.38×10^{-23} JK^{-1}), T is the droplet temperature and γ is the interfacial energy.

The thermodynamic parameter B is defined as [21]:

$$B = 4c^3v_o{}^2\gamma^3/27kT \tag{8.4}$$

In our view both the frequency of the monomer attachment to the nucleus f^* and the chemical potential difference $\Delta\mu$ can be influenced by an electric field.

Electric field effect on nucleation thermodynamics
An electric field in a solution or a crystalline bulk material changes the chemical potential and thus the chemical potential difference between the two phases. This changed chemical potential difference then induces changes in the nucleation and growth rate. The contribution of the electric field E to the chemical potential difference $\Delta\mu_\varepsilon$ can be expressed with the following equation [21]:

$$\Delta\mu_\varepsilon = \Delta\mu + c_\varepsilon E^2 \tag{8.5}$$

where $\Delta\mu$ is the chemical potential difference in absence of an electric field and c_ε is a function of the relative permittivities:

$$c_\varepsilon = 3\varepsilon_0\varepsilon_m(\varepsilon_c - \varepsilon_m)\upsilon_0 / 2(\varepsilon_c + \varepsilon_m) \tag{8.6}$$

where ε_0 is the vacuum permittivity, ε_c is the relative permittivity (dielectric constant) of the crystalline material, ε_m is relative permittivity of the solution and υ_o is the molecular volume of the crystalline material. The nucleation work $W*$ in presence of an electric field can then be expressed by the following equation:

$$W^* = 16\pi\upsilon_0^{\,2}\gamma^3 / 3(\Delta\mu + c_\varepsilon E^2)^2 \tag{8.7}$$

where γ is the interfacial energy of the medium.

When the relative permittivity of the crystalline material is higher then the relative permittivity of the solution, $\varepsilon_c > \varepsilon_m$, the term c_ε is positive and the chemical potential difference is increased, lowering the nucleation work. When $\varepsilon_c < \varepsilon_m$ the nucleus formation is inhibited by the electric field. If $\varepsilon_c = \varepsilon_m$ the electric field has no effect on nucleation [21].

By replacing the chemical potential equation that takes into account the electric field effect (eq. 8.5) into the equation of the stationary nucleation rate (eq. 8.2) the equation of the stationary nucleation rate that takes into account the electric field effect and can be expressed as the following:

$$J_s = zf^*C_0 \, exp \, [-B/(\, kTlnS + c_\varepsilon E^2)^2] \tag{8.8}$$

Thus according to equation 8.8 the nucleation rate in the electric field changes as the chemical potential difference changes due to the applied electric field. Since in the case of INA-1,4-dioxane system, the relative permittivities of INA ($\varepsilon_c = 2.209$) [22] and of the solution ($\varepsilon_m = 2.25$) [23] are almost equal, the contribution of the electric field to the chemical potential difference is estimated to be less than 10^{-7} kT, and therefore its effect on the nucleation work and nucleation rate should be small. Thus for the used system the electric field should have no effect on nucleation thermodynamics in the used solution system.

Electric field effects on nucleation kinetics

The electric field may not only affect the nucleation thermodynamics, but also the nucleation kinetics. The basic idea is that an electric field could align solute molecules having a permanent dipole moment, and in such a way changes the fraction of collisions that lead to successful attachment of the molecule to the nucleus. The molecules with preferred orientation all collide with the nucleus in a specific orientation. If this orientation coincides with the orientation of the molecules in the nucleus, the number of successful attachments goes up, thus the frequency of the monomer attachment to the nucleus f^* increases.

Since the used model compound INA has a relatively large permanent dipole moment (4.03 D at 25 °C [24]), it should be possible to align the INA molecules by a sufficiently strong constant electric field. The 1,4-dioxane is a non-polar solvent (its dipole moment is 0.75 Debye [25]), and thus should be unaffected by the electric field. If this mechanism would play a role, it is expected that the head-to-tail-like forms, I, III, IV or V, of INA would form rather than the head-to-head-like form II (Figure 8-2). The effect of the electric field on molecules with permanent dipole moment is depicted in Figure 8-5.
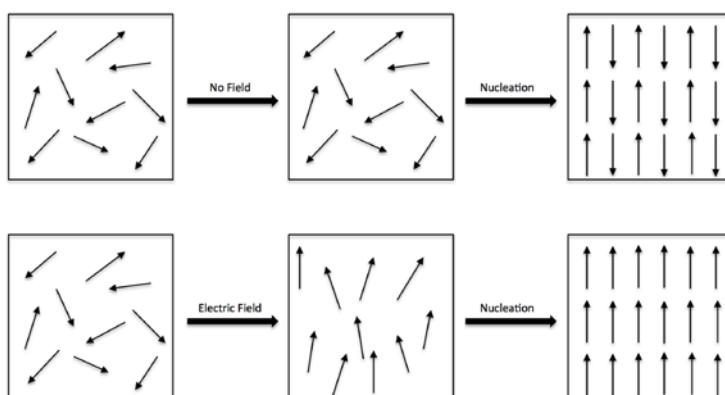
Figure 8-5. The electric field effect on nucleation kinetics [26]. In the absence of an electric field, no orientation of the INA molecules can be observed. In the presence of a sufficiently high electric field, the INA molecules tend to orientate in parallel to the electric field.

A large enough electric field could align polar molecules parallel to the field. The permanent dipole moment p of the molecule interacts with the applied electric field E and this results in a torque τ, which tends to align the molecule along the electric field direction. The maximum torque τ_{max} acting on the INA molecule can be calculated by multiplying its permanent dipole moment p (13 $\times 10^{-30}$ C m [24]) with the largest applied electric field E_{max} (5.6×10^5 V m^{-1}):

$$\tau_{max} = pE_{max} \qquad\qquad (8.9)$$

which gives a maximum torque of 7.28×10^{-24} Nm ($0.0017\ kT$). This maximum torque may be not large enough to align the INA molecules parallel to the electric field in the 1,4-dioxane solution. However, it may reduce the thermodynamic rotation of INA molecules in solution, and thus change the kinetics during nucleation.

Electromigration

Electromigration is the transport of molecules towards an electrode caused by the electric field. For instance, electromigration is the cause of the negatively charged molecules moving in solution to the positive electrode (anode), where crystallization takes place [27]. According to Hammadi et al. electromigration is causing the increased solution concentration around the anode [20] in the presence of an electric field. Thus the electromigration is responsible for the localized crystal growth on the electrode in our case. In our view the INA molecules are carrying the electrons in the used solution system, and are attracted by the Coulomb force towards the positive electrode (anode). The solvent molecules are not affected directly by the electric field, due to their non-polar nature. Thus the INA molecules are probably attracted to the anode causing a local solution concentration increase, which is the highest near the anode [28], and nucleation and crystal growth take place on the anode surface.

8.3.3.1 Fluid dynamics induced by the electric field

When the inhomogeneous electric field was present, the clear solution was moving around the electrodes above 2 kV potential difference, suggesting that electromigration was occurring. The observed circular fluid motion was probably induced by the Lorentz-force [29] that is acting on the charged INA molecules, and forcing them on a circular trajectory in the electromagnetic field [30]. The electromagnetic field must be created by the superposition of the applied electric field and the magnetic field present in the Crystalline station plus the Earth's magnetic field. In the homogeneous field setup, the INA-1,4-dioxane solution remained still even at the highest electric field, regardless of any magnetic field sources nearby.

To investigate further the induced fluid dynamics by the electric field, a suspension of INA in 1,4-dioxane was prepared and investigated visually in both

setups. The suspension started to move around the electrodes above 2 kV potential difference in the inhomogeneous field setup, again due to the Lorentz force acting on the INA molecules in the electromagnetic field, which was generated by the superposition of the applied electric field and the Earth's magnetic field. When a small magnetic stirrer bar was placed in the gap between the bottom of the vial and the end of the copper electrodes, the fluid motion apparently increased, and even a crystal bridge formed between the anode and the cathode (Figure 8-6).
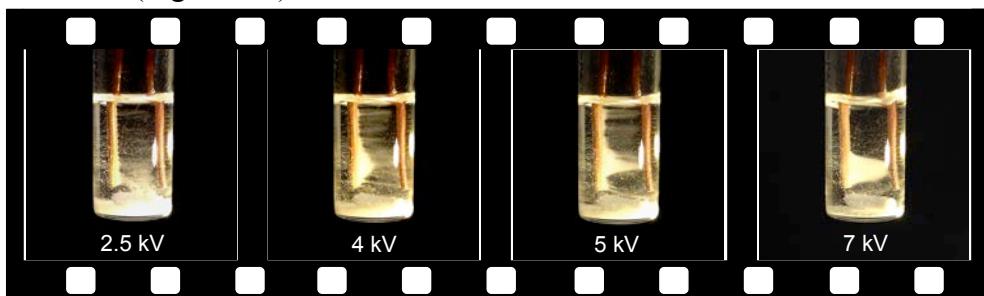
Figure 8-6. Induced fluid dynamics by an inhomogeneous static electric field in the presence of a magnetic stirrer bar. Around 5 kV potential difference a crystal bridge started to form between the electrodes.

In the homogeneous field setup, the induced fluid motion was not observed. However, the INA crystals in the bottom of the setup started to migrate towards the anode, and a pile of INA crystals was observed next to the anode when the electric field was at the maximum. The induced flow dynamics was perhaps absent because of the different nature of the electromagnetic fields created by the homogeneous electric field lines superposed on the Earth's magnetic field. Since electromigration and as a result fluid motion is present in the inhomogeneous field setup, it was expected that the nucleation thermodynamics and kinetics are changed. Induction time and crystal growth rate were measured in the presence and absence of the electric field to investigate further the electric field effects on nucleation.

8.3.3.2 Induction time probability

Induction time measurements of INA solutions were performed for 20-20 samples at a supersaturation ratio of $S = 2.05$ with and without the electric field. At this supersaturation ratio the induction time t varied between 90 and 900 seconds. This large variation of induction times under equal supersaturation

conditions reflects the stochastic nature of the nucleation process [31]. Figure 8-7 shows the experimentally obtained induction time probabilities for INA systems at the supersaturation ratio of $S = 2.05$. It can be seen that there is no significant difference in the induction time probabilities with and without the electric field. It must be noted that in the absence of the electric field nucleation takes place in the bulk solution, and not on the anode surface.
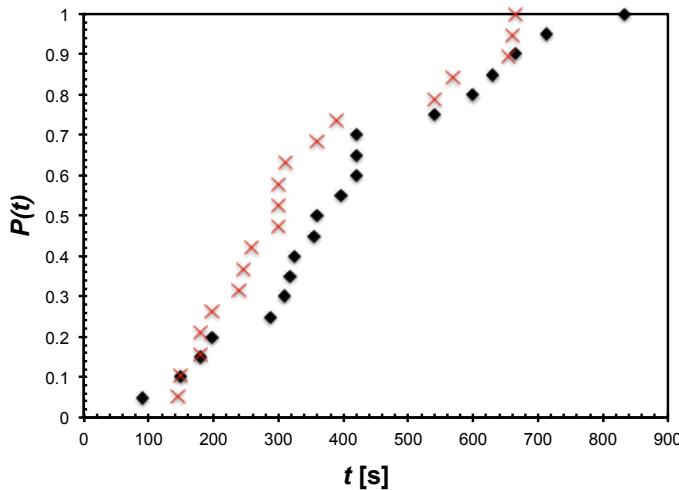
Figure 8-7. Experimentally obtained probability distribution *P(t)* of the induction time for INA at supersaturation ratio of $S = 2.05$ in the presence ($\times$) and absence ($\blacklozenge$) of the inhomogeneous electric field. No significant change can be observed.

A possible explanation for the insignificant change in induction time probabilities is that the relative permittivity of the crystalline material ε_c and of the solution ε_m is almost equal in the used system. Thus the chemical potential difference and the induction time probability should not be affected by the electric field.

8.3.3.3 Crystal growth rate and local supersaturation increase

Crystal growth rate measurements
In presence of the 5.6×10^5 V m^{-1} inhomogeneous electric field, the crystal growth rate on the anode was estimated to be around 130 μm min^{-1} by image analysis, which is two orders of magnitudes higher than the growth rate of organic crystals in general [32]. To obtain more comparable data for the crystal growth rate of INA in 1,4-dioxane systems, the INA crystal growth rate on the anode was measured in the absence of the electric field as well using the same

parameters as were used for the previous measurements. To obtain nucleation and crystal growth on the anode, the electric field had to be turned on until the first crystal appeared on the anode, then it was turned off for the rest of the measurement. Via this method, the growth rate of INA was measured to be around 8.3 μm min^{-1} in the absence of the electric field, which is 15 times lower than the measured crystal growth rate in the presence of the electric field. The crystal growth rate can be higher in the presence of the electric field, because of the migration of the charged INA molecules towards the anode (electromigration), which increases the local supersaturation [14].

From the crystal growth rate results, the local supersaturation ratio increase can be easily estimated. The crystal growth rate R - supersaturation ratio S relation can be expressed by the following equation for organic crystals at relatively low supersaturations [33]:

$$R = K(S-1)^2 \tag{8-10}$$

where K is a constant. It is assumed that the attachment frequency is the same with and without the electric field, and thus the rate constant K is not changing. Since the crystal growth rate was 15 times higher on the anode in the presence of the electric field, than in the absence, the following relation can be expressed for the supersaturation ratio in the presence and absence of the electric field:

$$15 = \frac{K(S_E-1)^2}{K(S_0-1)^2} \tag{8-11}$$

where S_E is the supersaturation ratio around the anode in the presence of the electric field, and S_0 is the supersaturation ratio around the anode in the absence of the electric field. Since the supersaturation ratio around the anode in the absence of the electric field S_0 was 2.05 during the crystal growth rate measurements at 25 °C:

$$S_E = 3.87 \times 2.05 - 2.87 = 5.06 \tag{8-12}$$

Thus $S_E = 5.06$, which is 2.5 times higher than S_0. This shows that the local supersaturation increase at the anode was more than doubled due to the applied electric field. At relatively higher supersaturations the crystal growth rate R - supersaturation ratio S relation becomes a linear relationship [33]. The

calculated local supersaturation ratio for that case results in $S_E = 16.8$. This would mean 8.2 times higher supersaturation ratio in the presence of the electric field than in the absence around the anode. This significantly increased supersaturation ratio due to electromigration is more likely to cause the polymorphic change of INA than the weak alignment of the molecules or the electric field induced chemical potential difference.

8.4 Conclusions

This research showed that a strong electric field affects cooling crystallization of isonicotinamide in 1,4-dioxane. Two experimental setups were built in order to examine effects of the electric field. An inhomogeneous electric field setup was placed in the Crystalline station with an on-board camera system that offered *in situ* investigation of the experiments in a controlled crystallization environment. A more or less homogeneous electric field was generated in the homogeneous field setup but without a precise temperature control.

In the absence of the electric field nucleation took place in the bulk solution, while in the presence of the field, the nucleation was localized, and crystals formed on the surface of the anode. The localized nucleation was due to the generated concentration gradient with the highest solution concentration around the anode.

When the electric field was not turned on, the metastable, chain-like form I was crystallized in both experimental setups. When the inhomogeneous electric field was turned on, both form I and form II of isonicotinamide were crystallized. By applying a strong, more or less homogeneous, constant electric field during the crystallization, only the stable form II was crystallized.

Electric current measurements in the homogeneous field setup showed that there was only current developing between the electrodes when isonicotinamide was present in the solution. The clear solvent showed no current even at the largest applied potential difference. Since the measured current was extremely low, redox reactions could be ruled out in the used system.

Three possible effects of the electric field on the crystallization were identified. The electric field might change the nucleation thermodynamics and/or kinetics, or the electric field could induce the transport of molecules towards an electrode (electromigration).

Image analysis from the Crystalline station showed that the applied electric field induced a circular fluid motion of the clear solution in the inhomogeneous

field setup. However, the induced fluid dynamics was not observed in the homogeneous field setup. Probably the induced fluid dynamics was observed due to the Lorentz-force acting on the isonicotinamide molecules in the inhomogeneous electric field that is superposed on the Earth's magnetic field.

Induction time probability measurements performed in the absence and presence of the electric field showed no significant effect of the electric field, suggesting that the nucleation thermodynamics was unchanged in the process. However, the crystal growth rate measurements showed significant difference. It was found that in the presence of the electric field, the growth rate of the INA crystals formed on the anode was 15 times higher than in the absence of the electric field. Probably the cause of the increased growth rate and thus the increased local supersaturation is the electromigration effect. From the crystal growth rate measurement results, the increased local supersaturation created by the electric field around the anode was estimated to be at least 2.5 times higher than in the absence of the electric field. Probably this significantly increased local supersaturation around the anode is the cause of the observed polymorphic change.

References

[1]   J. Haleblian, W. McCrone *Journal of Pharmaceutical Sciences* 1969, 58, 911.

[2]   J. H. OH, B. G. Swanson *Journal of the American Oil Chemists' Society* 2006, 83, 1007-1014.

[3]   E. Nauha, H. Saxell, M. Nissinen, E. Kolehmainen, A. Schäfer, R. Schlecker *CrystEngComm* 2009, 11, 2536.

[4]   M. Tristani-Kendra, C.J. Eckhardt *Journal of Chemical Physics* 1984, 81, 1160.

[5]   I. G. Goldberg, J. A. Swift *Crystal Growth & Design* 2012, 12, 1040-1045.

[6]   J. Bernstein *Polymorphism in Molecular Crystals* Clarendon Press: Oxford, 2002.

[7]   A. Y. Lee, D. Erdemir, A. S. Myerson *Annual Review of Chemical and Biomolecular Engineering* 2011, 2, 259-280.

[8]   I. Weissbuch, R. Popovitz-Biro, M. Lahav, L. Leiserowitz *Acta Crystallographica Section B* 1995, 51, 115.

[9]   F. J. J. Leusen *Journal of Crystal Growth* 1996, 166, 900.

[10]   J. W. Mullin *Crystallisation,* 4th Edition Butterworth-Heinemann Ltd.: Oxford, 2001.

[11]   D. Kashchiev *Journal of Crystal Growth* 1972, 13-14, 128-130.

[12]   K. V. Saban, J. Thomas, P. A. Varughese, G. Varghese *Crystal Research and Technology* 2002, 11, 1188-1199.

[13]   A. Ziabicki, L. Jarecki *Macromolecular Symposium* 1996, 104, 65-87.

[14]   J. E. Aber, S. Arnold, B. A. Garetz, A. S. Myerson *Physical Review Letters* 2005, *94*, 145503.

[15]   I. S. Ahuja, I. Prasad *Inorganic and Nuclear Chemistry Letters* 1976, 12, 777.

[16]   J. H. ter Horst, P. W. Cains *Crystal Growth & Design* 2008**,** 8, 2537-2542.

[17]   W. P. Purcell *The Journal of Physical Chemistry* 1964, 68, 2666.

[18]   S. A. Kulkarni, E. S. McGarrity, H. Meekes, J. H. ter Horst *ChemComm*, 2012, 48, 49830-4985.

[19]   S. Jiang, J. H. ter Horst *Crystal Growth & Design* 2011, 11, 256-261.

[20]   Z. Hammadi, S. Veesler *Progress in Biophysics and Molecular Biology* 2009, 101, 38-44.

[21]   D. Kashchiev, Nucleation: Basic Theory with Applications, Butterworth-Heinemann: Oxford, 2000.

[22]   J. A. Riddick, W. B. Bunger, T. K. Sakano *Organic solvents: physical properties and methods of purification.* Wiley Interscience: New York, 1986, 312.

[23]   http://macro.lsu.edu/HowTo/solvents/Dielectric%20Constant%20.htm

[24]   W. P. Purcell, J. A. Singer *J. Phys. Chem.* 1965, 69, 691-693.

[25]   G. R. Mahajan, A. C. Kumbharkhane *International Journal of Bioscience, Biochemistry and Bioinformatics* 2012, 2, 117-121.

[26]   A. Ziabicki, L. Jarecki *Macromolecular Symposium* 1996, 104, 65-87.

[27]   E. Nieto-Mendoza, B. A. Frontana-Uribe, G. Sazaki, A. Moreno *Journal of Crystal Growth* 2005, 275, e1437-e1446.

[28]   M. Taleb, C. Didierjean, C. Jelsch, J. P. Mangeot, B. Capelle, A. Aubry *Journal of Crystal Growth* 1999, 200, 575.

[29]   G. Sazaki, A. Moreno, K. Nakajima *Journal of Crystal Growth* 2004, 262, 499-502.

[30]   Jackson, John David *Classical electrodynamics,* 3rd ed. Wiley: New York, 1999.

[31]   S. S. Kadam, S. Kulkarni, R. Coloma Ribera, A. I. Stankiewicz, Andrzej, J. H. ter Horst, H. J. M. Kramer *Chemical Engineering Science* 2012, 72, 10-19.

[32]   N. Radacsi, A. I. Stankiewicz, Y. L. M. Creyghton, A. E. D. M. van der Heijden, J. H. ter Horst *Chemical Engineering & Technology* 2011, 34, 624-630.

[33]   K. Sangwal *Additives and Crystallization Processes: From Fundamentals to Applications* Wiley: Chichester 2007.

9   On the reliability of sensitivity test methods for submicron-sized RDX and HMX particles[5]

Submicron-sized RDX and HMX crystals were produced by electrospray crystallization and submicron-sized RDX were produced by plasma-assisted crystallization. In order to test the quality of the submicron-sized energetic materials, a series of small-scale sensitivity tests were carried out. Impact and friction sensitivity tests and ballistic impact chamber tests were performed to determine the product sensitivity. Rather than reflecting the quality of the particles, we found the sensitivity tests to be unreliable for submicron particles. The used impact test was not accurate enough, while the friction and ballistic impact chamber tests the submicron-sized crystals were distributed among the grooves of the porcelain plate or among the sand grains of the sandpaper used in these tests. These observations stress the need for revisiting the current standards used for determining the hazardous properties like friction and impact sensitivity of energetic materials in the case where the sample consists of submicron-sized crystals. Recommendations have been suggested to develop new test methods that only use the interactions between the particles and therefore allow the application of sensitivity tests for submicron/nano-sized energetic materials.

9.1 Introduction

Reduced sensitivity energetic materials have been widely investigated in the past decade [1-5]. These materials offer safer handling and storage. If the explosive material has a higher internal quality, it is considered to be less sensitive to mechanical or thermal effects [6]. It has been demonstrated that the higher the product quality of the solid energetic ingredients, the less sensitive a plastic bonded explosive containing these energetic materials becomes [7]. The product quality of crystalline materials is determined by the crystallization process applied to produce these materials. It was recently shown that crystallization of submicron-sized energetic RDX resulted in a reduced sensitivity product [8-12]. Smaller crystals are considered to contain less inclusions and defects, providing a higher quality. Submicron-sized crystals cannot contain micron-sized inclusions, which usually generate line dislocations and other defects. Voids should also be smaller as this can increase the threshold for critical hot spot formation. With energetic materials, it is easy to test this hypothesis by performing sensitivity tests. The application of nano- or submicron-sized crystals of energetic materials is believed to decrease the defect content considerably and therefore to further decrease the sensitiveness of the explosives. Moreover, Pivkina et al. [13] have reported an increase of the burning rate for nano-sized RDX powder as compared to that for conventional RDX.

Submicron-sized energetic crystals of RDX and HMX were produced by two novel crystallization techniques. Electrospray crystallization is an advanced crystallization process, which uses high voltage to generate a mist of ultrafine solution droplets, from which submicron-sized crystals are formed upon solvent evaporation [14]. Plasma crystallization is an innovative crystallization method, which was developed for submicron-sized RDX production by a surface dielectric barrier discharge (SDBD) treatment [15]. Both methods are producing submicron-sized crystals by electrostatic charging of the droplets to such an extent that the electrostatic forces overcome the surface tension of the droplets, and the droplets disrupt into smaller droplets to create more surface. As a result, crystallization commences in the small, confined volume, offered by the few micron droplets.

In this chapter structural characterization is performed by X-ray diffraction and density measurements to check the effect of the electrospray and plasma crystallization procedures on the crystallinity and polymorphism of the produced

materials. The influence of the particle size reduction process on the product quality is verified with impact, friction and ballistic impact chamber (BIC) tests. The reliability of the sensitivity test results for submicron energetic materials will be discussed.

9.2 Experimental Methods

9.2.1 Materials

Two conventional and four different submicron-sized energetic materials were used. Class 2 RDX (cyclotrimethylene trinitramine, HMX content 2.4%) with an average size of around 350 μm and class 6 HMX (octahydrotetranitrotetrazocine) with an average size of around 150 μm were used as a reference. Both were purchased from Chemring Nobel AS, Norway. Figure 1 shows the SEM images of the used submicron-sized RDX and HMX crystals. Spherical RDX crystals between 200-600 nm (see SEM image in Figure 9-1a) and spherical HMX crystals between 200-500 nm (Figure 9-1b) or donut-shaped HMX crystals around 1 μm size (Figure 9-1c) were produced by electrospray crystallization. Spherical RDX crystals between 400-900 nm were produced by plasma crystallization (Figure 9-1d).
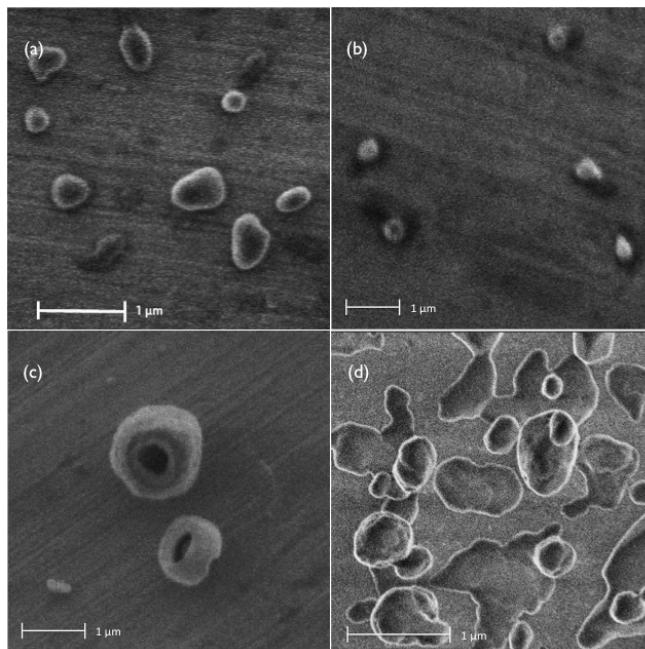
Figure 9-1. SEM pictures of the investigated materials. **(a)** RDX synthetized by electrospray crystallization, **(b)** electrosprayed HMX, **(c)** donut-shaped HMX created by electrospray crystallization and **(d)** RDX prepared by plasma crystallization.

9.2.2 Characterization tests

For morphological and size characterization of the crystalline samples, a Philips XL30 FEG scanning electron microscope and FEI Nova nanoSEM 650 electron microscope were used. No conductive coating was applied to the samples and only low electron beam energies (<2 kV) were used since voltages exceeding 2 kV at higher magnifications resulted in decomposition of the energetic materials.

X-ray diffraction (XRD) was carried out with a Philips PW3020 X-ray diffractometer. The obtained X-ray diffraction pattern was treated by "X'Pert HighScore" and matched to ICSD FIZ and ICDD databases for XRD phase identification. RDX is known to exist in five polymorphic forms (α, β, γ, δ and ϵ) [16] with the α form being the most stable one [17]. HMX has four different crystal structures, three pure crystallization phases, α, β and δ, and a solvate/hydrate phase γ [18] and β-HMX is the most stable form [19].

Density measurements were carried out with a Micrometrics AccuPyc 1340 gas pycnometer using helium. With a sample mass of around 1 g and with a

cycle of 10 measurements, the average absolute density of the samples was determined.

Sensitivity tests
Sensitivity measurements, which require relatively small sample sizes, were used since only around 1 g material of each sample was available for testing.
The sensitivity to friction was determined by a BAM Friction Apparatus (according to the international guidelines UN 3(b)(i) [20]. The sample was placed on a roughened porcelain plate, which was rigidly attached to the sliding carriage of the friction apparatus. A roughened cylindrical peg was placed on the top of the sample. The cylindrical peg was also made of white technical porcelain. Its length was 15 mm, its diameter was 10 mm and its roughened spherical end surface has a radius of 10 mm. The porcelain plate moved forward and back under the porcelain peg. The smallest load of the peg, which causes deflagration, crackling or explosion of the test sample at least once in six consecutive trials was the outcome of the friction sensitivity test. The quantity of the test sample was approx. 10 mm^3. The BAM friction test method is recommended in the UN-recommendations for the transport of dangerous goods and it is standardized as EN 13631-3 as a Harmonized European Standard [20].

For the impact sensitivity test, a BAM Fallhammer device was used (according to the international guidelines UN 3(a)(ii)) [20]. The temperature during the test was set at 23.1 °C. The sample was confined between two cylinders and guided by a ring. The cylinders had a diameter of around 9.995 mm and a height of 10 mm, while the ring had an external diameter of 16 mm, a height of 13 mm and a bore of around 10.01 mm [21]. The volume of the nano-RDX was approx. 40 mm^3, and the drop-weight was 5 or 1 kg. The drop height was varied between 15-50 cm. The smallest impact energy, which causes deflagration, crackling or explosion of the test sample at least once in six consecutive trials was the outcome of the impact sensitivity test. This method is the recommended test method in the UN-recommendations for the transport of dangerous goods and it is standardized as EN 13631-4 as a so-called Harmonized European Standard [20]. For both tests, the temperature during the test was measured to be 23.1 °C.

The BIC is an instrumented version of a drop-weight impact test. BIC tests were conducted to obtain information on the growth and extent of the reactions by impacting explosives under a fixed impact condition. The standard determination of the drop height corresponding to a 50% probability of initiation has only a limited meaning [22], while in the BIC tests more information can be

obtained about the reaction. The BIC is a quasi-confined chamber [23] in which a striker squeezes the explosive sample against an anvil when being struck by a drop-weight (Figure 9-2). A piece of sandpaper is placed at the bottom of the chamber to ensure a large enough shear in case the material is impact insensitive [22]. A 9,983 g drop-weight is released from a height of 1.5 m yielding an impact velocity of 5.35±0.09 m/s at the striker [24]. The impact will accelerate the 229 g striker and squeeze the RDX powder on top of the sandpaper between the striker and anvil until a reaction occurs. The used impact chamber had an internal diameter of 40 mm and was equipped with a pressure gauge, four fiber optic detectors to observe the start of reaction in the energetic material, and a 30 cm long, 4.5 mm gun barrel opposite the pressure gauge as automatic pressure relief. A 40 mm^3 spoon and a vertically placed tube with a 5 mm internal diameter were used to transfer the loose RDX or HMX powder to the sandpaper. Withdrawal of the tube yielded an RDX or HMX pile with a 9–10 mm base [25]. The striker was placed into the chamber and a bayonet insert prevented its free upward movement. A laser was horizontally aligned just above the top surface of the striker and the interruption of the laser beam, which was measured with a photodiode, recorded the start of the deformation.
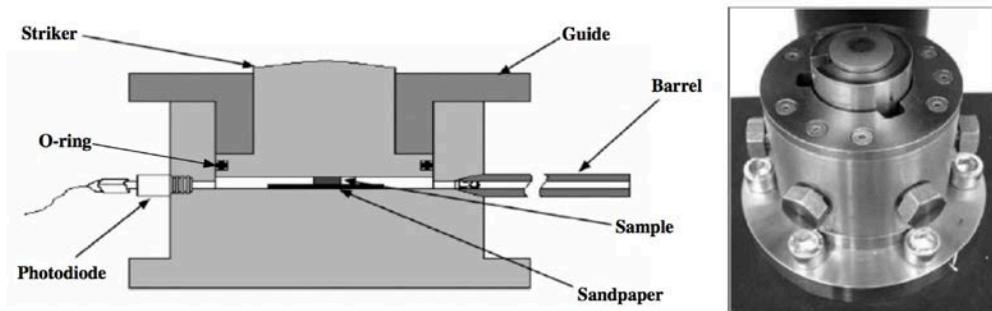
Figure 9-2. Schematics of the ballistic impact chamber reactor. Left: cross-section of the reactor chamber. Right: the chamber with the striker on the top and the holes for detectors on the side.

9.2.3 Surface roughness measurements

A portable roughness meter, Perthometer M3A, was used to perform surface roughness measurements on the BAM porcelain friction plates.

9.3 Results

9.3.1 Structural analysis (XRD)

X-ray powder diffraction showed that the product was crystalline in all cases. The crystal form of RDX was the stable α-form after re-crystallization in both the electrospray and plasma crystallization processes. However, both the spherical and donut-shaped HMX produced by electrospray crystallization showed a difference in crystal form, i.e. γ-HMX was produced rather than the stable β-form. The γ-HMX was not stable at room temperature [26]; therefore, the crystal structure was investigated one week and 6 months after production. One week after the production, the material was still the γ form, but after 6 months of storage at normal conditions, both the γ and β crystal forms were present. Thus the produced γ-HMX started to transform to the stable form. Cooling crystallization of HMX was also performed from the same solvent, acetone, to investigate the solvent effect on the crystal form. It is known that under conditions of high supersaturation – as can occur during electrospray crystallization –metastable polymorphs could form [27]. Furthermore, the presence of charges introduced by the electrospray process may also affect the intra- and intermolecular configurations of the HMX molecule, inducing the formation of, in this case, the γ-polymorph rather than the stable β-polymorph. K.Y. Lee et al. [26] also produced submicron-HMX in the γ-form by means of a solvent/non-solvent crystallization technique that confirms that the metastable polymorph is formed due to high supersaturations (which generally also occurs during solvent/non-solvent crystallization).

9.3.2 Product density

The results of the density measurements are shown in Table 9-1. No significant difference was shown in the average absolute density for the conventional RDX and submicron-sized RDX. The electrosprayed, spherical γ-HMX has a lower average absolute density than the conventional, β-form. The γ-HMX density is 1.82 g cm^{-3} from literature [21], which is close to the measured value of the electrosprayed γ-HMX. With respect to the standard deviation, the difference is negligible between the measured value and the value reported in the literature. The electrosprayed, donut-shaped γ-HMX has a density that is in between the

literature value of the β- and γ-form and close the density measured for the conventional HMX.

Table 9-1. Measured average absolute density (ρ_a) of the conventional and the produced materials with the standard deviation (*SD*), the temperature (*T*) during the measurements and the density values of conventional RDX and HMX from literature (ρ_l) [21]. The density values represent the average of 10 consecutive measurements.

Name	ρ_a (g/cm^3)	*SD* (g/cm^3)	*T* (°C)	ρ_l (g/cm^3)
Conventional α-RDX	**1.8042**	**0.0028**	**22.70**	**1.82**
Electrosprayed α-RDX	**1.8188**	**0.0197**	**22.37**	**1.82**
Plasma-made α-RDX	**1.7791**	**0.0138**	**22.71**	**1.82**
Conventional β-HMX	**1.8954**	**0.0102**	**22.35**	**1.96**
Electrosprayed γ-HMX (spherical)	**1.8372**	**0.0239**	**22.57**	**1.82**
Electrosprayed γ-HMX (donut)	**1.8959**	**0.0187**	**22.45**	**1.82**

9.3.3 Product sensitivity and reactivity

Friction and impact sensitivity
Friction and impact sensitivity tests were performed with the produced submicron-crystals of RDX and HMX and both of the raw materials. Table 9-2 shows the results obtained from friction sensitivity tests, where 360 N is the highest possible load. No ignition occurred, even with the highest possible load, for any of the produced submicron-sized crystals. The conventional RDX needed a load of 144 N for reaction and the conventional HMX ignited at a load of 252 N.

Table 9-2 shows the results obtained from the impact sensitivity tests. The submicron-sized RDX produced by electrospray crystallization needed 10 J impact energy for ignition (5 kg weight dropped from 20 cm height), while the conventional RDX (from which the submicron-sized RDX was produced) needed 5 J energy for ignition (1 kg weight dropped from 50 cm). The plasma-made submicron-sized RDX showed no change in impact sensitivity. The submicron-sized spherical γ-HMX crystals produced by electrospray needed 10 J energy for ignition (5 kg weight dropped from 20 cm height) and the 1 μm

sized donut-shaped γ-HMX needed 30 J impact energy for ignition (5 kg weight dropped from 60 cm height), whereas the conventional β-HMX had an impact sensitivity of 5 J. In all cases the submicron-sized crystals, produced by electrospray crystallization, were less sensitive than the conventional explosive crystals. In the case of 1 μm-sized donut-shaped HMX the difference between the impact sensitivity values is significant, implying that the donut-shaped HMX can probably absorb more impact energy originating from its shape (more elastic energy can be stored).

Table 9-2. Impact and friction sensitivity of 500 nm RDX and 400 nm HMX compared with conventionally sized RDX and HMX.

	Friction sensitivity (N)	Impact sensitivity (J)
Conventional α-RDX	144	5
Electrosprayed α-RDX	>360	10
Plasma-made α-RDX	>360	5
Conventional β-HMX	252	5
Electrosprayed γ-HMX (spherical)	>360	10
Electrosprayed γ-HMX (donut)	>360	30

BIC test
BIC tests were performed to measure the reaction time and pressure evaluation of the produced energetic materials. Surprisingly, none of the produced materials underwent ignition with the standard P180 sandpaper. The crystals were squeezed onto the surface of the sandpaper, and the white submicron powder material was distributed among the grains of the sandpaper (see Figure 9-3A). Sandpapers can be categorized by the density of the grains, the grit size, and the sandpaper backing type. Several different sandpaper backings exist; however, the ERL or BIC standards do not define the backing type, just the grit size (P180). The sandpaper backing was identified as a main factor for the BIC test outcome. In general P180 sandpaper with a textile backing (Klingspor, USA) is used in the BIC tests in our laboratory at TNO. In this research,

sandpapers with textile, paper and adhesive backings (grit number between P180, P400, P800 and P1200, all from Klingspor, USA) were used with all the four produced explosives and conventional RDX and HMX as references. When the P180 sandpaper was used with a paper backing, the submicron crystals were still squeezed onto the sandpaper surface, but the sample was partly burned (see Figure 9-3B). The sensors of the BIC instrument did not recognize ignition. In case sandpaper with higher grit numbers (P400, P800 or P1200) was used, partial ignition occurred, and all the sample material was burnt. There was no visible difference in reaction between the P400, P800 and P1200 sandpapers, when the sandpaper backing was constant. However, using different sandpaper backings resulted in slightly different reactions. Figure 9-3C shows P1200 sandpaper with paper backing after a BIC test. It can be seen that the material completely burnt and the sandpaper was partly destroyed. When the same P1200 grit number was used with adhesive backing, the sandpaper was destroyed in a larger part (see Figure 9-3D). In both cases the energetic sample material was the electrosprayed γ-HMX (spherical). No reaction time or pressure could be measured with the sensors of the BIC test machine with any of the produced (submicron) materials.
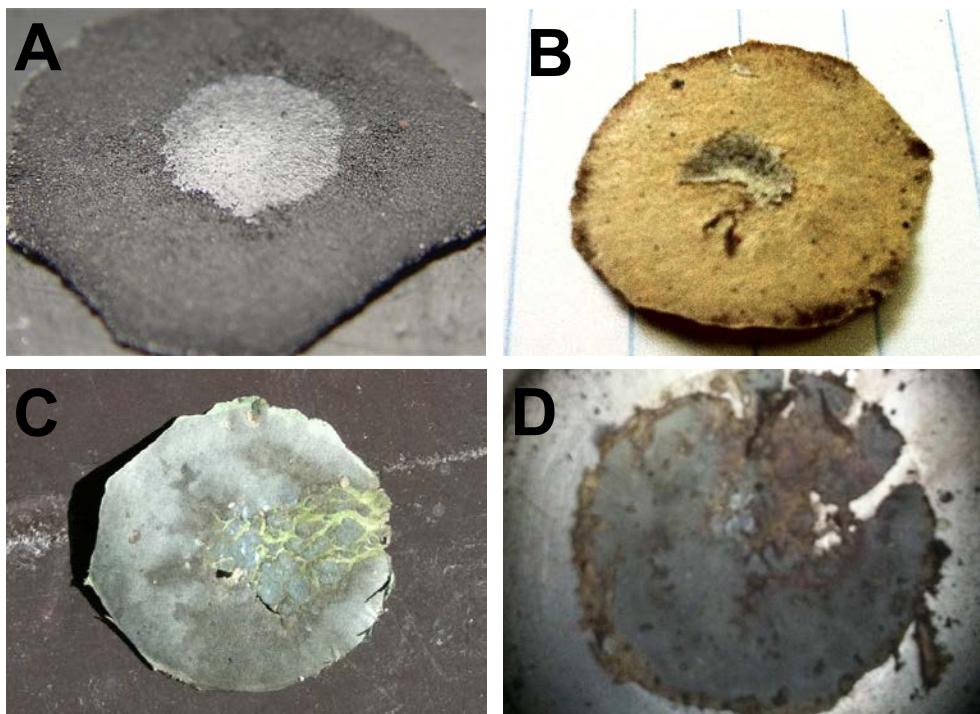
Figure 9-3. **A.** Electrosprayed HMX nanoparticles distributed among the sandpaper grains of a P180 sandpaper with textile backing after a BIC test. **B.** Electrosprayed HMX nanoparticles squeezed onto the surface of the P180 sandpaper with paper backing after a BIC test. The top part of the sample is burnt slightly. **C.** Partial ignition of electrosprayed HMX nanoparticles after a BIC test using P1200 sandpaper with paper backing. **D.** Partial ignition of electrosprayed HMX nanoparticles after a BIC test using P1200 sandpaper with adhesive backing.

The conventional RDX and HMX samples were measured with two different sandpapers to investigate the difference on reaction time (the time between the impact and reaction) and pressure evaluation depending on the sandpaper backing. P180 sandpapers with paper and textile backings were used in the BIC tests. Table 9-3 shows the measured values for the conventional RDX and HMX. The reaction time was always higher for samples placed on sandpaper with a paper backing, than on sandpaper with a textile backing. The measured maximum pressure build-up slightly increased for RDX and significantly decreased for the HMX samples.

Table 9-3. BIC test results of the conventional RDX and HMX with paper and textile sandpaper backings. The time between impact and reaction (t) was higher for samples placed on a paper backing. The measured maximum pressure build-up (P) slightly increased for RDX and significantly decreased for HMX when using a paper backing. The submicron-sized HMX-product (electrosprayed, spherical) gave no reaction in the BIC tests, *i.e.* not a reaction that was detected by the fiber optic detectors.

| Name	t (μs)	P (MPa)
Conventional RDX (paper backing)	**410**	**>4.9**
Conventional RDX (textile backing)	**261**	**4.79**
Conventional HMX (paper backing)	**462**	**1.34**
Conventional HMX (textile backing)	**220**	**2.85**

9.4 Discussion

Impact and friction sensitivity tests and BIC test were performed to determine the product quality. Indications were found that these methods are not eligible for measuring the sensitivity of submicron-sized energetic materials. In this chapter the reliability of the abovementioned three sensitivity tests for submicron-sized RDX and HMX crystals is discussed.

9.4.1 Friction sensitivity test

The BAM friction sensitivity test has been developed to simulate a hazardous situation that could occur with an energetic material under realistic circumstances when transporting or handling these materials. Therefore, this test gives just an indicative value of the sensitivity. The BAM friction apparatus was not able to measure the friction sensitivity for the produced submicron-sized energetic materials since no ignition occurred, even at the highest possible load. It is known that the roughness of the porcelain plates determines the result of the sensitivity test [28]. The depth of the grooves on the used plate was between 9 – 32 μm according to the manufacturer (BAM), which are sufficiently large to contain submicron particles. The surface roughness of the used porcelain plates was studied with a portable roughness meter (Perthometer M3A). The roughness depth of the grooves was found to be between 5 μm and 17.5 μm, which was smaller than the given value by the manufacturer, but large enough for submicron-sized particles to be distributed among the grooves. Thus, in the case of a submicron material, friction sensitivity could probably not be measured,

because the submicron-sized crystals were distributed among the grooves of the porcelain plate (Figure 9-4) and did not undergo friction.

Furthermore, it is known that the measured friction sensitivity is partially dependent upon the nature of the rubbing surfaces. Hence, a result obtained with porcelain may not be related to the effect of for instance steel. Moreover, when the rod is heavily loaded, as is necessary with relatively insensitive samples, the test is no longer a pure friction test and becomes, at least partially, also a thermal test [29]: with loads of 80 N and more, substantial heating occurs at the interface between the porcelain surfaces. Movement of the porcelain peg could cause the test sample to be pushed away, thus leaving a little amount of material to experience friction forces between the contact surfaces [30].
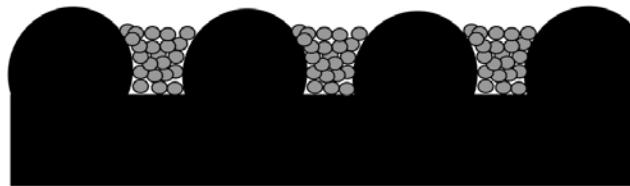
Figure 9-4. Schematic cross-section of a ceramic plate with 500 nm crystals in the grooves.

9.4.2 Impact sensitivity test

The BAM impact sensitivity test has also been developed to simulate a hazardous situation that could occur with an energetic material under realistic circumstances when transporting or handling these materials. Therefore, this test also gives only an indicative value, with an accuracy of plus/minus one level (one level is 1 J when the 1 kg drop-weight is used, and 2.5 J with the 5 kg drop-weight in the BAM impact test). It was noted that there was a gap between the coaxial cylinders and the ring of the confinement device. The gap was measured to be around 9 μm, which is large enough for submicron-sized crystals to escape. The weight of the samples together with the confinement device was measured before and after 10 tests, for which no ignition occurred. The samples were studied for mass loss, but none was measured. Apparently the submicron particles, despite the gap, did not escape the sample holder. This is probably due to the fact that submicron particles tend to agglomerate because of the large surface energy, and generally form 20-30 μm clusters [31]. As a conclusion, the

BAM impact test seems to be a reliable, but not a very accurate sensitivity test method for particles down to 500 nm.

9.4.3 Ballistic impact chamber test

Every drop height impact test procedure suffers from the fact that it mixes the plastic energy required to deform and heat the sample with the elastic energy stored in the machine during the impact test [32]. This stored elastic energy provides the energy to rebound the drop-weight. During impact the vertical movement of the drop-weight and the striker is accompanied by the radial movement of both the crystalline energetic material and the sandpaper. Differences in properties of the sandpaper will influence directly its sliding motion and thereby forces exerted on the radially flowing particles. Since the BIC test is very similar to the ERL/Bruceton Impact Machine (STANAG 4489, MIL-STD-1751A), probably our observations are valid for the ERL/Bruceton Impact Machine as well.

9.4.4 Recommendations

The previous results showed that conventional friction sensitivity methods could not be used for submicron-sized energetic materials. There is a need for a standard small-scale sensitivity test method, which is suitable for an accurate measurement of the sensitivity of energetic samples with a mass less than 1 g, regardless of the size of the particles.

Since the BAM friction test was not able to measure the friction sensitivity of the submicron-sized samples, a strikingly different device is suggested. There are several problems with the BAM friction test. In the BAM friction test the friction forces come from two sources: the friction between the sample particles and the sliding ceramic surfaces and the friction between the sample particle grains. First, friction occurs between the sample material and the ceramic friction plate due to the sliding motion. This friction force causes the friction between the sample particles by making the plains of grains sliding on each other as described in the Browning-model [33]. If the friction force between the sample particles and the sliding ceramic plate were eliminated, the plate roughness would not play a role, and the test could be applicable for submicron- or nano-sized energetic crystals. Furthermore, the thermal effect caused by the friction between the ceramic surfaces and the sample would also be eliminated.

Hereby a friction device is suggested that would only produce the friction between the sample particles, which would allow us to obtain reliable and accurate friction sensitivity results. In fact, there was a special friction apparatus developed by Wim Prinse at TNO, The Netherlands, more than 30 years ago [34] that produced friction only between the sample particles. In this device the sample was placed in a chamber formed by a moving piston (in vertical position) on the bottom, and a cylindrical guide around it (see Figure 9-5A). Both the piston and the guide were made from stainless steel. The force on the piston was adjustable, and it was pressed until the chamber was completely filled with the sample. A durable glass (Pyrex) closed the chamber on the top, which was fixed into a sliding stainless steel plate. A constant force held the piston guide to this unit consisting of the glass plate and the sliding plate. The adjustable constant force was applied on the piston, which pressed the sample to the glass plate. Since the force F acting on a fix area A was known, the pressure p on the sample could be calculated by the equation:

$$p = F / A \tag{9-1}$$

An O-ring was placed between the guide wall and the piston to provide perfect sealing. A second piston (placed horizontally), working with compressed air, was connected to the sliding plate containing the glass. This piston moved the sliding plate rapidly in one (horizontal) direction. The moving glass plate initiated friction between the particles in the sample. As the sample ignited, tremendous pressure was built in the chamber, which moved the piston downwards. As soon as the sample burnt, the external force on the piston pushed it up towards the glass plate. Figure 9-5B shows an example of the measured time-pressure curve by this friction machine. The diagram shows that when ignition occurs, the piston moves downwards corresponding with the pressure that is built up during the explosion. After the sample is burnt, the piston moves upwards, leaving less pressure in the chamber.
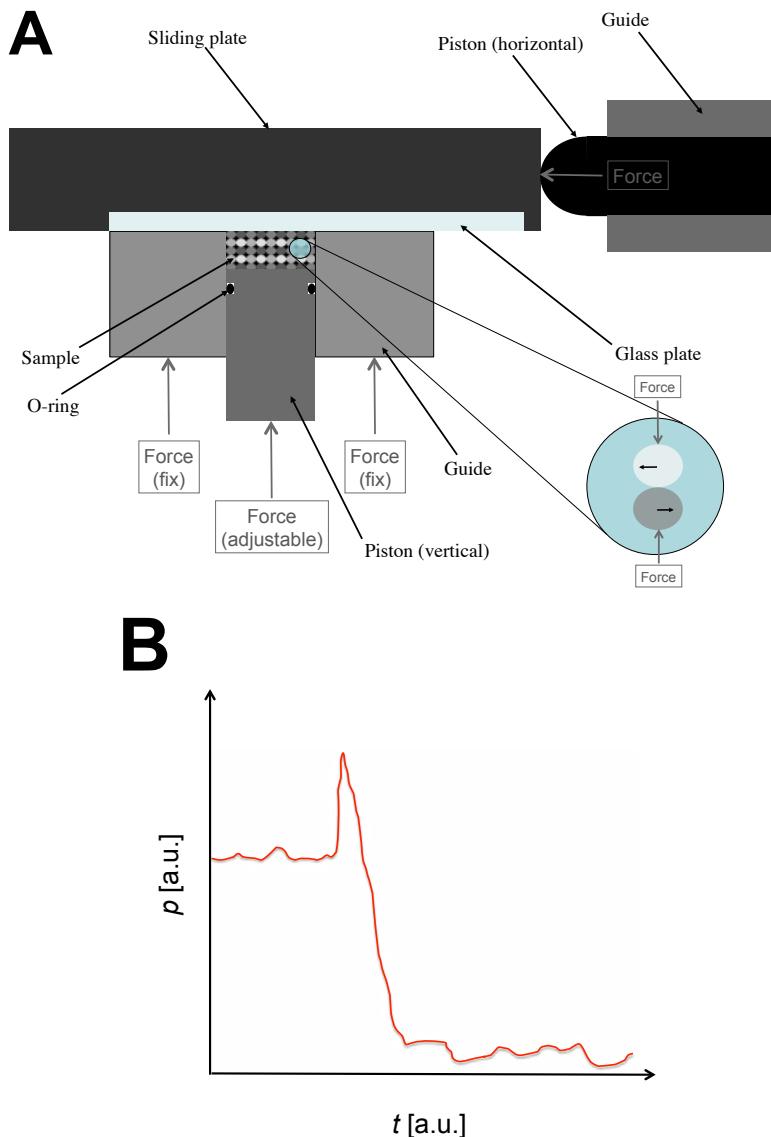
Figure 9-5. A. Schematic cross-section of the suggested friction apparatus for reliable friction sensitivity measurements. **B.** Example of a possible result obtained by the suggested friction test machine. The graph shows the pressure p increasing upon initiation (peak), and then decreasing to close to zero in time t.

This friction test device was successfully used for measuring the sensitivity of tetrazene in the past [34]. Thus because of the particle-particle friction, this device should be a reliable measurement method of the friction sensitivity of submicron-sized energetic materials. Unfortunately, we could not perform experiments with the proposed device, since it was disassembled in the 1980's.

However, there are models available that prove our claims to be correct [33, 35, 36].

The frictional heating is identified as a possible cause of ignition in the drop-weight system [37]. In a drop-weight test, like the BIC test, the frictional heating between the particles in the sample and induced by the impact of the drop-weight and the sample on the anvil will lead to a temperature rise of the sample [37]. This initiation mechanism is present in most sensitivity test methods, and it can be seen that frictional heating is present in the BAM impact and friction tests, as well as in the BIC test. If the frictional heating between the anvils and the sample would be excluded, only the particle-particle frictional heating would occur, allowing more reliable results. The interactions between the microscopic sample grains were investigated by Gruau et al. in detail [35]. They found that frictional heating leads to ignition when the levels and the durations of pressure and plastic shear rate are sufficient [35]. The criteria for ignition was first described by Browning and Scammon [36] who derived a relationship between the macroscopic pressure $<p>$ and the macroscopic plastic shear strain rate $\dot{\gamma}_{pl}$.

Gruau et al. also found that in a nearly adiabatic framework, the macroscopic temperature rise due to plastic dissipation does not exceed 40 K in a low velocity impact test [35]. They suggested to investigate ignition not at macroscopic scale but rather at microscopic scale, and established a model based on local friction between the explosive sample grains [36]. They have investigated the connection between the macroscopic pressure and plastic shear rate by representing it as a three dimensional microstructure (Figure 9-6.)
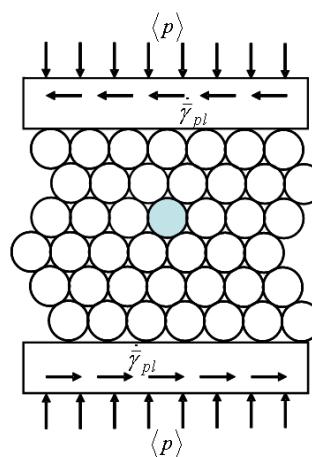
Figure 9-6. Schematics of microscopic identical sample grains subjected to a compressive macroscopic pressure $<p>$ and a shear strain $\dot{\gamma}_{pl}$ as suggested by Gruau et al. [35].

This ignition mechanism is the same as we suggested in the proposed friction sensitivity test device. Thus by eliminating the friction between the test apparatus surface and the sample material, the sensitivity test measurements can be made more reliable for submicron-sized energetic particles.

9.5 Conclusions

Sensitivity of submicron-sized RDX and HMX were tested with impact, friction and BIC test methods. The BAM impact sensitivity test results seem to be applicable for submicron-sized energetic materials, but inaccurate. The BAM friction test and the BIC test gave questionable results. Using the submicron-sized explosive materials there was no ignition with the BAM friction apparatus even the highest possible load was applied. The BIC test, which is similar in many ways to ERL machine with Type 12 tools showed no ignition of the submicron-sized materials, but the sample was squeezed among the grains of the sandpaper that was applied in the bottom of the test chamber. There is a need for a standard sensitivity test method, which can accurately measure the sensitivity of even nano-sized explosives. A friction initiation set-up as developed at TNO more than 30 years ago, might be a technique that will provide a more reliable measurement of the friction sensitivity of submicron- or nano-sized energetic materials by eliminating the friction between the test apparatus surface and the sample material.

References

[1]   A. E. D. M. van der Heijden, R. H. B. Bouma *Handbook of Material Science Research – Energetic Materials: Crystallization and Characterization*, Editors: Charles René and Eugene Turcotte, 2010.

[2]   J. W. Kim, J.-K. Kim, H.-S. Kim, K.-K. Koo *Crystal Growth & Design* 2009, 9, 2700-2706.

[3]   C. Spyckerelle, G. Eck, P. Sjöberg, A.-M. Amnéus *Propellants, Explosives, Pyrotechnics* 2008, 33, 14.

[4]   A. E. D. M. van der Heijden, R. H. B. Bouma, A. C. van der Steen *Propellants, Explosives, Pyrotechnics* 2004, 29, 304-313.

[5]   A. E. D. M. van der Heijden, R. H. B. Bouma *Crystal Growth & Design* 2004, 4, 999-1007.

[6]   R. M. Doherty, D. S. Watt *Propellants, Explosives, Pyrotechnics* 2008, 33, 4.

[7]   A. E. D. M. van der Heijden, Y. L. M. Creyghton, E. Marino, R. H. B. Bouma, J. H. G. Scholtes, W. Duvalois *Propellants, Explosives, Pyrotechnics* 2008, 33, 25-32.

[8]   V. Stepanov, L. N. Krasnoperov, I. B. Elkina, X. Zhang *Propellants, Explosives, Pyrotechnics* 2005, 30, 178-183.

[9]   P. Redner, D. Kapoor, R. Patel, M. Chung, D. Martin *25th Army Science Conference*, Orlando, Florida, November 27-30, 2006.

[10]   D. Spitzer, C. Baras, F. Ciszek, M. R. Schäfer *37th Annual ICT Conference*, Karlsruhe, Germany, June 27-30, 2006, P-144.

[11]   V. Stepanov, V. Anglade, W. Balas, A. Bezmelnitsyn, L. N. Krasnoperov *39th Annual ICT Conference,* Karlsruhe, Germany, June 24-27, 2008, P-54.

[12]   H. Qiu, V. Stepanov, A. R. Di Stasio, T. Chou, W. Y. Lee *Journal of Hazardous Materials* 2011, 185, 489-493 .

[13]   A. Pivkina, P. Ulyanova, Y. Frolov *Propellants, Explosives, Pyrotechnics* 2004, 29, 39-48.

[14]   N. Radacsi, A. I. Stankiewicz, Y. L. M. Creyghton, A. E. D. M van der Heijden, J. H. ter Horst *Chemical Engineering & Technology* 2011, 34, 624-630.

[15]   N. Radacsi, R. Ambrus, P. Szabó-Révész, A. E. D. M. van der Heijden, J. H. ter Horst *Crystal Growth & Design* 2012, 12, 3514-3520.

[16]   I. G. Goldberg, J. A. Swift *Crystal Growth & Design* 2012, 12, 1040-1045.

[17]   R. J. Karpowicz, S. T. Sergio, T. B. Brill *Industrial & Engineering Chemistry Product Research and Development* 1983, 22, 363-365.

[18]   H. H. Cady, L. C. Smith *Los Alamos Scientific Laboratory Report* LAMS-2652 TID-4500, Los Alamos National Laboratory: Los Alamos, NM, 1961.

[19]   P. Main, R. E. Cobbledick, R. W. H. Small, H. M. Krishna Murthy, M. Vijayan *Acta Crystallographica Section C* 1985, 41, 1351-1354.

[20]   *United Nations,* 4th Edition New York and Geneva, 2003.

[21]   R. Meyer, J. Köhler, A. Homburg *Explosives,* 6th Edition Wiley-VCH: Weinheim, 2007.

[22]   C. S. Coffey, V. F. DeVost *Propellants, Explosives, Pyrotechnics* 1995, 20, 105.

[23]   D. N. Griffin *American Rocket Society Technical Paper*, Palm Beach, Florida, 1961, 1706-61.

[24] B. Meuken, M. Martinez Pacheco, R. Verbeek, R. Bouma, L. Katgerman *Multifunctional Energetic Materials* MRS Symposia Proceedings No. 896, edited by N. N. Thadhani, R. W. Armstrong, A. E. Gash, W. H. Wilson, Materials Research Society, Warrendale, Pennsylvania, 2006, Paper No. 0896-H06-06.

[25] R. Bouma, A. G. Boluijt, H. J. Verbeek, A. E. D. M. van der Heijden *Journal of Applied Physics* 2008, 103, 093517.

[26] K-Y. Lee, D. S. Moore, B. W. Asay, A. Llobet *Journal of Energetic Materials* 2007, 25, 161–171.

[27] J. W. Mullin *Crystallisation,* 4th Edition Butterworth-Heinemann Ltd.: Oxford, 2001.

[28] J. J. J. P. A. Le Roux *Propellants, Explosives, Pyrotechnics* 1990, *15*, 243.

[29] V. J. Clancey *First International Symposium on Loss prevention and safety promotion in the process industries* Elsevier: Amsterdam, 1974, 253-259.

[30] R. K. Wharton, J. A. Harding *Journal of Energetic Materials* 1993, 11, 51-65.

[31] J. R. van Ommen, C. U. Yurteri, N. Ellis, E. M. Kelder *Particuology* 2010, 8, 572-577.

[32] C. S. Coffey, V. F. DeVost, D. L. Woody *Proceedings of the 9th Symposium on Detonation* Portland, Oregon, August 28 – September 1, 1989, OCNR 113291-7, 1243.

[33] R. V. Browning *Microstructural Model of Mechanical Initiation of Energetic Materials, APS Shock Compression of Condensed Matter Conference,* Seattle, Washington, August 13-18, 1995, 405-408.

[34] W. C. Prinse, J. J. Janswoude *Friction Initiation Meter (FIM). Description and preliminary results*, TNO, PML/TR report nr. T6128-I/T8012, 1979 (internal report)

[35] C. Gruau, D. Picart, R. Belmas, E. Bouton, F. Delmaire-Sizes, J. Sabatier, H. Trumel *International Journal of Impact Engineering* 2009, 36, 537-550.

[36] R. V. Browning, R. J. Scammon *Shock Compression of Condensed Matter* AIP Press: New York, 2001, 987-990.

[37] J. E. Balzer, J. E. Field, M. J. Gifford, W. G. Proud, S. M. Walley *Combustion and Flame* 2002, 130, 298-306.

10 Conclusions & perspectives

In this thesis Process Intensification in crystallization was discussed, whereby alternative forms of energy were used. Novel advances in the area of crystallization were introduced and also upgrades to the existing techniques were discussed. Electrospray crystallization and plasma-assisted crystallization were identified as inexpensive tools for producing submicron- or even nano-sized crystals. These produced submicron crystals can have beneficial properties, such as reduced sensitivity for explosives, or increased dissolution rates for pharmaceuticals. Electrospray crystallization for instance is ideal for small-scale production, while plasma-assisted crystallization has the potential to be used at larger scales. In this study, crystallization under the influence of an electrostatic field was also investigated. The latter method can be used for instance to control polymorphic fraction in a product, induce fluid dynamics in a solution or suspension or increase crystal growth rates. Results using the three aforementioned techniques were presented and possible further developments for creating a perfect crystallizer setup for nanoparticle production were discussed.

10.1 Electrospray crystallization

Electrospray crystallization is a cost-efficient and simple technique to produce submicron-sized crystals in a controlled process. As opposed to the conventional crystallization methods, which can require large amounts of material, electrospray crystallization only requires milligrams of materials. This could be highly beneficial especially during the discovery and early development stages of materials due to their limited availability. The relatively cheap cost of the experimental setup is also an added advantage to this technique.

In this study, it was shown that niflumic acid crystals in the size range of 200-800 nm could be produced by electrospray crystallization. In the presence of excipients, the produced submicron crystals had significantly increased dissolution rates compared to the conventionally sized drug particles. Increasing the dissolution rate of crystalline particles makes electrospray crystallization a highly desirable technique in the pharmaceutical industry. However, implementing electrospray crystallization in industrial settings remains challenging as it still suffers from low production rates [1]. In order to produce nanoparticles, a relatively low flow rate is required [1]. This makes the latter technique difficult to scale up [1]. To overcome this challenge, scaling out is proposed instead of scaling up. Several suggestions have been reported in the literature on out-scaling methods including the use of an array of capillaries, an array of holes in combination with a non-wetting material, multiple jet mode operation, serrations, grooves, etc. [2, 3]. But even under the use of hundreds of nozzles, the targeted industrial production rate still remains difficult to achieve, since orders of magnitude changes are needed.

Therefore, it is suggested to use electrospray crystallization as a simple and cheap way to investigate properties of nanoparticles, e.g. when the nano-sized product is still in the research phase. Generally, only small quantities are available of (very expensive) drug materials in research, so it is advantageous to adopt a production technique that uses only small quantities rather than the conventional techniques that require larger amounts of (expensive) materials. The range of sizes that can be produced by electrospray crystallization should be broad enough in order to study the effect of particle size on the properties of the active pharmaceutical ingredient, namely the dissolution rate, crystallinity, hydrophobicity, etc. Furthermore, electrospray crystallization could be also used for early stage polymorph screening of (expensive) materials.

The scaling up possibilities of electrospray crystallization are further discussed in subchapter 10.5.

10.2 Plasma crystallization

Similarly to electrospray crystallization, cold plasma crystallization is a method to synthesize nano-sized particles. It was shown in this thesis that RDX crystals in the size range of 200-900 nm can be produced by Surface Dielectric Barrier Discharge (SDBD) with an increased internal quality. Also niflumic acid and Poloxamer 188 crystals were produced by plasma crystallization in the submicron-sized range. SDBD is already used at industrial scales for water treatment by ozone production. However, similar to electrospray crystallization, the current plasma crystallization process has a very low production rate. On the other hand, the potential for scale-up for plasma crystallization is better than what can be achieved with electrospray. The main limiting factors that determine the production rate in the plasma crystallization process are the amount of solute entering the reactor, the efficiency of the particle collection, and the plasma treatment of the nebulae. The amount of solute is in turn determined by the solution concentration and the carrier gas flow rate. The DC bias voltage and the SDBD plate size, position and arrangement determine the particle collection process in which charged particles are attracted by the grounded plate.

Using high concentrations of RDX to achieve high production rates is not possible with the Collison nebulizer. Solution concentrations close to the saturation concentration led to unwanted crystallization and scaling in the micro-channels of the nebulizer, which resulted in full blockage after 1-2 minutes of operation. Thus, there is a strong relation between the clogging and the solution concentration. Therefore it is important to know the temperature dependent solubility of the used material in the solvent and use only solution concentrations that are substantially lower than the solubility at room temperature. In the case of RDX, around 20% of the saturation concentration can be used without clogging. The gas flow rate and thus the aerosol injection into the reactor are limited by the micro-channels of the nebulizer. The 11 L min^{-1} gas flow rate that was achieved with the 6-hole nebulizer head corresponds to 4.3 mL min^{-1} solution sprayed by the nebulizer. However, significant scaling occurs within the nozzle, in the tube between the reactor and the nebulizer, in the knee tube of the nebulizer and on the discharge electrodes

of the SDBD plate. Approximately 10% of the solute cannot reach the plasma because of this scaling. This amount of scaling in the current design cannot be avoided.

The efficiency of the particle collection is determined by the DC bias. As mentioned in *Chapter 6*, the DC bias potential difference has a limit. If the DC bias voltage exceeds the amplitude of the plasma exciting AC voltage, sparking can occur between the SDBD plate and the reactor wall. Thus in the current design the theoretical maximum of the DC bias voltage is 2.55 kV.

In principle, when using electrostatic collection, around 75 % collection efficiency can be achieved for particles in the size of around 500 nm [4]. To investigate the particle collection efficiency, the content of crystals in the outflowing gas was studied by applying a metal sheet above the gas outlet for 3 minutes during operation of the reference experiment. The sheet was investigated with SEM, and particles were observed on it. These particles seemed to be amorphous, and were likely not RDX. This indicates that the RDX that is not collected is either decomposed, or deposited within the reactor. Indications for decomposition of organic materials were observed as very small amounts of carbon deposition (less than 1 % of the injected solute) on the SDBD plate between the electrodes. Probably the organic molecules that had too much plasma exposure were decomposed and escaped the reactor chamber with the outflowing gas.

The product loss can be reduced by applying an improved geometry that minimizes scaling and decomposition of the solute. If the carrier gas would bring the aerosol at a proper distance above the plasma as a thin gas layer, the plasma treatment could be optimal for the production of nano-sized particles without decomposition.

An increase in the production rate could be achieved by applying a larger SDBD plate; however, cooling should also be introduced afterwards, because as shown in Figure 6-5, temperature increases with the increasing plate size. If the gas or solution were cooled, it would have a cooling effect directly on the gas above the plasma. However, this would decrease the solubility of the RDX in the solution resulting in clogging of the micro-channels of the nebulizer head. It might be better to apply an air- or water-cooling system or a Peltier element on the counter-electrode of the SDBD plate, which could offer an indirect cooling effect.

Table 1 shows a comparison between electrospray crystallization and plasma crystallization in terms of energy consumption, production rate, RDX impact sensitivity (internal quality) and dissolution rate.

Table 1. Comparison of electrospray crystallization with plasma crystallization

	Energy consumption [W]	Production rate [mg/h]	RDX impact sensitivity	Dissolved NIF with the excipients in 1 h [%]
Electrospray Crystallization	0.005	150	7.5	73
Plasma Crystallization	20-40	200	5	96

10.3 Cooling crystallization in electrostatic fields

Application of electric fields can make remarkable changes on crystallization processes. By applying a constant electric field during cooling crystallization, the produced crystal form can be controlled depending on the electric field strength and the dielectric properties of the solute and solvent. Crystallization in the presence of a 5.6×10^5 V m^{-1} constant electric field was used to produce the stable form II of isonicotinamide-1,4-dioxane system, where in the absence of the electric field the metastable form I was produced. In the presence of the electric field the crystals were growing on the surface of the anode, while in the absence of the electric field crystallization took place in the bulk solution.

Electric current measurements showed that there was only current developing between the electrodes when the solute (isonicotinamide) was present in the solution. The clear solvent showed no current even at the largest applied potential difference. Since the measured current was extremely low, redox reactions can be ruled out in the used system.

Three possible effects of the electric field on the crystallization were identified: The electric field might change the nucleation thermodynamics, nuclation kinetics, and cause electromigration (the transport of molecules towards an electrode).

An inhomogeneous electric field can be used to induce fluid dynamics of the isonicotinamide-dioxane solution. When a strong inhomogeneous electric field was applied for isonicotinamide-1,4-dioxane system, circular fluid motion was observed due to the Lorentz-force acting on the isonicotinamide molecules in the inhomogeneous electric field that is superposed on the Earth's magnetic field.

The electric field can also affect the crystal growth rate. By using the strong inhomogeneous electric field during cooling crystallization of isonicotinamide

in 1,4-dioxane, the crystal growth rate was approximately 15 times higher than in the absence of the electric field. Probably the cause of the increased growth rate and the induced fluid dynamics is the electromigration phenomenon. From the crystal growth rate measurement results, the increased local supersaturation created by the electric field around the anode was estimated to be at least 2.5 times higher than in the absence of the electric field, which might be the cause of the observed polymorphic change.

10.4 Implications of thesis findings and recommendations

10.4.1 Implications

As noted in the previous sections, three crystallization methods were introduced. Electrospray crystallization is an inexpensive approach, which can be used for submicron particle production. This could be highly desired in the pharmaceutical industry. A scaled up version of electrospray crystallization is plasma crystallization. The latter is a novel method for producing organic submicron crystals with increased internal qualities. On the other hand, electric field crystallization can be used to control polymorphism or increase crystal growth rate with attractive applications in industrial settings. While the aforementioned crystallization methods have numerous advantages over the conventional ones, several challenges remain to be overcome. For instance, the plasma setup still suffers from low production rates (product loss), also the theory behind the mechanism by which the electric field affects the polymorphic fraction is still not well understood. Future investigations of these three methods should focus on solving the stated issues. The next section focuses on recommendations for future crystallizer designs.

10.4.2 An outlook for making the perfect crystallizer for producing nanoparticles

In order to further advance the design of the current crystallizers, it is of paramount importance to understand the potential desired outcome from the crystallizer. For instance, electrospray crystallization can be used for small-scale production of active pharmaceutical compounds. However, electrospray crystallization has limitations on scaling up and only scaling out is possible by using multiple nozzle systems. It may however be possible to scale up

electrospray crystallization upon the development of a strikingly different setup free of nozzles.

Since the small nozzle diameter and the low solution flow rate are the main limiting factors in electrospray crystallization, the nozzle should be neglected, and a different geometry should be used to generate Taylor-cones. In this study, I suggest a partly immersed rotating drum with small pits on its surface is placed in a bath filled with solution (Figure 10-1). The drum material needs to be conductive, and connected to a DC power supply. A few centimeters above the drum a collector plate is positioned, which is connected to the zero electrode of the DC power supply. If 20-30 kV potential difference is applied between the rotating drum and the collector plate, the liquid in the small pits of the rotating drum will form individual Taylor-cones, and spraying will start towards the collector plate.
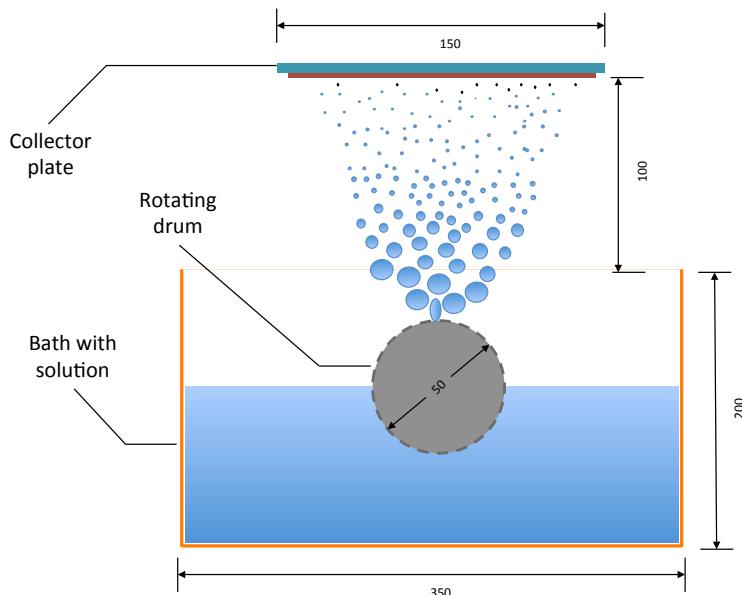
Figure 10-1. Cross-section of the proposed scaled-up electrospray crystallization setup.

For even large-scales, an improved SDBD plasma crystallizer is proposed. Its geometry could be a cylindrical SDBD reactor, with the length of around 30 cm and the discharge electrodes on the inner surface (Figure 10-2). The plasma geometry could also be optimized from the setup shown in Figure 6-3. By applying the plasma generating electrodes as a spiral, the advantage of the longitudinal and transversal arrangement could be combined. The particles

would experience an increased plasma exposure, at a more or less similar residence time. At the bottom of the setup, a modified nebulizer could produce the solution droplets by applying a reversed cone at the top of the nebulizer to direct the aerosol to the plasma. An extra carrier gas that is present as a thin layer above the discharge electrodes could bring the aerosol to a proper distance from the inner surface to charge the droplets equally. The top part of the setup could be a grounded metal cap where the crystals could be collected electrostatically.
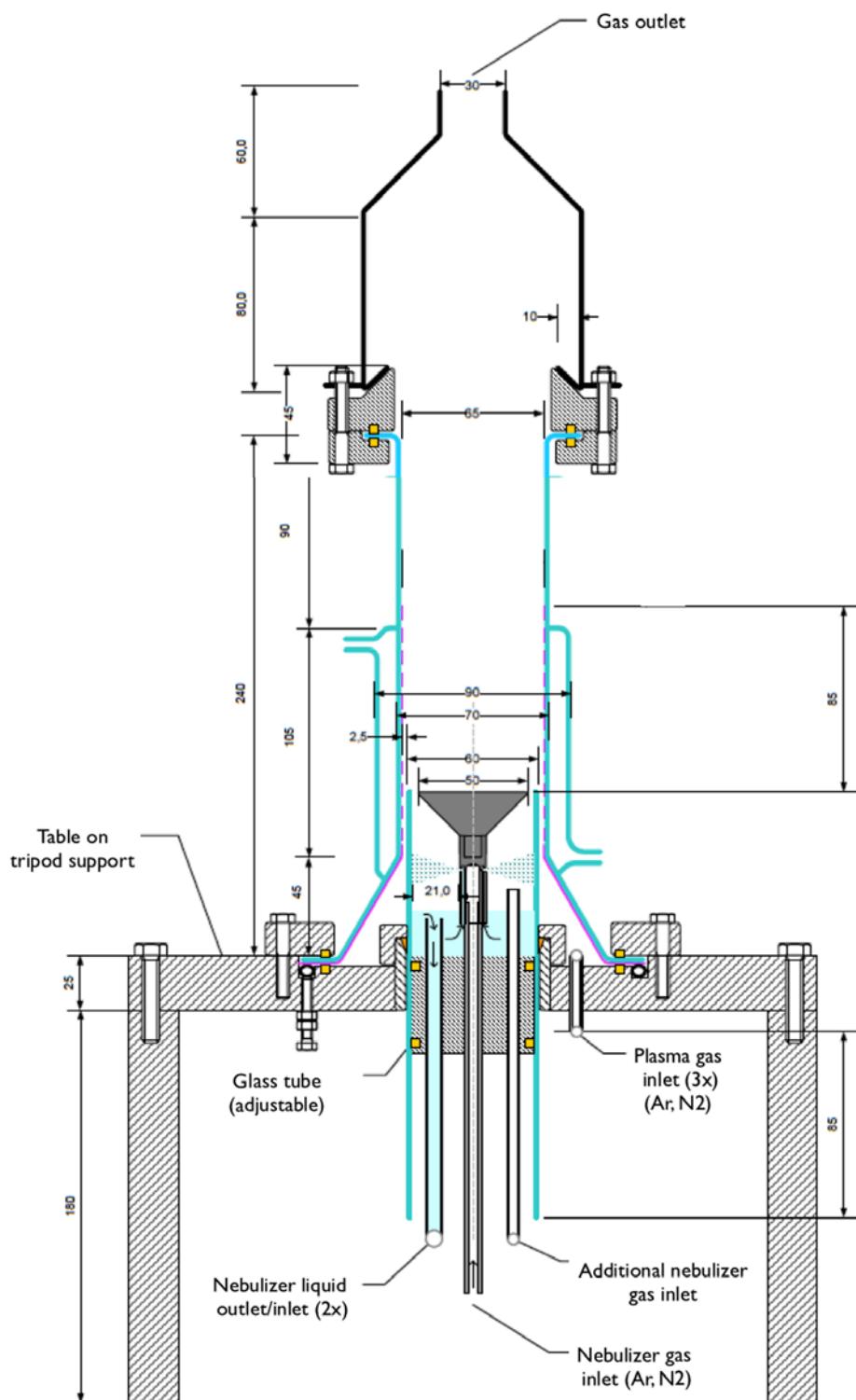
Figure 10-2. Cross-section of an improved plasma crystallization setup.

References

[1]   C. U. Yurteri, R. P. A. Hartman, J. C. M. Marijnissen *KONA Powder and Particle Journal* 2010, 28, 91-115.

[2]   W. Deng, A. Gomez *Journal of Aerosol Science* 2007, 38, 1062-1078.

[3]   W. Deng, C. M. Waits, B. Morgan, A. Gomez *Journal of Aerosol Science* 2009, 40, 907-918.

[4]   M. Rhodes *Introduction to Particle Technology,* 2nd Edition West Sussex: John Wiley & Sons Ltd., 2008.

Summary

Crystallization is one of the oldest separation and product formation techniques that continues to be in use today. Despite its long history, it only started to develop significantly in the past few decades. In this thesis, the application of Process Intensification in crystallization is investigated. Process Intensification is a set of often radically innovative principles in process and equipment design, which can bring significant benefits in terms of process and chain efficiency, capital and operating expenses, quality, wastes, process safety, etc. Alternative energy forms as basic elements of Process Intensification are investigated by applying electric fields and plasma technology in crystallization processes. Three main topics are discussed in this thesis:

a)   Submicron-sized and nano-sized particles can have beneficial product properties compared to conventionally sized crystalline products. **Electrospray Crystallization,** an advanced crystallization technique can serve as a tool to produce such submicron-sized particles. In this thesis, it was investigated whether electrospray crystallization can be used to produce 1. energetic materials with a reduced sensitivity and 2. submicron-sized pharmaceutical compounds for improved dissolution and absorption.

Electrospray crystallization of a solution is an integrated process of spraying and crystallization that uses a high voltage to produce a fine aerosol of droplets in the micron-size range. During the process, the emitted solvent droplets evaporate and a droplet disruption process (Coulomb-fission) occurs, which creates even smaller droplets. Due to solvent evaporation, eventually supersaturation is achieved and crystals of submicron particles can commence. Electrospray crystallization is an efficient, cost-effective and simple method for the production of submicron-sized crystals, but it suffers from a low production rate and it could be challenging to scale up. In this thesis, the process parameters for establishing a stable jet for producing submicron-sized particles were determined. The operation window to establish a continuous jet and produce submicron-sized crystals is relatively narrow, but experimentally feasible to maintain. Energetic crystals of RDX and HMX were produced with a mean size of around 500 nm by electrospray crystallization. The produced explosive crystals were tested for impact

and friction sensitivity. The samples were remarkably insensitive to friction stimuli, while an insignificant difference for the impact sensitivity was observed. With similar process parameters, submicron-sized crystals of a poorly water-soluble active pharmaceutical ingredient, niflumic acid, were produced. In the absence of excipients, for the case of the submicron-sized niflumic acid, no significant difference was shown in the dissolution profile compared to the conventional one. However, upon mixing the excipients, D-Mannitol and Poloxamer 188, with the submicron-sized niflumic acid, the dissolution rate of the drug was enhanced. Thus, it is possible to increase the bioavailability of drugs by drastically reducing the crystal size, while preventing their aggregation by using the proper excipients.

b) **Plasma Crystallization** is a new crystallization technique, in which an atmospheric pressure cold ionized gas is used to generate submicron-sized crystals. This novel type of plasma, the Surface Dielectric Barrier Discharge (SDBD), is a plasma made by several self-terminating microdischarges on a surface. A nebulizer system sprays the solution aerosol into the plasma with the help of a carrier gas. The plasma charges and heats the droplets. Upon evaporation Coulomb-fission occurs, supersaturation increases, and nucleation and crystal growth take place within the small, confined volume offered by the small droplets. Compared to the electrospray crystallization, much higher production rates can be achieved. The energetic material, RDX, and the active pharmaceutical ingredient, niflumic acid, and its excipient, Poloxamer 188, were produced by plasma crystallization with a significant size reduction compared to the conventional products. While there was no measurable change in the sensitivity of RDX, a substantial increase in the dissolution rate of the submicron niflumic acid crystals was observed in the presence of the plasma-made excipient.

c) The effect of a constant high electric field was investigated during the cooling crystallization of isonicotinamide in 1,4-dioxane (**Electrostatic Crystallization**). Two experimental setups were built in order to examine the electric field effect, with a focus on crystal polymorphism control. An inhomogeneous electric field was generated in a controlled crystallization environment. A Crystalline station with an on-board camera system offered *in situ* investigation of the experiments. A more homogeneous

electric field was generated in a different setup, but without a precise temperature control. Image analysis from the Crystalline station experiments showed that the applied electric field induced fluid motion of the solution due to the Lorentz-force acting on the isonicotinamide molecules in solution. This induced fluid dynamics was further visualized by using a suspension of the isonicotinamide-1,4-dioxane system. Image analysis also showed that the nucleation was localized to the anode, and crystals were formed only on the anode surface. The electric field generated a concentration gradient, with the highest solution concentration around the anode.

The crystal growth rate was also measured with the help of the on-board camera system. It was found that in the presence of the electric field, the growth rate of the isonicotinamide crystals formed on the anode is 15 times higher than in the absence of the electric field. From this crystal growth rate increase, the local supersaturation ratio increase was estimated at the anode, and found to be at least 2.5 times higher in the presence of the electric field, than in the absence.

In the absence of the electric field, the metastable, chain-like form I isonicotinamide was crystallized in both experimental setups. In the inhomogeneous electric field, both form I and form II of isonicotinamide were crystallized. By applying a more or less homogeneous, constant electric field during the crystallization, only the stable form II was formed.

In addition, concerns regarding the reliability of standard small-scale sensitivity tests methods for submicron-sized explosives were discussed in this thesis, since the obtained results for the produced explosive materials are questionable. In order to test the quality of the produced submicron-sized energetic materials, a series of small-scale sensitivity tests were carried out. Impact and friction sensitivity tests and ballistic impact chamber test were performed to determine the product sensitivity. Concerns were found with the standard friction and ballistic impact chamber sensitivity test methods, and suggestions were made to improve these tests. The friction sensitivity for all submicron-sized crystals showed no ignition even at the highest possible load. The ballistic impact chamber tests showed also no or only partial ignition with all the submicron-sized explosives. The submicron-sized crystals were distributed among the grooves of the porcelain plate used in the friction test or among the sand grains of the sandpaper used in the ballistic impact chamber test. There is a need to revisit the ignition mechanism of these sensitivity test methods, and make suggestions for accurate measurement methods for the sensitivity of nano-sized explosives. Recommendations have been suggested to develop new tests that

only rely on the interactions between the particles making them applicable to conduct the sensitivity tests for submicron/nano-sized energetic materials. A friction initiation setup as developed at TNO more than 30 years ago, might be a technique that could provide a more reliable measurement of the friction sensitivity of submicron- or nano-sized energetic materials by allowing only the frictional heating between the sample particles and exclude any other sources of frictional heating, allowing more reliable results.

Samenvatting

Kristallisatie is één van de oudste scheidings- en productvormingstechnieken. Ondanks zijn lange geschiedenis is deze techniek pas in de laatste decennia significant ontwikkeld. In dit proefschrift is de toepassing van procesintensificatie in kristallisatie onderzocht. Procesintensificatie is een set van vaak radicaal innovatieve principes in het ontwerp van processen en apparaten, die significante voordelen kunnen hebben voor proces- en keteneffiëntie, kapitaal- en exploitatiekosten, kwaliteit, afval, procesveiligheid, etc. Een van de basiselementen van procesintensificatie is het gebruik van alternatieve vormen van energie. De potentie hiervan voor kristallisatieprocessen is onderzocht door het toepassen van elektrische velden en plasmatechnologie in kristallisatieprocessen. De drie hoofdonderwerpen van dit proefschrift worden hieronder besproken.

a) Deeltjes kleiner dan een micrometer kunnen voordelige producteigenschappen hebben in vergelijking met kristallijne producten van conventionele grootte. **Electrospray Kristallisatie,** een geavanceerde kristallisatietechniek, kan als gereedschap dienen voor de productie van dergelijke sub-micrometer deeltjes. In dit proefschrift is onderzocht of electrospray kristallisatie kan worden gebruikt voor de productie van: 1. Energetische materialen met een lagere gevoeligheid, en; 2. Farmaceutische ingrediënten voor een beter oplosgedrag en betere absorptie. Electrospray kristallisatie is een geïntegreerd proces van verneveling en kristallisatie, dat hoogspanning gebruikt voor de productie van een fijne aerosol van micrometer druppels. Tijdens het proces verdampen deze druppels gedeeltelijk en breken op (Coulomb fissie), wat nog kleinere druppels genereert. Door verdere verdamping van het oplosmiddel wordt uiteindelijk oververzadiging bereikt en kan kristallisatie van submicron deeltjes plaatsvinden. Electrospray kristallisatie is een efficiënte, kosteneffectieve en simpele methode voor de productie van kristallen kleiner dan een micrometer, een nadeel is echter de lage productiesnelheid terwijl het opschalen een uitdaging zal zijn. In dit proefschrift zijn de procesparameters bepaald voor het instellen van een stabiele jet voor de productie van submicron deeltjes. Het operatiebereik voor het instellen van een continue jet is relatief klein, maar wel experimenteel haalbaar. Energetische kristallen van RDX en HMX met een gemiddelde grootte van ongeveer 500 nm zijn geproduceerd met electrospray kristallisatie. Stoot- en wrijvingsgevoeligheid van de geproduceerde explosieve kristallen zijn bepaald. De monsters waren opmerkelijk ongevoelig voor

wrijvingsstimuli, terwijl voor de stootgevoeligheid een insignificant verschil werd gemeten. Met vergelijkbare procesparameters zijn submicron kristallen van een slecht water-oplosbaar farmaceutische stof, nifluminezuur, geproduceerd. In afwezigheid van hulpstoffen werd geen significant verschil in het oplossingsprofiel van deze kristallen in vergelijking met de conventionele gevonden. Echter, in aanwezigheid van de hulpstoffen D-mannitol en poloxamer 188 werd de oplossnelheid van het geneesmiddel vergroot. Het is dus mogelijk om de beschikbaarheid van geneesmiddelen te verhogen door de kristalgrootte drastisch te verlagen, terwijl de aggregatie voorkomen kan worden door de juiste hulpstoffen toe te voegen.

b) **Plasma Kristallisatie** is een nieuwe techniek, waarbij bij atmosferische druk een koud gas wordt geïoniseerd en wordt gebruikt om submicron kristallen te genereren. Deze nieuwe vorm van plasma, de Surface Dielectric Barrier Discharge (SDBD), wordt gemaakt door verschillende micro-ontladingen op een speciaal geprepareerd oppervlak. De verneveelde oplossing wordt in het plasma gebracht met behulp van een draaggas. Het plasma verwarmt de druppels en maakt het oppervlak geladen. Tijdens de verdamping treedt Coulomb-fissie op en verhoogt de oververzadiging, waardoor nucleatie en kristalgroei plaatsvinden binnen het kleine volume van de druppels. In vergelijking met electrospray kristallisatie, kunnen veel hogere productiesnelheden worden bereikt. Met behulp van plasma kristallisatie zijn kleine kristallen van het energetisch materiaal RDX, de farmaceutische stof nifluminezuur en de farmaceutische hulpstof Poloxamer 188 geproduceerd. De gevoeligheid van RDX was onveranderd maar er werd wel een aanzienlijke verhoging van de oplossnelheid gemeten voor de kleine nifluminezuur kristallen in aanwezigheid van door plasmakristallisatie gemaakte deeltjes van de hulpstof.

c) Het effect van een constant en hoog elektrisch veld op de koelkristallisatie van isonicotinamide in 1,4-dioxaan is onderzocht (**Electrostatic Crystallization**). Hiervoor werden twee opstellingen gebouwd. Onder gecontroleerde temperatuurcondities werd een inhomogeen elektrisch veld gegenereerd gedurende het kristallisatieproces. De gevormde kristallen konden worden gevisualiseerd door een camerasysteem. Een meer homogeen elektrisch veld kon worden gerealiseerd in een andere opstelling met een minder goede temperatuurcontrole. Beeldanalyse liet zien dat het elektrisch veld de vloeistof in beweging bracht, waarschijnlijk door Lorentzkrachten uitgeoefend op de isonicotinamide moleculen in de oplossing. Deze beweging werd ook gezien in suspensies van isonicotinamide in dioxaan.

Beeldanalyse gaf ook aan dat in aanwezigheid van een elektrisch veld nucleatie van isonicotinamide plaatsvond op het anode-oppervlak. Het elektrisch veld genereerde een concentratiegradiënt doordat isonicotinamide door de anode werd aangetrokken waardoor rond de anode lokaal een hogere oververzadiging heerste.

De kristalgroeisnelheid werd ook gemeten met het *on-board* camerasysteem. Er werd gevonden dat in aanwezigheid van het elektrisch veld de groeisnelheid van de isonicotinamide-kristallen op de anode 15 maal hoger is dan in afwezigheid van het elektrisch veld. Op basis van deze toename in de kristalgroeisnelheid, kon geschat worden dat de lokale oververzadiging bij de anode minstens 2,5 maal hoger was in aanwezigheid van het elektrisch veld dan in afwezigheid ervan.

In afwezigheid van het elektrisch veld kristalliseerde in beide experimentele opstellingen de metastabiele fase I van isonicotinamide. In het inhomogene elektrische veld kristalliseerden zowel fase I als II van isonicotinamide. In een min of meer homogeen, constant elektrisch veld werd alleen de stabiele fase II gevormd.

Verder zijn in dit proefschrift vraagtekens gezet bij de betrouwbaarheid van standaard, kleine schaal gevoeligheidstesten voor submicron explosieve deeltjes. Om de kwaliteit van de geproduceerde submicron energetische materialen te testen, is een serie kleine schaal gevoeligheidstesten uitgevoerd. Stoot- en wrijvingsgevoeligheidstesten en *ballistic impact chamber* testen zijn uitgevoerd om de gevoeligheid van het product te bepalen. De standaard wrijvingsgevoeligheidstesten en de *ballistic impact chamber* testen lieten onduidelijkheden zien en er zijn suggesties gedaan om deze testen te verbeteren. In alle gevallen bleken de submicron kristallen in de wrijvingsgevoeligheidstest niet te initiëren, zelfs niet bij de hoogst mogelijke belasting. Ook de testen met de *ballistic impact chamber* lieten geen of slechts gedeeltelijke initiatie zien bij alle submicron explosieven. De submicron kristallen werden verdeeld over de groeven op het porseleinen plaatje dat gebruikt wordt bij de wrijvingsgevoeligheidstesten of tussen de korrels van het schuurpapier dat gebruikt wordt tijdens de *ballistic impact chamber* test. Er is een noodzaak om het initiatiemechanisme van deze gevoeligheidstesten te herzien en suggesties te doen voor nauwkeurige methodes om de gevoeligheid van explosieve nanodeeltjes te meten. Aanbevelingen zijn gedaan voor het ontwikkelen van nieuwe testmethodes die alleen berusten op de interacties tussen de deeltjes, zodat deze toepasbaar worden voor gevoeligheidsmetingen aan energetische submicron/nanomaterialen. Een wrijvingsinitiatie-opstelling, zoals 30 jaar geleden ontwikkeld bij TNO, zou een techniek kunnen zijn waarmee meer

betrouwbare metingen van de wrijvingsgevoeligheid van energetische submicron/nanomaterialen uitgevoerd kunnen worden. Daarbij wordt alleen wrijvingswarmte tussen de deeltjes in het monster gegenereerd en worden alle andere vormen van wrijvingswarmte vermeden, hetgeen meer betrouwbare resultaten moet opleveren.

(Vertaald door Antoine van der Heijden, Joop ter Horst en Marloes Reus)

Acknowledgements

I would like to express my deepest gratitude to all the people who were helping and supporting me during the 4 years of my Ph.D. work.

First of all, I would like to thank my family and instructors, who motivated me to study science, and supported me in my career. Mom, Dad, Dóri and Zoli: you never stopped loving me, and without your support I would had never been able to get my Ph.D. You all mean a lot to me, and I always wanted to make you proud!

During my studies I met three very special instructors, who inspired me and kept my passion for science alive. My high school physics teacher, Tibor Szilágyi, lit the first spark, which further developed into a fiery interest in science at the university after the interesting lectures and discussions with Prof. József Pálinkás and Prof. István Lovas. Thank you all for your persistent support and for answering my questions all the time!

Next, I would like to give my gratitude to Prof. Andrzej Stankiewicz for giving me the opportunity to be part of his group. Our regular discussions, your support and belief in my success helped me a lot morally to do my best in my Ph.D. research. Thank you Andrzej for your continuous support, being so direct with me, coming to my house in The Hague, and coming to my wedding in Hungary. You also invited me to participate in the Delft Skyline Debates, which I consider as a big honour, and you offered me your strong support for my future career.

I would also like to thank Dr. Joop ter Horst and Dr. Antoine van der Heijden for guiding me all the time and being my daily supervisors. Thank you very much Joop and Antoine for the coaching, I have learnt a lot from both of you. Joop, I am very glad you gave me the opportunity to be an organizer at the BIWIC 2011 Conference and the opportunity to participate in many other crystallization conferences. I would also like to thank you for inviting me to all the DACG meetings. I always enjoyed your sense of humour while we shared meals, this kept even the heaviest scientific discussions light. You are a very bright scientist, who can easily inspire others. Antoine, you were a very helpful supervisor, and gave me your trust in all cases. Thanks for your consistent support and for the nice discussions during our regular meetings.

of help and support in my work. Thank you all for the good times, for the fun and for the nice discussions. I would also like to thank Mahinder for helping me with all the tax issues, and Dennis for helping me with IKA and with the Dutch translations.

There are many other people close to me outside my office at P&E. Albert, Ana, Alex, Aylin, Brian, Daniel, Ernesto, George (both), Guido, Herman, Iza, Mahsa, Magda, Marloes, Marta, René, Richard, Rob, Samir, Sasha, Sayee, Sergio, Shanfeng, Sukanya, Stephanie, Thijs, Tomek: thank you for everything!

I would also like to thank Caner Yurteri for the introduction to electrospray and technical discussions on it, and Prof. Andreas Schmitt-Ott, Dr. Ruud van Ommen and Dr. George Biskos for teaching me all the details about nanoparticle technology.

Furthermore, I highly appreciate the work of Willem Duvalois, Ruud Hendrikx, John Koman, Bastian de Bes, Kristina Djanashvili and Emile van Veldhoven with the sample analysis.

I would also like to thank my collaborators from Hungary for all the help and kindness. First of all I would like to thank Professor Piroska Szabó-Révész and Dr. Zoltán Aigner for the opportunity to work together.

I would like to thank Prof. Michael Zaworotko, Prof. Masakuni Matsuoka and Prof. Dimo Kashchiev for the stimulating discussions.
During my Ph.D. journey I had the privilege to be part of 3 different groups at TNO, and I have gained many new friends during the years. I would like to thank all the help and kindness from all the colleagues at TNO. I had a lot of fun during the years with my office mates, Ashwini, Elena, Rogier, Willem and Monique. I would also like to thank the managers of my groups who made it possible for me to work at TNO. Andre, Ton and Huub: you are all great bosses!

I would also like to acknowledge Marcel, Linda, Paul, Flavia, Cristiaan, Berend, Willem, Viola, Alfons, Berry, Job, Rick and all the people I had lunch with every day I was at TNO.

Finally, I would also like to express my gratitude to all the students I supervised during the years. Yvar, Remco, Lèon, Coen, Bob, Jean and Nick – you were all great students and helped me a lot with your experimental and theoretical work.

Curriculum vitae

Norbert Radácsi was born on December 5th in Debrecen, Hungary. After finishing his secondary school with cum laude distinction at Ady Endre High School in Debrecen in 2000, he pursued a master's degree in physics at the University of Debrecen. One year later, he enrolled in the general medicine program in parallel to his physics studies at the same university. In 2006, he obtained his M.Sc. degree in physics. Then he volunteered at the Hungarian Defence Force and became a military pilot. He flew with the JAK-52 military training aircraft, and in the meantime he obtained his private pilot license for Cessna-150. In 2008 he went to The Netherlands to obtain his Ph.D. at the Delft University of Technology. He worked at the Process & Energy Department of the faculty of 3ME and at TNO, a Dutch organization for applied scientific research. During his Ph.D. he received guidance from Prof. A. I. Stankiewicz, Dr. J. H. ter Horst, Dr. A. E. D. M. van der Heijden and Dr. Y. Creyghton. Apart from his research, Norbert enjoys swimming, airsoft, hiking, flying, travelling, reading and photography.

Publications

Journal publications

1. <u>N. Radacsi</u>, A. E. D. M. van der Heijden, J. H. ter Horst, Crystallization of Isonicotinamide in a Strong Electric Field, In preparation for journal submission

2. <u>N. Radacsi</u>, R. H. B. Bouma, E. L. M. Krabbendam-la Haye, J. H. ter Horst, A. I. Stankiewicz, A. E. D. M. van der Heijden, On the Reliability of Sensitivity Test Methods for Submicron-sized RDX and HMX Particles, Submitted for publication to *Journal of Energetic Materials*

3. R. Ambrus, <u>N. Radacsi</u>, T. Szunyogh, A. E. D. M. van der Heijden, J. H. ter Horst, P. Szabó-Révész, Analysis of Niflumic Acid Nanocrystals Prepared by Electrospray Crystallization, Submitted for publication to *Journal of Pharmaceutical and Biomedical Analysis*

4. <u>N. Radacsi</u>, Y. L. M. Creyghton, A. E. D. M. van der Heijden, A. I. Stankiewicz, J. H. ter Horst, Cold Plasma Synthesis of High Quality Organic Nanoparticles at Atmospheric Pressure, Submitted for publication to *Journal of Nanoparticle Research*

5. <u>N. Radacsi</u>, R. Ambrus, P. Szabó-Révész, A. E. D. M. van der Heijden, J. H. ter Horst, Atmospheric Pressure Cold Plasma Synthesis of Submicron-sized Pharmaceuticals with Improved Physico-chemical Properties *Crystal Growth & Design* 2012 DOI: 10.1021/cg301026b

6. <u>N. Radacsi</u>, R. Ambrus, T. Szunyogh, P. Szabó-Révész, A. I. Stankiewicz, A. E. D. M. van der Heijden, J. H. ter Horst, Electrospray Crystallization for Nano-sized Pharmaceuticals with Improved Properties, *Crystal Growth & Design* 2012, 12, 3514-3520.

7. <u>N. Radacsi</u>, A. I. Stankiewicz, Y. L. M. Creyghton, A. E. D. M. van der Heijden, J. H. ter Horst, Electrospray Crystallization for High-Quality Submicron-Sized Crystals, *Chemical Engineering and Technology* 2011, 34, 624-630.

Publications in conference proceedings

1. <u>N. Radacsi</u>, Y. L. M. Creyghton, A. E. D. M. van der Heijden, R. Ambrus, A. I. Stankiewicz, J. H. ter Horst, Plasma Crystallization for Submicron-sized Drugs with Outstanding Properties, *In proceedings of 10th International Workshop on Crystal Growth of Organic Materials (CGOM10),* June 11-14, 2012, Limerick, Ireland, p. 120-122.

2. <u>N. Radacsi</u>, A. I. Stankiewicz, Z. Aigner, Y. L. M. Creyghton, A. E. D. M. van der Heijden, J. H. ter Horst, Electrospray Crystallization: A Simple Technique to Create High Quality Nanocrystals, *In the conference proceedings of 18th International Symposium on Industrial Crystallization (ISIC18),* September 13-16, 2011, Zürich, Switzerland, p. 168-169.

3. <u>N. Radacsi</u>, A. I. Stankiewicz, Z. Aigner, Y. L. M. Creyghton, A. E. D. M. van der Heijden, J. H. ter Horst, Electrospray Crystallization for Submicron-sized Crystals with Improved Properties, *In proceedings of 18th Industrial Workshop on Industrial Crystallization (BIWIC),* September 7-9, 2011, Delft, The Netherlands, p. 211.

4. <u>N. Radacsi</u>, L. Wassink, A. I. Stankiewicz, Y. L. M. Creyghton, A. E. D. M. van der Heijden, J. H. ter Horst, Electrospray Crystallization for Less Sensitive Energetic Nanoparticles, *In the conference proceedings of 17th Industrial Workshop on Industrial Crystallization (BIWIC),* September 8-10, 2010, Halle, Germany, p. 109-117.

5. <u>N. Radacsi</u>, L. Wassink, A. I. Stankiewicz, Y. L. M. Creyghton, A. E. D. M. van der Heijden, J. H. ter Horst, Electrospray: A Simple Technique to Create Nanosized RDX, *In the conference proceedings of 41st International Annual Conference of ICT: Energetic Materials for High Performance, Insensitive Munitions, and Zero Pollution),* June 29 – July 2, 2010, Karlsruhe, Germany, 132-1.

Oral presentations

1. Crystallization in electrostatic fields for controlling crystals polymorphism. *4th European Conference on Crystal Growth (ECCG4)* June 17-20, 2012, Glasgow, UK

2. Plasma Crystallization for Submicron-sized Drugs with Outstanding Properties, *10th International Workshop on Crystal Growth of Organic Materials (CGOM10),* June 11-14, 2012, Limerick, Ireland

3. Electrospray Crystallization: a Simple Technique to Create Nano-sized Crystals with Improved Properties. *11th Nederlandse Process Technology Symposium (NPS-11),* October 24 – 26, 2011, Papendal, The Netherlands

4. Electrospray Crystallization: A Simple Technique to Create High Quality Nanocrystals. *18th International Symposium on Industrial Crystallization (ISIC18),* September 13-16, 2011, Zürich, Switzerland

5. Electrospray Crystallization for Submicron-sized Crystals with Improved Properties. *British Association for Crystal Growth (BACG) Symposium,* July 10-12, 2011, London, UK

6. Electrospray Crystallization for Less Sensitive Energetic Nanoparticles. *17th Industrial Workshop on Industrial Crystallization (BIWIC),* September 8-10, 2010, Halle, Germany